



LIBRARY
Michigan State
University

This is to certify that the
dissertation entitled
PROTON COUPLED ELECTRON TRANSFER MEDIATED BY A SALT
BRIDGE
presented by
James A. Roberts

has been accepted towards fulfillment
of the requirements for
Ph.D. degree in Chemistry

Major professor

Date 9-15-97

PLACE IN RETURN BOX to remove this checkout from your record.
TO AVOID FINES return on or before date due.
MAY BE RECALLED with earlier due date if requested.

DATE DUE	DATE DUE	DATE DUE
<hr/>	<hr/>	<hr/>
<hr/>	<hr/>	<hr/>
<hr/>	<hr/>	<hr/>
<hr/>	<hr/>	<hr/>
<hr/>	<hr/>	<hr/>

ABSTRACT
PROTON COUPLED ELECTRON TRANSFER MEDIATED BY A SALT BRIDGE

By

James A. Roberts

PROTON COUPLED ELECTRON TRANSFER MEDIATED BY A SALT
BRIDGE

By

James A. Roberts

A DISSERTATION

Submitted to
Michigan State University
in partial fulfillment of the requirements
for the degree of

DOCTOR OF PHILOSOPHY

Department of Chemistry
1997

ABSTRACT
PROTON COUPLED ELECTRON TRANSFER MEDIATED BY A SALT BRIDGE

By

James A. Roberts

Many proteins and enzymes derive their function through the mediation of electron transfer processes by proton transfer. The coupling of proton motion to charge separation is a basic mechanism of biological energy conversion systems. However, the inherent complexity of biological systems does not allow for the direct measurement of coupled proton and electron kinetics. To this end the design of electron transfer complexes incorporating design features of fixed distance electron transfer in combination with photoinduced proton transfer have been prepared.

Tris-bipyridyl ruthenium(II) complexes functionalized with hydrogen-bonding salt-bridges permit a photoinduced excited state electron transfer to be established. Initial intramolecular rate constant. However, a comparative study of switched interface systems investigations based on the excited state electron transfer donor chemistry of $[(bpy)_2Ru(Me-bpy)COOH(PF_6)_2]^{2+}$, $[(bpy)_2Ru(Me-bpy)COO^-(PF_6)]^+$ and $[(bpy)_2Ru(Me-bpy)AmH^+(PF_6)_3]^{3+}$ (bpy = 2,2'-bipyridine, Me-bpyCOOH = 4-methyl,4'-carboxylic acid-2,2'-bipyridine, Me-bpyAmH⁺ = 4-methyl,4'-amidinium-2,2'-bipyridine) complexed with the complimentary salt-bridge functionalized 3,5-dinitrobenzene show rates for electron transfer dependent upon the orientation of the salt-bridge interface. When the arrangement is donor-amidinium-carboxylate-acceptor (AMH⁺,COO⁻) the observed intramolecular electron transfer rate constant is a factor of 2 less than for the same donor-acceptor system bridged by a (COOH)₂ interface. The rate for the (COO⁻,AMH⁺)

interface orientation indicates a rate enhancement of 4 relative to that observed for the switched analog.

Energetics of bipyridyl systems are not convenient to a clear electron transfer measurement as the energy of the interface functionalized and non-functionalized bipyridyl ligands are similar. Thus systems designed with alkylated bipyridyl ligands $[(\text{tmb})_2\text{Ru}(\text{Me-bpy})\text{COOH}(\text{PF}_6)_2]^{2+}$, $[(\text{tmb})_2\text{Ru}(\text{Me-bpy})\text{COO}^-(\text{PF}_6)]^{2+}$ and $[(\text{tmb})_2\text{Ru}(\text{Me-bpy})\text{AmH}^+(\text{PF}_6)_3]^{2+}$ ($\text{tmb} = 4,4',5,5'$ -tetramethyl-2,2'-bipyridine $\text{Me-bpyCOO}^- = 4$ -methyl,4'-carboxylate 2,2'-bipyridine) and ester modified bipyridyl ligands $[(\text{decb})_2\text{Ru}(\text{Me-bpy})\text{COOH}(\text{PF}_6)_2]^{2+}$ and $[(\text{decb})\text{Ru}(\text{Me-bpy})\text{AmH}^+(\text{PF}_6)_3]^{2+}$ ($\text{decb} = 4,4'$ -diethylcarboxy-2,2'-bipyridine) were used. For the (tmb) systems, the observed intramolecular electron transfer rate is 36 times greater for the $(\text{COO}^-, \text{AmH}^+)$ interface system relative to the $(\text{AmH}^+, \text{COO}^-)$ system. Reductive electron transfer, with the (decb) functionalized Ru(II) complexes, toward the protonated residue of the metal complex exhibits a fast intramolecular rate constant. However, a comparative study of switched interface systems is hampered by large changes in the electron transfer donor potential.

ACKNOWLEDGMENTS

My advisor, Professor Dan Nocera, has provided me the freedom to explore science in an environment that has always been exceptional and invigorating. My understanding and awareness of the big picture and machinery of science have changed as a result of the five years spent in his research group. I would also like to thank my committee members Professors Babcock, Cukier and Dunbar and also Professor Blanchard who served on my committee on extremely short notice.

Special thanks to Yongshu Deng and Eric Saari who spent the last eventful weeks like me, deeply entrenched in the sometimes overwhelming process of finishing. Thanks also to Dr. Al Barney who helped to maintain my focus during the final days and to Linda Krause who always kept things on a **To my family,** about her this thesis would assuredly have been much more of a burden. Finally I would like to thank Wanda Hartmann for her diligent proofreading when things were not running smoothly.

The Nocera group, most directly J.P. and Deng for a continuous supply of compounds, and the rest of the group Adrian, Al, Jude, Jean, Mark Mortellaro, Nick, Ann, Carolyn, Claudia, Doug, Dan, Dimitris, Erik, Janice, Jeff, Mark Torgerson, Sara, and Zoe, have provided a sound environment in which to develop as a scientist. Most importantly I would like to thank Wanda, who has for the last 2 1/2 years been a source of inspiration and support during the trying times of graduate school.

And Finally, I would like to thank Al and Kathy Barney and also Dan, Amy and Ariel Engstrom for their hospitality during my last homeless days at Michigan State University.

ACKNOWLEDGMENTS

My advisor, Professor Dan Nocera, has provided me the freedom to explore science in an environment that has always been exceptional and invigorating. My understanding and awareness of the big picture and machinery of science have changed as a result of the five years spent in his research group. I would also like to thank my committee members Professors Babcock, Cukier and Dunbar and also Professor Blanchard who served on my committee on extremely short notice.

Special thanks to Yongshi Deng and Eric Saari who spent the last eventful weeks like me, deeply entrenched in the sometimes overwhelming process of finishing. Thanks also to Dr. Al Barney who helped to maintain my focus during the final days and to Linda Krause who always kept things on a lighter note, without her this thesis would assuredly have been much more of a burden. Finally I would like to thank Wanda Hartmann for her diligent proofreading when things were not running smoothly.

The Nocera group, most directly J.P. and Deng for a continuous supply of compounds, and the rest of the group Adrian, Al, Jude, Jean, Mark Mortellaro, Niels, Ann, Carolyn, Claudia, Doug, Dan, Dimitris, Eric, Janice, Jeff, Mark Torgerson, Sara, and Zoe, have provided a sound environment in which to develop as a scientist. Most importantly I would like to thank Wanda, who has for the last 2 1/2 years been a source of inspiration and support during the trying times of graduate school.

And Finally, I would like to thank Al and Kathy Barney and also Dan, Amy and Ariel Engebretson for their hospitality during my last homeless days at Michigan State University.

CHAPTER 3	57
PHOTOINDUCED ELECTRON TRANSFER WITHIN AN ELECTRON DONOR-ACCEPTOR ASSEMBLY JUXTAPOSED BY A HYDROGEN-BONDING INTERFACE	57
INTRODUCTION	57
RESULTS	61
<i>Electronic Absorption and Luminescence spectroscopy</i>	61
<i>Luminescence and Lifetime Measurements</i>	63
DISCUSSION	72
TABLE OF CONTENTS	

TABLE OF CONTENTS.....	VI
LIST OF FIGURES.....	IX
LIST OF TABLES.....	XIII

CHAPTER 1	1
INTRODUCTION.....	1
ELECTRON TRANSFER	1
<i>Fixed Distance Systems</i>	3
<i>Model systems</i>	5
<i>Rigid donor-acceptor systems</i>	10
NON-COVALENT INTERACTIONS	13
PROTON TRANSFER	17
<i>Proton transfer in biological systems</i>	17
NON-COVALENT SYSTEMS IN ELECTRON TRANSFER	18
PROTON COUPLED-ELECTRON TRANSFER	24
<i>Incorporation of Ruthenium Systems into the study of PCET</i>	32
ORGANIZATION OF THE THESIS	39
CHAPTER 2	41
EXPERIMENTAL METHODS.....	41
MATERIALS.....	41
ELECTROCHEMISTRY	41
OPTICAL SPECTROSCOPY	47
PHOTOPHYSICAL MEASUREMENTS	50
<i>Infrared spectroscopy</i>	51
<i>Nano-Second Lifetime Measurements</i>	52
<i>Pico-second Lifetime measurements</i>	53
SYNTHESIS OF RUTHENIUM COMPLEXES	55

APPENDIX A.....	149
-----------------	-----

CHAPTER 3	57
PHOTOINDUCED ELECTRON TRANSFER WITHIN AN ELECTRON DONOR-ACCEPTOR ASSEMBLY JUXTAPOSED BY A HYDROGEN-BONDING INTERFACE.....	57
INTRODUCTION	57
RESULTS	61
<i>Electronic Absorption and Luminescence spectroscopy</i>	61
<i>Luminescence and Lifetime Measurements</i>	65
DISCUSSION	72
CHAPTER 4	78
PHOTOINDUCED ELECTRON TRANSFER WITHIN A SYNTHETICALLY MODIFIED RUTHENIUM DONOR ACCEPTOR PAIR:THE EFFECT OF SWITCHING THE SALT-BRIDGE INTERFACE.....	78
INTRODUCTION	78
RESULTS	83
<i>Electrochemistry</i>	83
<i>Electronic Absorption and Luminescence photophysical characterization</i>	83
<i>Association Constants</i>	87
<i>Determination of Ru(II)polypyridyl complex energetics</i>	94
<i>Luminescence and Lifetime Measurements</i>	94
DISCUSSION	101
CHAPTER 5	109
PHOTOINDUCED REDUCTIVE ELECTRON TRANSFER WITHIN AN ELECTRON DONOR-ACCEPTOR PAIR:ASSESSMENT OF THE REVERSAL OF THE ELECTRON TRANSFER DIRECTION	109
INTRODUCTION	109
RESULTS	113
<i>Electronic Absorption / Emission Spectroscopy</i>	113
<i>Luminescence Spectra</i>	117
<i>Lifetime Quenching Electron Transfer Measurements</i>	124
DISCUSSION	133
LIST OF REFERENCES	138
APPENDIX A	149

DETERMINATION OF THE ACID-BASE PROPERTIES OF A SERIES OF ELECTRON TRANSFER DONOR-ACCEPTOR PAIRS: ASSESSMENT OF THE pK_a^* AND ΔpK_a IN AQUEOUS SOLUTION.....	149
INTRODUCTION.....	149
RESULTS.....	153
<i>Absorption/Emission Ground State and Excited State Acid-Base Reactions of the Ruthenium Complexes</i>	153
<i>Ground State Acid-Base Properties of the Free Ligands</i>	164
<i>Excited State Acid-Base Properties of the Ruthenium Complexes; Lifetime Measurements</i>	165
<i>Ground State Acid-Base Properties of Salt-Bridge Functionalized 3,5-Dinitrobenzene Electron Transfer Quenchers</i>	170
DISCUSSION.....	171
reaction centers	8
Figure 3. Electron transfer model systems (a) Biphenyl bridged model system of McClendon (b) Peptide linked chromophore-quencher system of Meyer and (c) rigid covalent norbornadiene system of Paddon-Row.	9
Figure 4. Non-covalent electron transfer systems implementing guanine-cytosine base-pair recognition for donor-acceptor separation. Conformationally flexible system (a), conformationally rigid system (b) two point (c) and four point (d) hydrogen bonding of quinones by functionalized porphyrins.	20
Figure 5. Non-covalent systems based on asymmetric hydrogen-bonding (a) and by metal ligation (b)	21
Figure 6. Non-covalent cyclodextrin porphyrin assembly for the investigation of electron transfer to quinone.	22
Figure 7. Zn(II)-porphyrin-3,4-dicarboxylic acid donor-acceptor symmetric interface system. (a) Zn(II)-Fe(III) diporphyrin symmetric interface system with phenyl spacer (b).	27
Figure 8. Photophysical scheme for tris-bipyridyl ruthenium(II) complexes. 1MLCT , 3MLCT , $^1\pi\pi^*$, and ^3d-d refer to the singlet and triplet charge transfer, the singlet intraligand and the triplet metal centered states respectively. k_1 and k_{12} represent decay processes.	37
Figure 9. Bipyridyl ligated systems. Symmetric dicarboxylic acid (a) asymmetric amidinium-carboxylate (b) and asymmetric carboxylate-amidinium (c) salt-bridge interfaces for electron transfer studies.	62
Figure 10. Biexponential fit of lifetime decay indicating concentration-dependent and concentration-independent components of a representative lifetime decay for $[(bpy)_3Ru^{2+}(Me-bpy)AmH^+]$ (1.0×10^{-4} M) with complementary 3,5-dinitrobenzoate [1.5×10^{-4} M]	68

Figure 11. Concentration-independent component (●) and concentration dependent component (■) for the lifetime titration of $[(bpy)_3Ru^{2+}(Me-bpy)AmH]^+$ (1.0×10^{-4} M) with 3,5-dinitrobenzoate in CH_2Cl_2 at 22°C. 69

Figure 12. Energetic scheme for the excitation of the $Ru(II)$ polypyridyl complexes $[(bpy)_3Ru^{2+}(Me-bpy)AmH]^+$, $[(bpy)_3Ru^{2+}(Me-bpy)COOH]^+$, $[(bpy)_3Ru^{2+}(Me-bpy)COO]^-$ 74

LIST OF FIGURES

Figure 13. Tetramethyl bipyridyl $Ru(II)$ complexes for electron transfer through the salt-bridge interface formed by the association of the complementary quenchers 3,5-dinitrobenzoate and 4-aminobenzoate. 74

Figure 1. Photosynthetic reaction center mimics, coupled porphyrin model systems design of (a) Osuka et al. and (b) a tetrad system of Gust and Moore. 7

Figure 2. Model system for the assessment of electric field effects in photosynthetic reaction centers 8

Figure 3. Electron transfer model systems (a) Biphenyl bridged model system of McClendon (b) Peptide linked chromophore-quencher system of Meyer and (c) rigid covalent norbornadiene system of Paddon-Row. 9

Figure 4. Non-covalent electron transfer systems implementing guanine-cytosine base-pair recognition for donor-acceptor separation. Conformationally flexible system (a), conformationally rigid system (b) two point (c) and four point (d) hydrogen bonding of quinones by functionalized porphyrins. 20

Figure 5. Non-covalent systems based on asymmetric hydrogen-bonding (a) and by metal ligation (b) 21

Figure 6. Non-covalent cyclodextrin porphyrin assembly for the investigation of electron transfer to quinone. 22

Figure 7. Zn(II)-porphyrin-3,4-dicarboxylic acid donor-acceptor symmetric interface system. (a) Zn(II)-Fe(III) diporphyrin symmetric interface system with phenyl spacer (b). 27

Figure 8. Photophysical scheme for *tris*-bipyridyl ruthenium(II) complexes. 1MLCT , 3MLCT , $^1\pi\pi^*$, and ^3d-d refer to the singlet and triplet charge transfer, the singlet intraligand and the triplet metal centered states respectively. k_r and k_{nr} represent decay processes. 37

Figure 9. Bipyridyl ligated systems. Symmetric dicarboxylic acid (a) asymmetric amidinium-carboxylate (b) and asymmetric carboxylate-amidinium (c) salt-bridge interfaces for electron transfer studies. 62

Figure 10. Biexponential fit of lifetime decay indicating concentration-dependent and concentration-independent components of a representative lifetime decay for $[(bpy)_3Ru^{2+}(Me-bpy)AmH]^+$ (1.0×10^{-4} M) with complementary 3,5-dinitrobenzoate (1.5×10^{-4} M). 68

- Figure 11. Concentration-independent component (●) and concentration dependent component (■) for the lifetime titration of $(bpy)_2Ru^{2+}(Me-bpy)AmH^+$ [1.0×10^{-4} M] with 3,5-dinitrobenzoate in CH_2Cl_2 at $22^\circ C$69
- Figure 12. Energetic scheme for the excitation of the Ru(II)polypyridyl complexes $[(bpy)_2Ru^{2+}(Me-bpy)AmH^+]^{3+}$, $[(bpy)_2Ru^{2+}(Me-bpy)COOH]^{2+}$ $[(bpy)_2Ru^{2+}(Me-bpy)_2Ru^{2+}(Me-bpy)COO^-]^{+}$ in CH_3CN at $22^\circ C$74
- Figure 13. Tetramethyl bipyridyl Ru(II) complexes for electron transfer through the salt-bridge interface formed by the association of the complimentary quenchers 3,5-dinitrobenzoate (a), 3,5-dinitrobenzoic acid (b) and 3,5-dinitrobenzamidinium (c). 81
- Figure 14 Absorption and Absolute emission of the three Ru(II) electron transfer complexes: $[(tmb)_2Ru^{2+}(Me-bpy)AmH^+]^{3+}$ (line), $[(tmb)_2Ru^{2+}(Me-bpy)COO^-]^{+}$ (dashed line), and $[(tmb)_2Ru^{2+}(Me-bpy)COOH]^{2+}$ (dotted line).84
- Figure 15 Association constant determination from Absorption titration of $[(tmb)_2Ru^{2+}(Me-bpy)AmH^+]^{3+}$ (3.0×10^{-5} M) with 3,5-dinitrobenzoate in CH_2Cl_2 . Inset plot shows the change in absorbance at 495 nm through the titration.90
- Figure 16. Association constant determination from Absorption titration of $[(tmb)_2Ru^{2+}(Me-bpy)AmH^+]^{3+}$ (3.0×10^{-5} M) with benzoate in CH_2Cl_2 . Inset plot shows the change in absorbance at 470 nm through the titration.91
- Figure 17. Association constant from the ratio of biexponential fit function prefactors (A_1 and A_2) of the lifetime decay of $[(tmb)_2Ru^{2+}(Me-bpy)COO^-]^{+}$ (0.10 mM) titrated with 3,5-dinitrobenzamidinium.92
- Figure 18 Concentration-dependent (■) and concentration-independent (●) observed rate constants for the quenching of $[(tmb)_2Ru^{2+}(Me-bpy)COO^-]^{+}$ (0.10 mM) by 3,5-dinitrobenzamidinium in CH_2Cl_295
- Figure 19. Top panel. Lifetime decay data for the quenching reaction between $[(tmb)_2Ru^{2+}(Me-bpy)COO^-]^{+}$ and 3,5-dinitrobenzamidinium. Biexponential fitting of the decay data is indicated with the solid line. Bottom panel. Relative percentages of the biexponential fitting of the decay data from Top panel.96
- Figure 20. Concentration-dependent (■) and concentration-independent (●) observed rate constants for the quenching of $[(tmb)_2Ru^{2+}(Me-bpy)COOH]^{2+}$ (0.06mM) by 3,5-dinitrobenzoic acid in CH_2Cl_297
- Figure 21. Concentration-dependent (■) and concentration-independent (●) observed rate constants for the quenching of $[(tmb)_2Ru^{2+}(Me-bpy)AmH^+]^{3+}$ (0.064mM) by 3,5-dinitrobenzoate in CH_2Cl_298
- Figure 22. Ru(II)polypyridyl complexes for reductive electron transfer quenching (a) $[(bpy)_2Ru^{2+}(Me-bpy)AmH^+]^{3+}$ (b) $[(bpy)_2Ru^{2+}(Me-bpy)COO^-]^{+}$, (c) $[(decb)_2Ru^{2+}(Me-bpy)AmH^+]^{3+}$ and (d) $[(decb)_2Ru^{2+}(Me-bpy)COOH]^{2+}$. Figures investigated.154

shown are the salt-bridged complexes formed from the 1:1 association with N,N'-dimethylaminobenzoate and N,N'-dimethylaminobenzamidinium	112
<i>Figure 23.</i> Absorption and emission spectra for amidinium functionalized electron transfer donor complexes [(bpy) ₂ Ru ²⁺ (Me-bpy)AmH ⁺] ³⁺ and [(decb) ₂ Ru ²⁺ (Me-bpy)AmH ⁺] ³⁺ in aerated CH ₃ CN solution.	114
<i>Figure 24.</i> Absorption and emission spectra of carboxylate functionalized electron transfer donor complexes [(bpy) ₂ Ru ²⁺ (Me-bpy)COO-] ⁺ and [(decb) ₂ Ru ²⁺ (Me-bpy)COOH] ²⁺ in aerated CH ₃ CN solvent.	115
<i>Figure 25.</i> Absorption titration of [(bpy) ₂ Ru ²⁺ (Me-bpy)AmH ⁺] (2.0 x 10 ⁻⁵ M) by N,N'-dimethylaminobenzoate in CH ₃ CN.....	118
<i>Figure 26.</i> Absorption titration of [(decb) ₂ Ru ²⁺ (Me-bpy)AmH ⁺] ³⁺ (2.0 x 10 ⁻⁵ M) with N,N'-dimethylaminobenzoate in CH ₃ CN	119
<i>Figure 27.</i> Absorption titration of [(bpy) ₂ Ru ²⁺ (Me-bpy)AmH ⁺] ³⁺ with N,N'-dimethylaminobenzamidinium in CH ₃ CN.	120
<i>Figure 28.</i> Absorption titration of [(decb) ₂ Ru ²⁺ (Me-bpy)COO-] ⁺ with N,N'-dimethylaminobenzamidinium in CH ₃ CN.	121
<i>Figure 29.</i> Concentration-independent (●) and concentration-dependent (■) observed rate constants for the quenching of [(bpy) ₂ Ru ²⁺ (Me-bpy)AmH ⁺] ³⁺ by N,N'-dimethylaminobenzoate in CH ₃ CN.....	125
<i>Figure 30.</i> Ratio of pre-exponential factors A ₁ (■) and A ₂ (●) from biexponential fitting of the quenching data for [(bpy) ₂ Ru ²⁺ (Me-bpy)AmH ⁺] ³⁺ with N,N'-dimethylamino-benzoate.	126
<i>Figure 31.</i> Concentration-independent (●) and concentration-dependent (■) observed rate data for the quenching of [(decb) ₂ Ru ²⁺ (Me-bpy)AmH ⁺] ³⁺ by N,N'-dimethylaminobenzoate in CH ₃ CN.....	127
<i>Figure 32.</i> Marcus fit of bimolecular electron transfer rates constants for the kinetic determination of redox potentials of the reductive quenchers N,N'-dimethylaminobenzoate and N,N'-dimethylaminobenzamidinium in CH ₃ CN μ = 0.1 22 ^o C.....	130
<i>Figure 33.</i> Ru(II)polypyridyl complexes used in the aqueous acid-base property determinations. (a),(b) [(x-bpy) ₂ Ru ²⁺ (Me-bpy)COOH] ²⁺ {(a) x = H and (b) x = (CH ₃) ₄ }, and (c),(d) [(x-bpy) ₂ Ru ²⁺ (Me-bpy)AmH ⁺] ³⁺ {(c) x = H and (d) x = (CH ₃) ₄ }.....	152
<i>Figure 34.</i> Absorption pH titration of [(bpy) ₂ Ru ²⁺ (Me-bpy)COOH][(PF ₆) ₂]. The spectrum for the intraligand π-π* region is shown at the left and the spectrum in the dπ-π* MLCT region at the right. The inset of each of the plots shows the change of the absorption (λ = 286 and 456 nm) over the pH range investigated.....	154

Figure 35. Absorption pH titration of $[(\text{tmb})_2\text{Ru}^{2+}(\text{Me-bpy})\text{COOH}][(\text{PF}_6)_2]$. The spectrum for the intraligand $\pi-\pi^*$ region is shown at the left and the spectrum of the $d\pi-\pi^*$ MLCT region is shown at the right. The inset of each of the plots shows the absorption ($\lambda = 290$ and 447 nm) over the pH range investigated.....155

Figure 36. Absorption pH titration of $[(\text{bpy})_2\text{Ru}^{2+}(\text{Me-bpy})\text{AmH}^+][(\text{PF}_6)_3]$. The spectrum for the intraligand $\pi-\pi^*$ region is shown at the left and the spectrum of the $d\pi-\pi^*$ MLCT region is shown at the right. The inset of each of the plots shows the absorption ($\lambda = 286$ and 457 nm) over the pH range investigated.....157

Figure 37. Absorption pH titration of $[(\text{tmb})_2\text{Ru}^{2+}(\text{Me-bpy})\text{AmH}^+][(\text{PF}_6)_3]$. The spectrum for the intraligand $\pi-\pi^*$ region is shown at the left and the spectrum of the $d\pi-\pi^*$ MLCT region is shown at the right. The inset of each of the plots shows the absorption ($\lambda = 289$ and 440 nm) over the pH range investigated.....158

Figure 38. Emission pH titration for $[(\text{bpy})_2\text{Ru}^{2+}(\text{Me-bpy})\text{COOH}][(\text{PF}_6)_2]$. The inset of the plot indicates the changes of the emission intensity at 630 nm over the pH range investigated.....160

Figure 39. Emission pH titration for $[(\text{tmb})_2\text{Ru}^{2+}(\text{Me-bpy})\text{COOH}][(\text{PF}_6)_2]$. The inset of the plot indicates the changes of the emission intensity at 630 nm over the pH range investigated.....161

Figure 40. pH dependence of the lifetime measurements. Top trace (●) is for the complex $[(\text{bpy})_2\text{Ru}^{2+}(\text{me-bpy})\text{COOH}][(\text{PF}_6)_2]$, bottom trace (■) is for the complex $[(\text{tmb})_2\text{Ru}^{2+}(\text{Mebpy})\text{COOH}][(\text{PF}_6)_2]$ 167

Figure 41. pH dependence of the lifetime measurements. Top trace (●) is for the complex $[(\text{bpy})_2\text{Ru}^{2+}(\text{Me-bpy})\text{AmH}^+][(\text{PF}_6)_3]$, bottom trace (■) is for the complex $[(\text{tmb})_2\text{Ru}^{2+}(\text{Mebpy})\text{AmH}^+][(\text{PF}_6)_3]$ 168

Table 9. Photophysical Characterization for $(\text{decb})_2\text{Ru(II)}$ and $(\text{bpy})_2\text{Ru(II)}$ complexes in CH_3CN 123

Table 10. Redox potentials and rate constants for the bimolecular quenching reactions between $\text{Ru}(\text{bpy})_3^{2+}$ and the reductive electron transfer quenchers..... 131

Table 11. Rates for concentration-dependent and concentration-independent quenching of $(\text{decb})_2\text{Ru(II)}$ and $(\text{bpy})_2\text{Ru(II)}$ salt-bridge electro transfer complexes..... 132

LIST OF TABLES

Table 1. Electrochemical data for the three (bpy) ₂ Ru(II) complexes	63
Table 2. Emission Characterization of (bpy) ₂ Ru(II) complexes	67
Table 3. Observed electron transfer rates for concentration-dependent and concentration-independent electron transfer of bipyridine based donor-acceptor complexes in CH ₂ Cl ₂ at 22 ⁰ C.	70
Table 4. Electrochemical data for (tmb) ₂ Ru(II) complexes in CH ₃ CN at 22 ⁰ C. E _{1/2} (V) vs. SCE.	86
Table 5. Ru(II) polypyridyl emission characterization data in CH ₂ Cl ₂ 22 ⁰ C. Excitation by Xe/Hg lamp at 435.8 nm	88
Table 6. Rates for concentration-dependent and concentration-independent quenching of (tmb) ₂ Ru(II) electron transfer complexes.	99
Table 7. Absorption data for (decb) ₂ Ru(II) and (bpy) ₂ Ru(II) complexes.....	116
Table 8. Emission Data for (decb) ₂ Ru(II) and (bpy) ₂ Ru(II) complexes in CH ₃ CN.	123
Table 9. Photophysical Characterization for (decb) ₂ Ru(II) and (bpy) ₂ Ru(II) complexes in CH ₃ CN.	123
Table 10. Redox potentials and rate constants for the bimolecular quenching reactions between Ru(bpy) ₃ ²⁺ and the reductive electron transfer quenchers.....	131
Table 11. Rates for concentration-dependent and concentration-independent quenching of (decb) ₂ Ru(II) and (bpy) ₂ Ru(II) salt-bridge electron transfer complexes.	132

Traditionally, the study of photoinduced electron transfer has been dominated by the determination of distance, conformational, and stereoelectronic relationships to the observed electron transfer rate. The myriad of systems designed to incorporate these issues have occupied the literature significantly for the past twenty years since Marcus' original description of activated electron transfer in the 1950's [2].

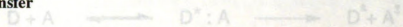
Subsequent to Marcus' theory, photoinduced electron transfer reactions were composed of bimolecular interactions between donor and acceptor in homogeneous solution. Deactivation of an electronically excited donor by either oxidative or reductive quenching species is shown schematically in Eq (1.1). Typical of bimolecular reactions is the oxidative and reductive quenching of $\text{Ru}(\text{bpy})_3^{2+}$ with viologen, aromatic nitro, aromatic amine and inorganic complex quenchers [3]. In these bimolecular electron transfer reactions, organization of donor and acceptor in a specific distance or

CHAPTER 1

INTRODUCTION



Electron Transfer



Theoretical descriptions of electron transfer have been presented in the past at a

(1.1)

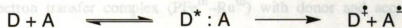
level of detail and sophistication that was not experimentally accessible. However, with conformational arrangement is inherently difficult and the electron transfer information the advent of fast laser techniques, and with the design of fixed distance donor-acceptor gleaned from such experiments is either rate limited by the diffusional encounter of the systems, the study of electron transfer reactions have become accessible at a level befitting of the theoretical framework. Of particular significance, is the ability to probe products. However, in 1981 Satoh [4] introduced ion-pairing in bimolecular electron fast vibrational events occurring as a result of, or promoting, an electron transfer event transfer reactions with the system composed of $\text{Ru}(\text{bpy})_3^{2+}$ and $\text{Fe}(\text{CN})_6^{3-}$, effectively [1].

organizing donor and acceptor in solution. This addition of electrostatic complementarity

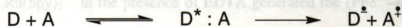
Traditionally, the study of photoinduced electron transfer has been dominated by the determination of distance, conformational, and stereoelectronic relationships to the observed electron transfer rate. The myriad of systems designed to incorporate these issues have occupied the literature significantly for the past twenty years since Marcus' original description of activated electron transfer in the 1950's [2]

Subsequent to Marcus' theory, photoinduced electron transfer reactions were composed of bimolecular interactions between donor and acceptor in homogeneous solution. Deactivation of an electronically excited donor by either oxidative or reductive quenching species is shown schematically in Eq (1.1). Typical of bimolecular reactions is the oxidative and reductive quenching of $\text{Ru}(\text{bpy})_3^{2+}$ with viologen, aromatic nitro, aromatic amine and inorganic complex quenchers [3]. In these bimolecular electron transfer reactions, organization of donor and acceptor in a specific distance or

cytochrome *c* (Fe^{3+}) produced the covalently attached $(\text{NH}_3)_5\text{Ru}(\text{III})$ (histidine-33), creating a electron transfer complex ($\text{Ru}^{\text{III}}-\text{Ru}^{\text{III}}$) with donor and acceptor fixed in distance by the protein. Bimolecular reduction of the surface bound $(\text{NH}_3)_5\text{Ru}(\text{III})$



$\text{33Ru}(\text{III})$ by $\text{Ru}(\text{bpy})_3^{2+}$ in the presence of EDTA generated the $(\text{Fe}^{\text{II}}-\text{Ru}^{\text{II}})$ complex. Subsequently, intramolecular electron transfer across a distance of approximately 11.8 Å



(1.1)

occurred with a rate constant of $30 \pm 3 \text{ s}^{-1}$. Further studies utilizing the cytochrome *c* conformational arrangement is inherently difficult and the electron transfer information protein in which the driving force of the reaction was enhanced by the substitution of the gleaned from such experiments is either rate limited by the diffusional encounter of the $\text{Fe}(\text{II})$ with $\text{Zn}(\text{II})$ were developed. Coupled with the variation of the $\text{Ru}(\text{II})$ complex complexes in solution or by the nuclear activation necessary to convert reactants to products. However, In 1981 Sutin [4] introduced ion-pairing to bimolecular electron transfer and electrochemical measurements were performed on the $\text{Ru}(\text{bpy})_3^{2+}$ and $\text{Fe}(\text{CN})_6^{3-}$ and ΔG transfer reactions with the system composed of $\text{Ru}(\text{bpy})_3^{2+}$ and $\text{Fe}(\text{CN})_6^{3-}$, effectively of the reaction, providing a determination of the electronic coupling (H_{ab}) and organizing donor and acceptor in solution. This addition of electrostatic complementarity

to the bimolecular system, characterized by moderate association ($\sim 350 \text{ M}^{-1}$) eliminated the diffusional dependence of previous non-specific bimolecular interactions.

Fixed Distance Systems

Bimolecular reactions are still of great interest to the study of electron transfer reactions [5] but more generally, the determination of specific contributions to electron transfer reactions over the past 15 years has developed around the incorporation of spacers tethering two electron transfer centers in a specific distance, stereochemical, or conformational arrangement.

The elegant flash quenching experiments performed by Gray et al. [6] spurred the development of fixed distance electron transfer systems. Formation of a metalloprotein electron transfer complex resulting from reaction of $(\text{NH}_3)_5\text{Ru(III)(H}_2\text{O)}$ with horse heart cytochrome *c* (PFe^{III}) produced the covalently attached $(\text{NH}_3)_5\text{Ru(III)}$ (histadine-33), creating a electron transfer complex ($\text{PFe}^{\text{III}}\text{-Ru}^{\text{III}}$) with donor and acceptor fixed in distance by the protein. Bimolecular reduction of the surface bound $(\text{NH}_3)_5(\text{histadine-33})\text{Ru(III)}$ by $\text{Ru}(\text{bpy})_3^{2+}$ in the presence of EDTA generated the ($\text{PFe}^{\text{III}}\text{-Ru}^{\text{II}}$) complex. Subsequently, intramolecular electron transfer across a distance of approximately 11.8 \AA occurred with a rate constant of $30 \pm 3 \text{ s}^{-1}$. Further studies utilizing the cytochrome *c* protein in which the driving force of the reaction was enhanced by the substitution of the Fe(III) with Zn(II) were developed. Coupled with the variation of the Ru(III) complex position at the surface of the protein, temperature dependence studies of the electron transfer and electrochemical measurements were performed to assess the ΔH , ΔS and ΔG of the reaction, providing a determination of the electronic coupling (H_{ab}) and

reorganizational energy (λ) for the system. Large reorganizational energy and significant decay of the electronic coupling through the protein separating the electron donor and acceptor were revealed. The attenuation of the electronic coupling (H_{ab}) found from these measurements (2.0 \AA^{-1}) was attributable to poor donor-acceptor overlap through the medium of the protein environment. [7]

Prompted by these initial findings, the assessment of electron transfer rates through protein matrices of many small protein complexes, modified by attachment of various ruthenium complexes have been undertaken. Blue copper proteins, azurin, plastocyanin, and histidine derivatives of Fe-cyt c and myoglobin were developed [8]. The surprising finding of these protein mediated electron transfer reactions was the large reorganizational energies ($\sim 1.0 \text{ V}$) fairly independent of the protein environment and the donor-acceptor electronic coupling, found to be significantly variable, with the parameters not well accounted for by semi-classical electron transfer descriptions. In stark contrast to these findings, the observations of Dutton [9], surveying a wide range of electron transfer reactions in proteins having variable distances between donor and acceptor were found to follow a "universal" model for the electron donor-acceptor coupling (H_{ab}) and distance (d) separating the donor and acceptor. This one-dimensional square barrier (β_{IDSB}) model proposed that a general relationship exists for the exponential decay of the maximum electron transfer rate constant $k_{\text{max}} \text{ (s}^{-1}\text{)} = 10^{13} \exp^{-1.4(d-3.6)}$ versus $d \text{ (\AA)}$, where $\beta = 1.4 \text{ \AA}^{-1}$ satisfactorily explaining all of the distant dependent rate data. However, the works of Onuchic and Beratan have suggested an alternative tunneling pathway model for the decay of the electron transfer within the protein environment [10]. This model accounts for dominant pathways for electron

transfer contributions from bonding interactions existent within the protein environment. Covalent, hydrogen bonding interactions and through-space jumps, are separately assigned decay components, which additively provide contributions to the electron transfer pathway. This model effectively predicts exponential decay dependent on the tunnel length and composition rather than the direct distance between donor and acceptor. A recent analysis comparing both of these electronic coupling models (Dutton and Onuchic-Beratan) applied to electron transfer in 23 protein systems has shown a clear distinction between the photosynthetic reaction center proteins and other electron transfer proteins [11]. However, the method of the of the analysis used in this investigation generalizes the Onuchic-Beratan tunneling pathway model incorporating only through-space interactions including the protein as a continuous medium with characteristic electronic bandwidth.

[17].

Model systems

The observation of long range electron transfer in both the photosynthetic reaction center and other protein electron transfer systems have prompted model system studies aimed at assessing the controlling factors. Simulation of the protein environment with small molecule model systems possessing design features representative of the secondary, structure of proteins has been a recent focus in the work of Isied, Wishart, and Ogawa [12]. Recent examples from Ogawa [13] have incorporated the use of β -sheets and β -turns separating donor and acceptor complexes. Preliminary results from this group have substantiated Gray et al. [14] in the prediction of different electronic coupling decay constants for α -helices (1.26 \AA^{-1}) and β -strands (1.00 \AA^{-1}).

Previously, Meyer [15] has incorporated the design feature of peptide spacers in ruthenium based inorganic chromophore-quencher assemblies. These model system data are not treated by either of the distant dependent decay models, due primarily to the short range of the electron transfer, but rather are analyzed by conventional Marcus relationships.

Although no account has been made in these model systems as to the dipole moment associated with the amino acid residues oriented parallel to the α -helical axis, the incorporation of electrostatic potential effects generated from the dipole induced field on electron transfer in systems such as these is an issue of significant current interest [16]. Electrostatic field effects have been incorporated into both theoretical and experimental studies of the photosynthetic reaction center in relation to possible mechanistic implications governing the rapidity of electron transfer over long distances [17].

Many model system designs encompassing the orientation and distance relationships of chromophores in electron transfer patterned after the photosynthetic reaction center have been developed [18]. Figure (1a), shows the design of Osuka [19] incorporating three porphyrin macrocycles; two in a close conformation and the third appended with a pyromellitimide acceptor representative of the arrangement of the chromophores found in the bacterial reaction center. The distinct narrow anion radical spectra of the pyromellitimide quencher in these systems provides a great advantage in the observation of a charge separated state owing to the electron transfer reactions relative to other similar quinone based reaction center mimics. Gust and Moore (1b) have

Figure 1. Photosynthetic reaction center mimics, coupled porphyrin model systems design of (a) Osuka et al. and (b) a tetrad system of Gust and Moore.

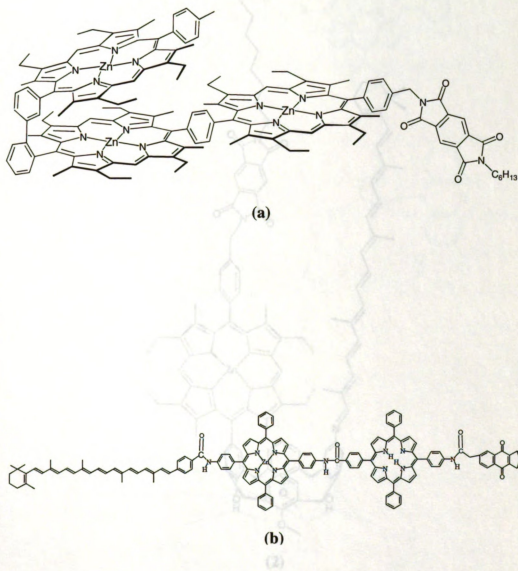


Figure 1. Photosynthetic reaction center mimics, coupled porphyrin model systems design of (a) Osuka et al. and (b) a tetrad system of Gust and Moore.

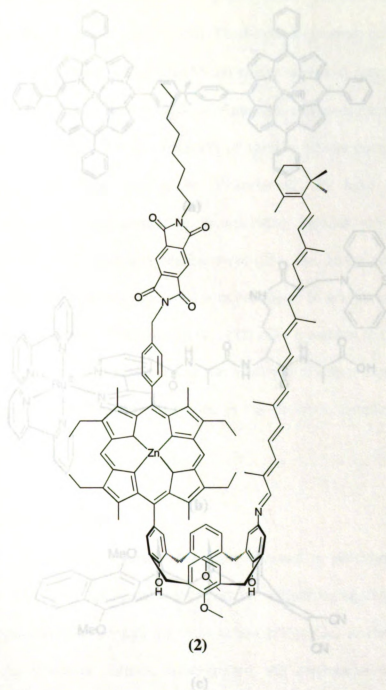
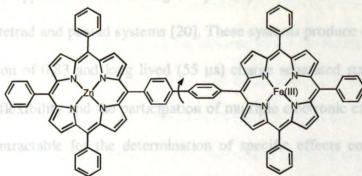


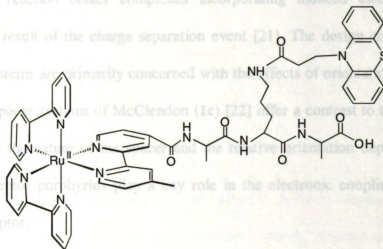
Figure 2. Model system for the assessment of electric field effects in photosynthetic reaction centers

taken a different approach to mimicking the photosynthetic reaction center with their design of triad, tetrad and pentad systems [20]. These systems produce quantum yields of ion-pair formation of 0.1-0.3 and lifetimes of 55 ns compared to the excited singlet states; however, the conformational flexibility and competition of multiple non-radiative decay pathways make these systems intractable for the determination of specific structural effects controlling electron transfer reactions. Yet other studies by Wasielewski (2) have shown model



(a)

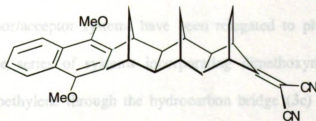
photosynthetic reaction center complexes incorporating induced electrostatic fields generated as a result of the charge separation event [21]. The design considerations of these model systems are primarily concerned with the effects of orientation and distance. The aromatic spacer systems of McClendon (1c) [22] offer a contrast to these studies by suggesting that the aromatic spacer may play a key role in the electronic coupling between the donor and acceptor.



(b)

Rigid donor-acceptor systems

Not all donor/acceptor systems have been relegated to photosynthetic reaction center models. The rigid donor-acceptor system of Meyer and Paddon-Row [23] have detailed the effects of distance, conformation, and conjugation within this one versatile system.



(c)

Perhaps the most important model system designed to address these issues are the

Figure 3. Electron transfer model systems (a) Biphenyl bridged model system of McClendon (b) Peptide linked chromophore-quencher system of Meyer and (c) rigid covalent norbornadiene system of Paddon-Row.

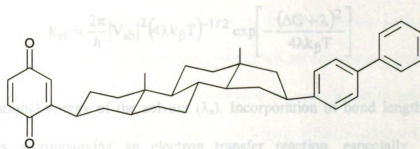
Miller [24]. The attachment of donor and acceptor groups at the 3 and 16 positions taken a different approach to mimicking the photosynthetic reaction center with their design of triad, tetrad and pentad systems [20]. These systems produce quantum yields of ion-pair formation of 0.83 and long lived (55 μ s) charge separated states; however, the conformational flexibility and the participation of multiple electronic excited states make these systems intractable for the determination of specific effects controlling electron transfer reactions. Yet other studies by Wasielewski (2) have shown model photosynthetic reaction center complexes incorporating induced electrostatic fields generated as a result of the charge separation event [21]. The design considerations of these model systems are primarily concerned with the effects of orientation and distance. The aromatic spacer systems of McClendon (1c) [22] offer a contrast to these studies by suggesting that the nature of the spacer and the relative orientation dependence of the donor and acceptor porphyrins play a key role in the electronic coupling between the donor and acceptor.

Rigid donor-acceptor systems

Not all donor/acceptor systems have been relegated to photosynthetic reaction center models. The series of systems incorporating dimethoxynaphthalene covalently attached to dicyanoethylene through the hydrocarbon bridge (3c) of Paddon-Row [23] have detailed the effects of distance, conformation, and conjugation within this one versatile system.

Perhaps the most important model system designed to address these issues are the rigid steroid spacer between donor and acceptor groups (4) investigated by Closs and

Miller [24]. The attachment of donor and acceptor groups at the 3 and 16 positions respectively of the 5- α -Androstane spacer allowed the creation of a fixed 10.3 Å distance separating the donor and acceptor. Tuning the free energy for the reaction over 2.5 V was accomplished through the introduction of a series of aromatic, and substituted quinone groups. The free energy dependence of the electron transfer rate results in the observation of a non-parabolic fall-off in the observed electron transfer for these systems providing



(4)

the first unambiguous verification of the Marcus inverted region predicted in Eqs. (1.1 - 1.2). Fitting of this data to Marcus theory however, required the incorporation of

$$k = A \exp \left[\frac{-\Delta G^*}{k_B T} \right] \quad (1.1)$$

$$\Delta G^* = \left[\frac{(\Delta G + \lambda)^2}{4\lambda} \right] \quad (1.2)$$

quantum mechanical considerations derived by Marcus [25], Levich and Dogonadze [26] based on the Fermi Golden Rule for the quantum mechanical probability for the transition of an electron between two states as given in Eq. 1.3. The assumption may be made from

$$k_{et} = \frac{2\pi}{\hbar} |V_{ab}|^2 FC \quad (1.3)$$

Eq.1.3 for non-adiabatic electron transfer that the Franck-Condon factor may be given in the form $FC = (4\lambda k_B T)^{-1/2} \exp(-(\Delta G + \lambda)^2 / 4\lambda k_B T)$, yielding the semi-classical expression for electron transfer as given in Eq. (1.4). In this form the electron transfer rate constant maintains a dependence upon the free energy for reaction (ΔG), the temperature (T), and

$$k_{et} = \frac{2\pi}{\hbar} |V_{ab}|^2 (4\lambda k_B T)^{-1/2} \exp \left[-\frac{(\Delta G + \lambda)^2}{4\lambda k_B T} \right] \quad (1.4)$$

the reorganizational energy of the solvent (λ_s). Incorporation of bond length and bond angle changes accompanying an electron transfer reaction, especially for highly exothermic reactions, may be represented by a single vibrational mode having energy $h\nu$ and additional reorganizational energy for this mode

$$k_{et} = \frac{2\pi}{\hbar} |V_{ab}|^2 \sum_{n=0}^{\infty} \left(e^{-S} \frac{S^n}{n!} \right) \exp \left[-\frac{(\Delta G + \lambda_s + n h\nu)^2}{4\lambda k_B T} \right] \quad (1.5)$$

$$S = \frac{\lambda_v}{h\nu} \quad (1.6)$$

λ_v ($S = \lambda_v/h\nu$). This expression originally derived by Closs and Miller [24] successfully accounts for the observation of the non-parabolic fall-off of the rate in the inverted region according to Eq. (1.5).

Despite advances made by the virtue of fixed distance electron transfer systems, non-covalent interactions and bond-making/bond-breaking reactions so important in yielding bonding energies (2-18 kcal/mol). This classification of hydrogen bonding,

many biological transformations have yet to be explored. The prevalence of these factors in biological systems provides new frontiers for electron transfer research.

Non-covalent interactions

The most common non-covalent interaction found in redox active systems is established by the hydrogen bond. The premier example of hydrogen bonding in biological systems is exemplified by the non-covalent, base-pair, self-association interactions found in the complementary strands of the DNA double helix. However, hydrogen-bonding interactions in biological systems are by no means restricted to this particular system. Hydrogen-bonding interactions have been implicated in mechanisms of catalytic enzyme reactions [27], the secondary and tertiary structure of proteins [28] and the stabilization of bound oxygen to hemoglobin and myoglobin [29]. Recent site directed mutagenesis studies have implicated hydrogen-bonding interactions in tuning the redox potentials of critical components of the photosynthetic reaction center [30].

Classifications of hydrogen-bonding interactions have been advanced based on the strength and internuclear separation of the interaction [31,32]. Measurements of hydrogen-bonding interactions typically involve NMR chemical shift of the hydrogen-bonded nucleus, and the determination of the internuclear distance between the heavy atoms by x-ray crystallography. Strong hydrogen-bonding interactions are exemplified by the interaction of F-H-F, having an interfluorine distance of 2.26 Å [32]. Typical energies for the hydrogen-bonding in these interactions may be > 24 kcal/mol. An intermediate range, of hydrogen-bonding interactions, is Low-Barrier-Hydrogen-Bonding, typically yielding bonding energies 12-18 kcal/mol. This classification of hydrogen bonding,

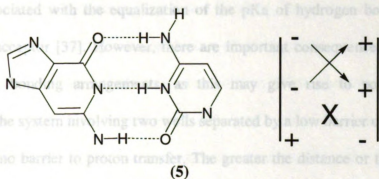
although established in solution, solid state and gas phase, remains a controversial issue [33] regarding the catalytic stabilization afforded by hydrogen-bonding interactions in enzymatic reactions. The final categorical class of hydrogen-bonding interactions are Traditional Hydrogen Bonds (THB), also called weak hydrogen-bonds, typically exhibiting bonding energies of < 12 kcal / mol. This thesis will focus on systems exhibiting the latter types of hydrogen bonds

Important aspects in the description of any hydrogen-bonding interaction are van der Waals, electrostatic and pKa effects [34]. Within symmetric or asymmetric hydrogen-bonding systems van der Waals interactions of the electron deficient proton with an neighboring electron rich anion influences a directional and close association of substituents. The association of two hydrogen bonding species in symmetric hydrogen bonding arrangements has been most commonly investigated. However, the investigation of non-symmetric hydrogen-bonding interactions via infrared measurements [35] has shown that the incorporation of asymmetry into the hydrogen-bonding interaction may substantially influence the thermodynamic association inherent to the system. Bolstered by the increased specificity of the directional interaction, pairing of the donor and acceptor are enhanced. Furthermore, addition of complimentary charges into an asymmetric hydrogen-bonding interaction may further augment the already enhanced association. Charges implemented within a hydrogen-bonding system yield complimentary electrostatic interactions, which may be described by a simple

$$E^H = \frac{q_1 q_2}{\epsilon r} \quad (1.8)$$

electrostatic model Eq. (1.8). In this expression, changes in the hydrogen-bond energy (E^H) are described by changes in Coulombic interactions between the partial effective

charges of the hydrogen bond donor and the hydrogen bond acceptor (q_1 and q_2). The presence of the distance (r) and the solvent dielectric (ϵ) modify the strength of the interaction between the charges as a function of distance and solvent dielectric. As shown in Eq (1.8) the strength of the hydrogen bonding is inversely proportional to the dielectric constant of the solvent and the distance between the charges. Additional electrostatic considerations enhancing the strength of the hydrogen bonding interactions have been shown by Jorgenson [36]. The Secondary Electrostatic Interaction (SEI) results in the development of enhanced Coloumbic attraction within hydrogen bonding interactions



exhibiting complimentary charges in a diagonal orientation in hydrogen-bonding substituents. For the case of guanine and cytosine (5) in the Watson-Crick hydrogen-bonding arrangement, there are both positive and negative secondary electrostatic interactions between the partial positive and negative charges of the nitrogen and oxygen atoms composing the hydrogen bond. Positive contributions to the hydrogen bond strength are found between the carbonyl oxygen and the imino nitrogen functionalities of the guanine with the cytosine amino and protonated imino functionalities represented schematically at the right of Figure (5). Furthermore, negative contributions to the hydrogen bond strength are found for the guanine amino and the cytosine protonated

imino functionalities. Description of hydrogen-bonding in terms of acid and base or ionizable residue concepts (pK_a), using the electrostatic argument shown in Eq. (1.8) predicts that the hydrogen bonding strength will increase linearly with increasing acidity (positive charge) of the hydrogen bonding donor or with increasing basicity of the hydrogen bonding acceptor (negative charge) reaching a maximum at $\Delta pK_a = 0$ [31].

Description of the hydrogen bonding interactions based on the pK_a of the participating substituents is a thermodynamic argument and a first approximation for a proton transfer process. While there is an expected definite relationship between the hydrogen bonding strength and the pK_a it has been shown in model compounds that there is no special stabilization associated with the equalization of the pK_a of hydrogen bond donor and hydrogen bond acceptor [37]. However, there are important consequences of short and strong hydrogen bonding arrangements, as this may give rise to potential energy descriptions for the system involving two wells separated by a low barrier or possibly to a single well with no barrier to proton transfer. The greater the distance or the weaker the interaction, the greater will be the barrier to, and the less likely will be, proton transfer. The derivation and interpretation of potential energy surfaces describing the internuclear proton lability or transfer between the two heavy atoms is difficult to describe solely from these primarily thermodynamic observations [38]. Theoretical approaches and implications of the nature and type of hydrogen-bonding interaction are diverse and both classical and quantum mechanical descriptions may be necessary to fully describe proton transfer reactions occurring in solution. [39]

Perhaps nowhere does the relevance of proton transfer have such a prominent role as in biological systems. The coupling of proton transfer to charge separation is a

Proton Transfer

The transfer of a proton between two chemical sites is the most fundamental of chemical reactions and may occur as a result of either thermal or electronic excitation. Photoinduced proton transfer reactions have been studied in a variety of intermolecular and intramolecular hydrogen bonding chemical systems for many years. Accompanying photoexcitation of an intramolecularly hydrogen bonded complex, a fast reorganization of molecular structure generally occurs resulting from the shift or transfer of the proton within the hydrogen bonded complex. Frequently, a signature of the photoinduced proton transfer within a hydrogen bonded complex is the observation of dramatically (4000 - 10000 cm^{-1}) Stokes-shifted emission resulting from the electronic and/or conformational change occurring in the production of the proton transfer tautomer [40].

Upon photoexcitation, the electronic composition of the chromophore is altered such that barring steric or strain considerations, the proton transfer reaction will proceed with a driving force for protonation/deprotonation determined by the change in the acidity or basicity of the chromophore. Complete proton transfer within hydrogen-bonded complexes results when a large change in the acidity or basicity of chromophore occurs in the excited state. The observation of an incomplete transfer or proton shift within the hydrogen-bonded complex may result in complexes in which there is a relatively small change in the excited state pKa of the chromophore relative to the ground state.

Proton transfer in biological systems

Perhaps nowhere does the relevance of proton transfer have such a prominent role as in biological systems. The coupling of proton transfer to charge separation is a

fundamental component of biological energy conversion mechanisms. These coupled events continue to emerge as fundamental components of structure/function relationships in a variety of proteins and enzymes including nitrogenase [41], non-heme iron containing proteins [42,43], multicopper oxidases [44] and reductases [45]. However, the significance of the effect of the coupling of proton motion to electron transfer is best demonstrated in the active site of cytochrome *c* oxidase. Despite similar separation of the two heme sites from the binuclear Cu_A center, electron transfer to heme *a* is 10^2 – 10^4 faster than to heme a_3 [46]. Proton transfer accompanying heme reduction is believed to be the origin of the slow electron transfer to heme a_3 and accordingly the controlling factor for directional electron transport via heme *a* [47]. In photosynthesis and respiration the photoinduced redox processes creates a proton potential across the mitochondrial membrane which is utilized for the production of ATP. Yet the inherent complexity of these systems does not allow the direct observation of the electron/proton transfer steps. Incorporating the design feature of non-covalent interactions specifically those containing hydrogen-bonding interactions between the electron transfer donor and acceptor may provide the means of differentiating these inherently coupled processes

Intramolecular electron transfer in each of these systems was conducted using time-

Non-covalent systems in electron transfer

The incorporation of hydrogen-bonding interactions in electron transfer systems are relatively few. Mataga, [48] has shown the effects of hydrogen-bonding interactions for a variety of organic based electron transfer systems incorporating single point acid/base complementary interactions of amino and alcohol functionalized compounds. Additionally, complementary hydrogen-bonding interactions utilizing DNA base-pair

recognition (guanine-cytosine) for the binding of electron transfer donor and acceptor moieties held at a fixed orientation and distance have been shown in the work of Sessler [49]. The electron transfer ensembles of Sessler (**4a**, **4b**) represent some of the first preparations of non-covalent electron transfer model systems. A primary issue in the use of non-covalent electron transfer systems is the strength of the interaction, and therefore the association constant maintaining the two interacting components in contact in solution. In (**4a**) the characterized by a heteroassociation constant of $3100 \pm 470 \text{ M}^{-1}$ in CD_2Cl_2 . Despite the association of the complimentary cytosine and guanine components of the electron transfer complex are significant association of the two components in low dielectric solvent, the orientation is such that the electronically excited zinc metalloporphyrin donor and 2-cytidiny benzoquinone acceptor are capable of through space interactions. Thus the conformational flexibility in this complex may lead to net electron transfer quenching by collisional interaction in addition to that through the hydrogen-bonding interface. To alleviate these concerns, further synthetic modifications of this system have led to the development of (**4b**). The association constant in this system is significantly greater ($8900 \pm 600 \text{ M}^{-1}$) than that of (**4a**). Determination of intramolecular electron transfer in each of these systems was conducted using time-resolved fluorescence measurements yielding unimolecular electron transfer rates of $4.2 \pm 0.7 \times 10^8 \text{ s}^{-1}$ and $8 \times 10^8 \text{ s}^{-1}$ for (**4a**) and (**4b**) respectively. While charge-separated intermediates have not been observed, these fluorescence data are consistent with electron transfer occurring through hydrogen-bonding interfaces. Control experiments are also consistent with electron transfer. Addition of ethanol to the solutions results in loss

Figure 4. Non-covalent electron transfer systems incorporating guanine-cytosine base-pair recognition for donor-acceptor separation. Conformationally flexible system (a), conformationally rigid system (b) two point (c) and four point (d) hydrogen bonding of quinones by functionalized porphyrins.

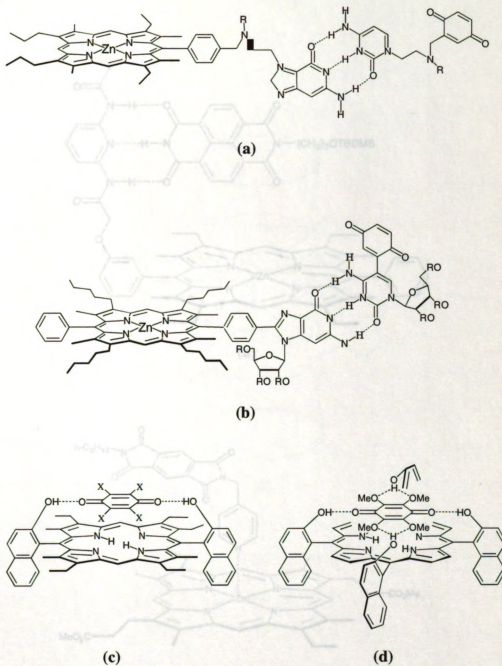
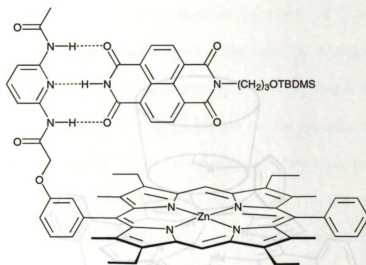
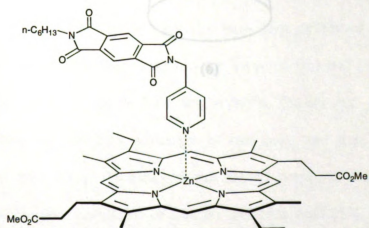


Figure 4. Non-covalent electron transfer systems implementing guanine-cytosine base-pair recognition for donor-acceptor separation. Conformationally flexible system (a). Conformationally rigid system (b) two point (c) and four point (d) hydrogen bonding of quinones by functionalized porphyrins.



(a)



(b)

Figure 5. Non-covalent systems based on asymmetric hydrogen-bonding (a) and by metal ligation (b)

of the biphasic decay corresponding to emission from the formation of bound and unbound donor in the return of the monoexponential decay of the uncomplexed zinc metalloporphyrin lifetime 1.4 ns ($7.1 \times 10^8 \text{ s}^{-1}$).

A beautiful set of experiments investigating the effects of hydrogen bonding in electron transfer systems has recently been undertaken by Mataga [50]. Efficient quenching of the porphyrin singlet excited state by 1,4,5-naphthalene-tetracarboxamide in benzene solution is observed. Quenched emission from the complex was not resolved despite an instrument response of 3-5 ns. The quenching was attributed to emission due to unbound donor. Static quenching of the complex, however, was observed. Efficient quenching, when coupled with the appearance of a new emission band associated with the formation of a charge transfer complex, suggests that electron transfer quenching is established as occurring at rates between 3-5 ns ($3.3 \times 10^{11} \text{ s}^{-1}$). An experimental advantage of this complex is the appreciable association ($1.6 \pm 10^4 \text{ M}^{-1}$ in CDCl_3 and $(1.3 \pm 10^3 \text{ M}^{-1})$ in C_6D_6). Further systems that have been developed for non-covalent hydrogen-bonding electron transfer reactions (6) those of (4c) and (4d) developed by Aoyama, Ogoshi [51], and co-workers and Hayashi, Ogoshi and co-workers [52], respectively. These systems take advantage of two point and four point hydrogen-bonding interactions between the para quinone and the porphyrin complex in systems reflective of the covalent complexes of Lindsey and Mauerzall [53]. Interestingly, for these complexes quenching of the fluorescence of the porphyrin is found to depend upon the binding of the quinone and not on the redox properties, suggesting that the close spatial relationship gives rise to large electronic coupling dominating the Franck-Condon

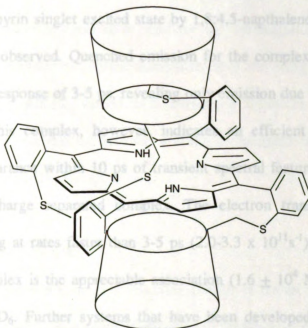


Figure 6. Non-covalent cyclodextrin porphyrin assembly for the investigation of electron transfer to quinone.

of the biphasic decay corresponding to emission from the formation of bound and unbound donor in the return of the monoexponential decay of the uncomplexed zinc metalloporphyrin lifetime 1.4 ns ($7.1 \times 10^8 \text{ s}^{-1}$).

A beautiful set of experiments investigating the effects of hydrogen bonding in electron transfer systems has recently been undertaken by Mataga [50]. Efficient quenching of the porphyrin singlet excited state by 1,8:4,5-naphthalene-tetracarboxamide in benzene solution is observed. Quenched emission for the complex was not resolved despite an instrument response of 3-5 ps, revealing only emission due to unbound donor. Static quenching of this complex, however, indicates an efficient quenching, when coupled with the appearance within 10 ps of transient spectral features associated with the formation of a charge separated complex. The electron transfer quenching is established as occurring at rates faster than 3-5 ps ($2.0\text{-}3.3 \times 10^{11} \text{ s}^{-1}$). An experimental advantage of this complex is the appreciable association ($1.6 \pm 10^4 \text{ M}^{-1}$) in CDCl_3 and ($1.3 \pm 10^5 \text{ M}^{-1}$) in C_6D_6 . Further systems that have been developed for non-covalent hydrogen-bonding electron transfer reactions are those of (4c) and (4d) developed by Aoyama, Ogoshi [51], and co-workers and Hayashi, Ogoshi and co-workers [52], respectively. These systems take advantage of two point and four point hydrogen-bonding interactions between the para quinone and the porphyrin complex in systems reflective of the covalent complexes of Lindsey and Mauerzall [53]. Interestingly, for these complexes quenching of the fluorescence of the porphyrin is found to depend upon the binding of the quinone and not on the redox properties, suggesting that the close spatial relationship gives rise to large electronic coupling dominating the Franck-Condon factor.

The use of non-covalent interactions between electron transfer donor and acceptor based on metal complex ligation by pyridyl containing acceptors have been performed by Sanders and co-workers [54] (**5a**). In this system a dramatic example of the effects of the solvent reorganizational energy are evidenced by comparison of complex (**5a**) to the additionally synthesized meso tetra-phenyl porphyrin analog. The intramolecular electron transfer rates observed in these two complexes are found to be $213 \times 10^8 \text{ s}^{-1}$ and $53.3 \times 10^8 \text{ s}^{-1}$ respectively. Further systems developed for the investigation of non-covalent interactions in electron transfer have been demonstrated in the design of (**6**) [55] two-cyclodextrin molecules covalently linked to a central porphyrin. In these systems the inclusion of a quinone or substituted quinone into the cyclodextrin cavity provides the acceptor for the electron transfer reaction.

Similar electron transfer rates for the aminopyrene-pyridine-*x* (where *x* = H, 2-methyl and 4-methyl) are found to be $\sim 1.0 \times 10^{10} \text{ s}^{-1}$. The

Proton Coupled-Electron Transfer

The coupling of proton transfer to electron transfer in model systems have been addressed with Oxo bridged di-Manganese OEC model complexes. These model systems have shown proton and electron transfer events to be coupled processes [56]. An earlier example showing the coupling of proton and electron transfer events involved the use of ruthenium oxo derivatives, [57]. While each of these systems incorporate the proton and electron transfer events the ultimate mechanism of the coupling of the proton to the electron transfer event is not resolved.

The work of Mataga employing electron transfer within single point hydrogen-bonding of 13 and 7H dibenzocarbazole and 1-aminopyrene with pyridine have shown the coupling of proton shift within the hydrogen-bonded pair to facilitate fast electron

transfer reactions [58]. The basic tenets for coupling of proton transfer to electron transfer were given in these studies, where it was assumed that the ionization potential of the donor would be reduced, and the electron affinity of the acceptor would be enhanced due to the presence of the hydrogen-bonding interaction. Furthermore, the hydrogen-bonding in the excited state was expected to give rise to greater delocalization of charge causing the proton to shift toward the acceptor further lowering the ionization potential of the donor and increasing the electron affinity of the acceptor. These factors were expected to facilitate a rapid electron transfer between donor and acceptor in contrast to expectation, based upon the assumption that the electronic coupling through a hydrogen-bonding interface would be reduced relative to a system composed of a direct attachment of the donor and acceptor. Observed intramolecular electron transfer rates for the aminopyrene-pyridine-*x* (where *x* = H, 2-methyl and 4-methyl) are found to be $\sim 1.0 \times 10^{10} \text{ s}^{-1}$. The basic shortcoming of this system is the single-point hydrogen bonding yielding meager ($< 10 \text{ M}^{-1}$) association constants even in non-polar hexane. [63]. In this system results of

kinetic To circumvent this issue, complementary hydrogen-bonding interactions of dicarboxylic acids in aprotic low dielectric solvents may be implemented giving rise to a more strongly associated hydrogen-bonding proton transfer interface. Wenograd [59] and Pitzer [60]. First described this interface in solvents with low dielectric constant. Many examples of the use of this interface in proton and electron transfer [61] systems have appeared since making this interface an exceptional experimental model. (a) where only a

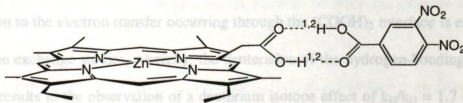
methyl Previous studies in the Nocera group [62] have elaborated the details of the symmetric dicarboxylic acid $(\text{COOH})_2$ interfaces (**7a**, **7b**) as a spacer between the electron transfer donor and acceptor. Electronic excitation of the zinc metalloporphyrin to

the singlet excited state when associated through the $(\text{COOH})_2$ interface to the electron transfer acceptor 3,4-dinitrobenzoic acid leads to the observation of fast intramolecular electron transfer ($k_{\text{es}} = 1 \times 10^{10} \text{ s}^{-1}$ and $k_{\text{et}} = 5 \times 10^{10} \text{ s}^{-1}$). Definitive evidence supporting the determination of electron transfer through the $(\text{COOH})_2$ interface is corroborated by addition of ethyl-3,4-dinitrobenzoate. In the presence of this non hydrogen-bonding complex only the electronically excited zinc metalloporphyrin complex is observed and there is no evidence of quenching. Furthermore, conclusive evidence of the coupling of the proton to the electron transfer occurring through the $(\text{COOH})_2$ interface is established in isotope exchange studies, whereby, the deuteration of the hydrogen-bonding interface protons results in the observation of a deuterium isotope effect of $k_{\text{H}}/k_{\text{D}} = 1.7$ on charge separation and $k_{\text{H}}/k_{\text{D}} = 1.8$ on the charge recombination reaction.

Further studies of the effect of symmetric dicarboxylic acid $(\text{COOH})_2$ interfaces were found in system **(7b)** where the symmetric $(\text{COOH})_2$ interface is isolated from the redox centers by the incorporation of a phenyl spacer [63]. In this system results of kinetic data in the observation of quenching of zinc metalloporphyrin emission as a function of added complimentary benzoic acid functionalized iron metalloporphyrin. It is proposed in this system that the incorporation of the phenyl spacer results in decreased effective electronic coupling between the redox centers, and furthermore proton transfer within the interface is decoupled from the electron transfer yielding an observed electron transfer rate of $7.6 \times 10^8 \text{ s}^{-1}$, significantly attenuated with respect to **(7a)** where only a methylene group is present between the porphyrin and the dicarboxylic acid interface. The electron transfer quenching results of **(7b)** are obscured by an energy transfer component.

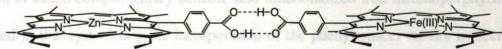
Zn(II)-porphyrin-3,4-dicarboxylic acid donor-acceptor symmetric interface system: (a) Zn(II)-Pc(III) diporphyrin symmetric interface system with phenyl spacer (b).

determination of electron transfer through the $(\text{COOH})_2$ interface is corroborated by addition of ethyl-3,4-dinitrobenzoate. In the presence of this non hydrogen-bonding complex only the electronically excited zinc metalloporphyrin complex is observed and there is no evidence of quenching. Furthermore, conclusive evidence of the coupling of the proton to the electron transfer occurring through $(\text{COOH})_2$ is established in isotope exchange experiments. A hydrogen bonding interface between the two porphyrins results in observation of a deuterium isotope effect of $k_H/k_D = 1.7$ on charge separation and $k_H/k_D = 1.8$ on the charge recombination reaction.



(a)

Further studies of the effect of symmetric dicarboxylic acid $(\text{COOH})_2$ interfaces were found in system (7b) where the symmetric $(\text{COOH})_2$ interface is isolated from the redox centers by the incorporation of a phenyl spacer [64]. In this system results of kinetic data in the observation of quenching of zinc metalloporphyrin emission as a function of added complementary benzoic acid functionalized iron metalloporphyrin. It is proposed that the phenyl spacer isolates the porphyrin redox centers from the hydrogen bonding interface. This results in an increased effective electronic coupling between the redox centers, and furthermore proton transfer within the interface is decoupled from the electron transfer yielding an observed electron transfer rate of $7.6 \times 10^8 \text{ s}^{-1}$, significantly attenuated with respect to (7a) where only a methylene group is present between the porphyrin and the dicarboxylic acid interface. The electron transfer quenching results of (7b) are obscured by an energy transfer component.



(b)

Incorporation of the non-covalent dicarboxylic acid interface in electron transfer systems presents a unique problem in electron transfer research. The interface resulting from the incorporation of the non-covalent dicarboxylic acid interface in electron transfer systems presents a unique problem in electron transfer research. The interface resulting from the incorporation of the non-covalent dicarboxylic acid interface in electron transfer systems presents a unique problem in electron transfer research. The interface resulting from the incorporation of the non-covalent dicarboxylic acid interface in electron transfer systems presents a unique problem in electron transfer research.

Figure 7 Zn(II)-porphyrin-3,4-dicarboxylic acid donor-acceptor symmetric interface system. (a) Zn(II)-Fe(III) diporphyrin symmetric interface system with phenyl spacer (b).

displacement from one side of the interface is compensated by the displacement of a determination of electron transfer through the $(\text{COOH})_2$ interface is corroborated by proton on the opposite side. As a result, protons are not pumped by an electron transfer addition of ethyl-3,4-dinitrobenzoate. In the presence of this non hydrogen-bonding event and proton motion does not lead to a net charge build-up within the interface. complex only the electronically excited zinc metalloporphyrin complex is observed and Subsequently, proton motion may influence an observed electron transfer rate through there is no evidence of quenching. Furthermore, conclusive evidence of the coupling of modification of the electron coupling matrix element between the electron donor and the proton to the electron transfer occurring through the $(\text{COOH})_2$ interface is established acceptor states.

in isotope exchange studies, whereby, the deuteration of the hydrogen-bonding interface protons results in the observation of a deuterium isotope effect of $k_{\text{H}}/k_{\text{D}} = 1.7$ on charge separation and $k_{\text{H}}/k_{\text{D}} = 1.8$ on the charge recombination reaction.

Further studies of the effect of symmetric dicarboxylic acid $(\text{COOH})_2$ interfaces were found in system **(7b)** where the symmetric $(\text{COOH})_2$ interface is isolated from the redox centers by the incorporation of a phenyl spacer [64]. In this system results of kinetic data in the observation of quenching of zinc metalloporphyrin emission as a function of added complimentary benzoic acid functionalized iron metalloporphyrin. It is proposed in this system that the incorporation of the phenyl spacer results in decreased effective electronic coupling between the redox centers, and furthermore proton transfer within the interface is decoupled from the electron transfer yielding an observed electron transfer rate of $7.6 \times 10^8 \text{ s}^{-1}$, significantly attenuated with respect to **(7a)** where only a methylene group is present between the porphyrin and the dicarboxylic acid interface. The electron transfer quenching results of **(7b)** are obscured by an energy transfer component.

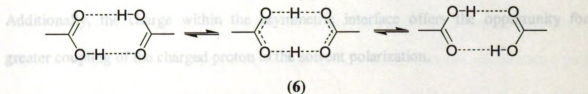
Incorporation of the non-covalent dicarboxylic acid interface in electron transfer transfer of the electron, upon the configuration of the interface presents [66]. The systems presents a unique problem in electron transfer research. The interface resulting electronic coupling is found to reach a maximum at a conformation in which the proton from this dicarboxylic acid $(\text{COOH})_2$ configuration is symmetric, and proton

displacement from one side of the interface is compensated by the displacement of a proton on the opposite side. As a result, protons are not pumped by an electron transfer event and proton motion does not lead to a net charge build-up within the interface. Subsequently, proton motion may influence an observed electron transfer rate through modification of the electron coupling matrix element between the electron donor and acceptor states.

Recently the incorporation of the dicarboxylic acid interface organizing electron transfer donor and acceptor complexes composed of benzoic acid functionalized trimethoxy phenyl (Zn^{II} and Fe^{III}) porphyrin complexes have appeared [65]. The results analyzed by the additive contribution of specific types of bonding interactions of the tunneling pathway. However, these analyses of the results are partially misinformative as it is merely assumes that the primary contribution to the electron transfer rate in each system is the coupling of the donor and acceptor over the nearly constant distance separating the donor and acceptor in each system. This particular study serves to further validate the use of non-covalent hydrogen-bonding interfaces as viable spacer systems for the observation of electron transfer reactions.

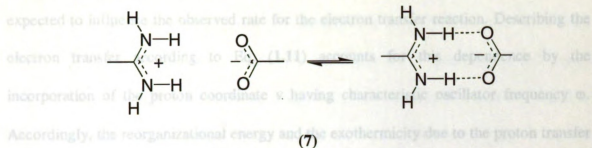
The two carboxylic acid functionalized systems (**7a**) and (**7b**) provide the benchmark for the investigation of a photoinduced proton transfer within a fixed distance electron transfer system. The theoretical assessment of the results of system (**7a**) show that the effect of the proton modulation of the observed electron transfer rate stems from the dependence of the electronic coupling matrix element (V_{ab}), responsible for the transfer of the electron, upon the configuration of the interface protons [66]. The electronic coupling is found to reach a maximum at a configuration in which the protons

are located equidistant within the interface. This configuration represents a maximum for the charge delocalization, facilitating the observation of fast electron transfer. Because the symmetric interface does not involve a net charge rearrangement upon proton transfer only a weak coupling of the protons with the solvent is expected.

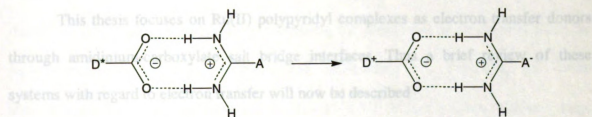
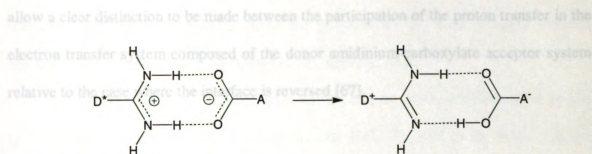


The use of the symmetric dicarboxylic acid interface has presented the initial framework for the determination of the involvement of the proton in the modulation of an observed electron transfer rate. However, the use of the symmetric dicarboxylic acid interface has several experimental limitations. The association of the carboxylic acids presents a small association (500 M^{-1}) constant even in solvents of low dielectric constant, and furthermore the homo-association of donor and acceptor complexes reduces the solution concentration of the desired electron transfer assembly. To alleviate these concerns and to potentially reveal more information concerning the modulation of the electron transfer rate by the proton interface, the incorporation of an asymmetric salt-bridging interface has been included in the PCET system design. This hydrogen-bonding arrangement presents several advantages over the symmetric analog. The directional and specific interaction of donor and acceptor by charge complementarity affords a strong interaction of donor and acceptor in solution and furthermore eliminates the potential formation of the homoassociated species. The most important aspect of the charged

asymmetric salt-bridge interface is the significantly enhanced association constant.



Additionally, the charge within the asymmetric interface offers the opportunity for greater coupling of the charged proton to the solvent polarization.



Synthetic modifications of tris-bipyridyl ruthenium complexes synthesized to

(8)

obtain information concerning the nature and the systematic details of electron transfer are numerous [68]. All systems take advantage of the well-documented photophysical properties of this class of compounds. Particularly advantageous aspects of these

molecules $k_{et} = \frac{2\pi}{h} |V|^2 (E_s k_B T)^{-1/2} \sum_{v=0} \left| \langle O_i | v f \rangle \right|^2 \exp \left[-\frac{(E_s + \Delta G + h\omega v)^2}{4E_s k_B T} \right]$ (1.11)

means by which these may be manipulated and controlled in an orderly manner to create tailor-made electron transfer components $\left| \langle O_i | v f \rangle \right|^2 = \left(e^{-S} \frac{S^p}{p!} \right)$ (1.12)

In either representation of the interface, shown in (8) the displacement of the proton is expected to influence the observed rate for the electron transfer reaction. Describing the electron transfer according to Eq. (1.11) accounts for this dependence by the incorporation of the proton coordinate v having characteristic oscillator frequency ω . Accordingly, the reorganizational energy and the exothermicity due to the proton transfer shown in Eq. (1.12) are given as the summation over the proton vibrational frequencies in Eq. (1.11). This additional contribution, Franck-Condon factors for the proton states, may allow a clear distinction to be made between the participation of the proton transfer in the electron transfer system composed of the donor amidinium-carboxylate acceptor system relative to the case where the interface is reversed [67].

Incorporation of Ruthenium Systems into the study of PCET

This thesis focuses on Ru(II) polypyridyl complexes as electron transfer donors through amidinium-carboxylate salt bridge interfaces. Thus a brief review of these systems with regard to electron transfer will now be described

Synthetic modifications of tris-bipyridyl ruthenium complexes synthesized to range in the molar absorptivity values arises largely from the introduction of asymmetry obtain information concerning the nature and the systematic details of electron transfer in the complexes via the incorporation of ligands having different electronic (σ donating and π bonding) composition. Reduction of the symmetry of the complex due to the ligand properties of this class of compounds. Particularly advantageous aspects of these environment may be achieved in the ground state through the synthetic manipulation of molecules are the well-characterized radiative and non-radiative decay properties and the ligand set surrounding the central metal. Upon charge transfer excitation, promotion means by which these may be manipulated and controlled in an orderly manner to create of an electron to the ligand based π^* orbital results in an inequivalence of one of the three tailor-made electron transfer complexes.

Absorption Spectroscopy of Ruthenium Bipyridyl Complexes

The ground and excited states of ruthenium tris-bipyridyl molecules have been well characterized over the past 30 years by a vast assortment of spectroscopic techniques [69]. Features present in the electronic absorption spectra consist of transitions found in ultra-violet region, characterized by intraligand π - π^* absorption in the 270 – 300 nm region. Typically the transitions have molar absorptivities $\epsilon \sim 4 - 10 \times 10^4 \text{ M}^{-1} \text{ cm}^{-1}$ and reflect the absorption cross sections observed for the free bipyridyl ligands. The π - π^* transitions gradually red shifting upon the introduction of more strongly electron withdrawing substituents at the periphery of the bipyridyl rings.

The spectral features of $\text{Ru}(\text{bpy})_3^{2+}$ complexes, however, are dominated by the split non-gaussian, metal-to-ligand charge transfer (MLCT) band in the 400 - 500 nm region. General consensus is that the bands originate from $^1\text{E}(\pi^*) \leftarrow 3 \text{ } ^1\text{A}_1(\text{d}\pi)$ transitions (D_3 point group symmetry), involving the promotion of an electron from the metal-centered $\text{d}\pi$ manifold to the ligand antibonding π^* . Typically, the molar absorptivities for these transitions are ($\epsilon \sim 6 - 15 \times 10^3 \text{ M}^{-1} \text{ cm}^{-1}$). This relatively large range in the molar absorptivity values arises largely from the introduction of asymmetry in the complexes via the incorporation of ligands having different electronic (σ donating and π bonding) composition. Reduction of the symmetry of the complex due to the ligand environment may be achieved in the ground state through the synthetic manipulation of the ligand set surrounding the central metal. Upon charge transfer excitation, promotion of an electron to the ligand based π^* orbital results in an inequivalence of one of the three ligands, effectively increasing the transition dipole and hence the molar absorptivity.

In a systematic study of the absorption of $\text{Ru}(\text{bpy})_3^{2+}$ complexes in 19 solvents spanning a range from nitromethane to water, slight shifts (the largest observed difference was found to be 310 cm^{-1}) of the absorption maxima in the $d\pi-\pi^*$ (MLCT) transition region have been observed. This solvent dependant shifting of the MLCT band has been given as evidence of the localization of the excited state electron at one bipyridyl ligand upon photoexcitation [70]. The consequence of solvent changes of the localization due to lower dielectric constant creating a configuration in which strong coupling of the hole at the metal and the electron at the ligand would be preferred for solvents having a higher dielectric constant, the opposite would be expected for a low dielectric thus a dependence upon the solvent is expected. The basis for these conclusions is drawn from the derivation of an expression for the change in the total polar spectral transition energy (ΔE_T) associated with a particular transition. However, caution has been advised in the over interpretation of this solvent dependant absorption data due primarily to the small observed shift found when a comparison is made to the solvent dependent shifts observed in charge transfer absorption spectra for organic complexes [71].

Luminescence Spectroscopy of Ruthenium Bipyridyl Complexes

Paris and Brandt first reported the luminescence of $\text{Ru}(\text{bpy})_3^{2+}$ in 1959 [72]. The observed luminescence was attributed to the π^*-d charge transfer. Initially, skepticism of this assignment arose from Porter [73] and from Crosby [74] who attributed this luminescence as d^*-d emission or as d^*-d phosphorescence influenced by spin-orbit

coupling considerations. However, the original contention of the π^* -d assignment prevailed, after considerable investigation during the 1960's [75].

More detailed studies have since shown that photoexcitation of the MLCT of $\text{Ru}(\text{bpy})_3^{2+}$ complexes results in the initial population of a singlet $^1\text{MLCT}$ excited state. Due to strong spin-orbital effects intersystem crossing occurs from this state with unity efficiency producing the emissive $^3\text{MLCT}$ excited state of the complex. Recent studies have shown that the appearance of the triplet excited state of the $\text{Ru}(\text{bpy})_3^{2+}$ occurs with a time constant of approximately 500fs [76]. The emissive $^3\text{MLCT}$ is known to contain a manifold of three closely lying (100 cm^{-1}) states. Deactivation of the excited state occurs by three major pathways: radiative decay, non-radiative decay to the ground state of the complex and thermally activated cross over to metal centered d-d excited states. The energy gap between the emissive the $^3\text{MLCT}$ and the non-emissive MC states may be determined by temperature dependence studies but is dependent upon the ligand composition surrounding the metal center. For $\text{Ru}(\text{bpy})_3^{2+}$ the metal centered states are located approximately 3600 cm^{-1} above the $^3\text{MLCT}$. Population of the MC states gives rise to extremely fast radiationless decay including decomposition of the complex by ligand substitution processes, While luminescence from the $^3\text{MLCT}$ of *tris*-bipyridyl complexes of ruthenium are found to be significantly red shifted approximately 6000 cm^{-1} from the absorption of the MLCT transition maxima.

The bandshape of luminescence spectra are generally nondescript at room temperature consisting of broad, fairly gaussian-shaped bands. Upon cooling, vibrational structure begins to appear, the spacing of which reflects dominant (medium frequency) vibrational modes of the bipyridyl ligands and to a lesser extent metal-nitrogen bond

vibrations. The quantum yield of emission of $\text{Ru}(\text{bpy})_3^{2+}$ complexes are typically found to be approximately 10% ($\phi_{\text{em}} \leq 0.10$) [68] upon excitation into the MLCT transition and has been found to be significantly independent of excitation wavelength.

$$I_e \approx \phi_{\text{em}} = \frac{k_r}{k_r + k_{\text{nr}}} = k_r \tau_0 \quad (1.7)$$

Large variations in the band position and quantum yield of the emission occur with ligand substitution where increasing delocalization of excited state electron density and electron withdrawing substituents causes the emission to progress to lower energy and decreased quantum yield. These effects are adequately understood through the application of energy gap law considerations as applied to ruthenium, and osmium complexes by Meyer [77].

Ligand variation and substitution of electron withdrawing and donating substituents may affect the decay of the $^3\text{MLCT}$ state of $\text{Ru}(\text{bpy})_3^{2+}$ complexes. Generally, it is found that a decrease in the energy gap between the ground and excited states decreases the radiative rate, consistent with the Energy Gap Law. Two mechanisms by which the excited state decay may be influenced by the energy gap of the complex are evident. The overlap of the initial and final states of the acceptor modes resulting from a change in the equilibrium displacement (ΔQ_e) or frequency ($\nu = \omega/2\pi$) between initial and final electronic states promotes deactivation of the complex by non-radiative decay. Additionally, the difference of the excited state energy relative to the ground state may increase or decrease k_{nr} through the efficiency of overlap of vibrational wavefunctions. Thus an increase in the vibrational overlap between ground and excited states through a

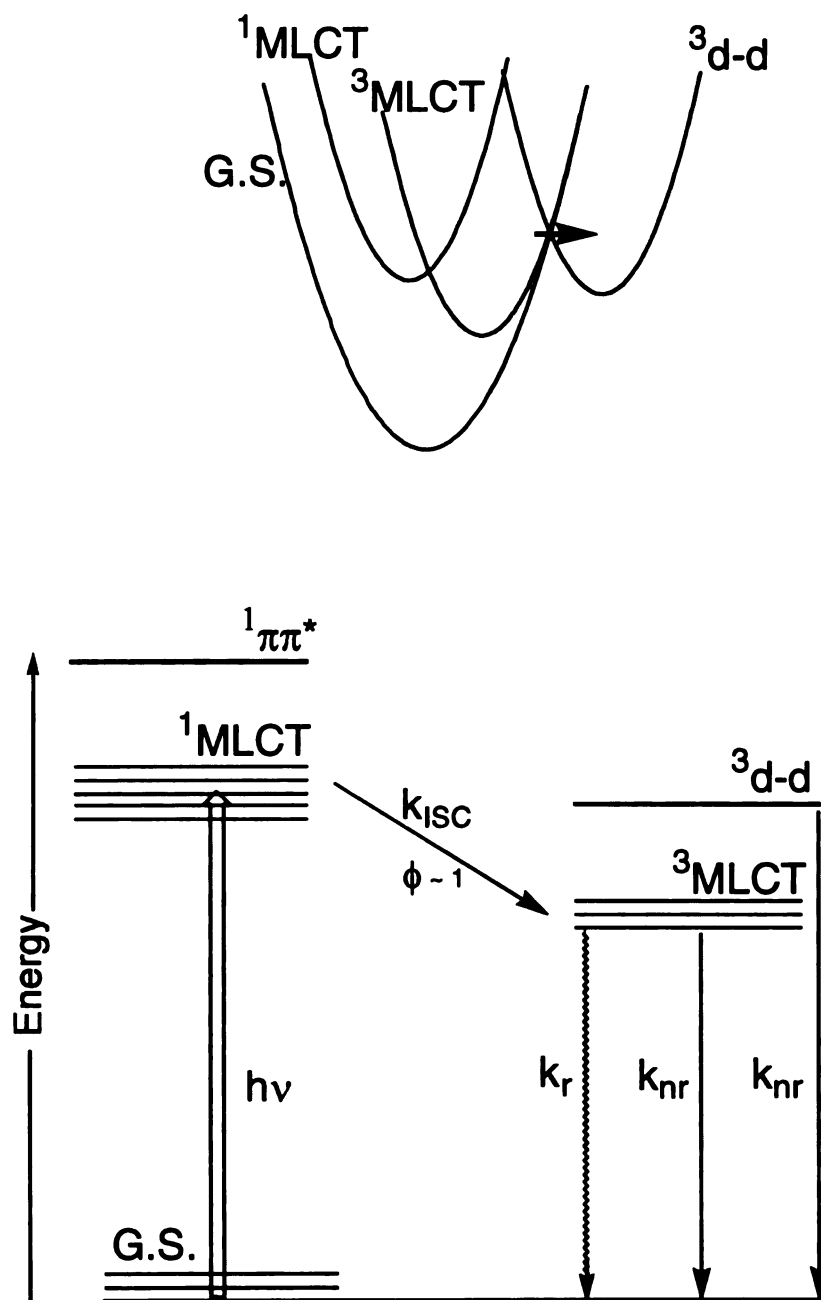


Figure 8. Photophysical scheme for *tris*-bipyridyl ruthenium(II) complexes. $^1\text{MLCT}$, $^3\text{MLCT}$, $^1\pi\pi^*$, and $^3\text{d-d}$ refer to the singlet and triplet charge transfer, the singlet intraligand and the triplet metal centered states respectively. k_r and k_{nr} represent decay processes.

change in the equilibrium displacement (ΔQ_e) or by a decrease in the energy gap (ΔE) results in the effective increase in the non-radiative decay k_{nr} of the complex.

As with the absorption profile the position of the emission band observed is largely dependent upon the nature of the ligand electronic composition and the nature of the solvent environment. With the introduction of electronically withdrawing or donating ligands emission maxima is observed to red or blue shift accordingly. The sensitivity of the emission to the solvent environment is attributable to the charge transfer nature of the transition, producing a significant dipole that may interact with the solvent dipoles. As expected, the more strongly the solvent interacts with the dipole of the complex, the more dramatically red shifted will be the emission maxima.

Non-radiative decay processes dominate the emissive properties of ruthenium complexes, and lifetimes of these complexes typically vary with ligand substitution. However, measurements of the lifetime of these complexes commonly yield decay constants of $1\mu s$ in polar aprotic solution.

The loss of the ligands in the excited state is particularly problematic in solvents of low dielectric in the presence of complexing counterions such as Cl^- , ClO_4^- and CNS^- . A mechanism for the photoanation reaction has been published, however, the direct experimental evidence supporting the mechanism remains largely speculation. Yet, recent evidence for imidazolyl ligands suggests that the de-ligation proceeds through the sequential removal of nitrogens from the metal center [78].

The complications of deligation are known and understood such that synthetic strategies for the circumvention of these processes may be incorporated into complex

design [68]. The placement of ligands surrounding the metal center having different σ and π characteristics allows the manipulation of the energetic levels of the complex such that the energy gap between the emissive MLCT state and the photochemical d-d MC state are separated to an extent that de-ligation (decomposition) processes are not competitive with deactivation of the complex via radiative and nonradiative channels.

Organization of the Thesis

The incorporation of each of hydrogen-bonding proton transfer in simple electron transfer systems composed of asymmetric salt-bridge hydrogen bonding interactions, as a potential means of providing insights to these two fundamental reactions is the subject of this thesis.

Chapter Two elaborates the experimental procedures used for the determination and characterization of ruthenium and porphyrin complexes. Electrochemical and photochemical determination of the free energy driving forces (ΔG) for each of the electron transfer reactions are given. This chapter additionally includes general details for the characterization of each of the chromophores in the solvents in which the electron transfer reactions were studied.

Chapter Three develops the PCET of synthetically functionalized tris-bipyridyl ruthenium complexes incorporating dicarboxylic acid and amidinium-carboxylate interfaces. Considerations of the excited state energetics on the PCET rate is presented.

Chapter Four is concerned with the introduction of the tetramethylated bipyridyl ruthenium complexes. This designed feature enforces localization of the MLCT transition toward at the interface, clearing up considerations of equilibrium distribution among

ancillary ligands. A consideration of the effects of the nuclear (proton) motion in the interface as it pertains to the observed electron transfer reaction is discussed. The effects of the coulombic field generated in the charged interface are assessed in relation to the potential role in the electron transfer reactions.

In Chapter Five a Ru(II) acceptor-salt bridge-donor system is detailed. This section includes a description of the electrochemical determination of the energetics of the various ligands composing the complex.

CHAPTER 2

EXPERIMENTAL METHODS

Materials

All Ru(II) polypyridine complexes were prepared in the laboratory of Professor Nocera at Michigan State University [79].

Electrochemistry

Electrochemical measurements were performed with the use of a workstation comprising an EG&G PAR 173 potentiostat/galvanostat a PAR 175 universal programmer, and a PAR 179 digital coulometer. The output of the digital coulometer was fed directly into a Houston Instrument Model 2000 X-Y recorder. Cyclic voltammograms were measured at room temperature by using a Pt-disk working electrode ($A = 0.08 \text{ cm}^2$), Pt-wire auxiliary electrode, and an Ag wire pseudo-reference potential electrode in a standard H-cell configuration. Redox couples for the ruthenium(II)polypyridyl

complexes, typically (2-5 mM) were measured in CH_3CN or CH_2Cl_2 solution containing 0.1 M tetrabutylammonium hexafluorophosphate (TBAH) as supporting electrolyte. Typical scan rates were 50 to 200 mV/sec. Oxidation-reduction couples were referenced to SCE via the use of an internal reference ferrocenium/ferrocene having a potential of 0.307 V vs. SCE [80]. The reversibility of each redox couple was determined through the measurement of the anodic to cathodic peak separation ΔE_p of the oxidative and reductive cycles for each complex and also from the $i_{p,a}/i_{p,c}$ ratios. For each of the redox couples, the typical measured anodic to cathodic peak separation ΔE_p varied from the theoretical 59 mV by 40mV. This deviation can be attributed to minimal uncompensated cell resistance and fluctuations due to slight thermal effects.

Cyclic voltammetry measurements in water were undertaken to assess pH effects. Experiments were conducted in H_2O at constant ionic strength maintained at 0.1 M with the use of LiCl and buffered for each pH range used as described previously [81]. The pH was adjusted with the addition of stock solutions of HCl and NaOH. The NaOH solution used in these measurements was prepared via standard techniques; the HCl solution was titrated against the NaOH standard to determine the solution normality. Serial dilutions of these stock solutions were performed to obtain the correct concentration for volumetric additions. During these measurements it was found that the use of a platinum electrode gave very irreversible and inconsistent results, having ΔE_p 's significantly greater than 100 mV. Thus a glassy carbon disk electrode was used for these experiments. For the best reversibility and most reproducible results, activation of the surface of a glassy carbon electrode was necessary. The glassy carbon activation procedure of Meyer [81] was altered slightly as follows: the potential of the electrode was held at 1.8 V for an initial

period of 25 minutes in an 0.1 M H_2SO_4 solution followed by cycling the electrode 5-10 times between a potential of 1.8 V for a period of 30 seconds followed by a potential of – 0.2 V for 15 seconds. This procedure was repeated for each point of the titration as the activation of the surface results in the formation of a fragile oxide layer that flakes off from the surface of the electrode upon extended immersion in solution.

Reduction potentials of the oxidative electron transfer quenchers were determined in CH_2Cl_2 solution containing TBAH ($\mu = 0.1$) as the supporting electrolyte. Quencher concentrations were typically 2-5 mM. The reduction potentials of the protonated quenchers 3,5-dinitrobenzamidinium (DNBAmH^+) and 3,5-dinitrobenzoic acid (DNBA) were performed using a glassy carbon electrode as the working electrode because the platinum electrode resulted in a quasi-reversible redox couple from which the determination of reduction potentials could not be determined with sufficient accuracy or reliability.

The effect of protonation on the redox potential of each of the quenchers in CH_2Cl_2 solvent was determined with DBU (1,8 Diazabicyclo[5.4.0]undec-7-ene) solution 2×10^{-3} M or through the direct addition of the DBU base in concentrated form by micro-pipet. For the direct DBU additions, it was found that the addition of base in excess of 200 μl resulted in excessive asymmetry of the current response and a dramatic reduction of the effective potential range over which the electrode response in CH_2Cl_2 could be measured. The use of DBU in these experiments thus required a thorough cleaning and polishing procedure between each measurement during repeated use. The cleaning procedure consisted of a brief 5-10 minute soaking in concentrated nitric acid, followed by thorough rinsing with house distilled H_2O , polishing of the electrode surface with

(BAS 100 μm polishing alumina) and brief sonication of the electrode in a small 25 ml beaker containing distilled/deionized H_2O . Cleanliness of the electrodes in these measurements was assumed upon the return of reversibility of the measurement of the ferrocenium/ferrocene redox couple.

Standard chronocoulometric techniques [80] were applied to the measurement of the diffusion coefficients for each of 13 nitro-aromatic oxidative quenchers $[\text{Ru}(\text{bpy})_3(\text{PF}_6)_2]^{2+}$ and also measurements were made for the 3,5 dinitroaromatic salt-bridge functionalized oxidative quenchers. For each of the nitroaromatics the same potential (-1.2 V) was set for the platinum electrode. For the determination of the diffusion coefficient of $[\text{Ru}(\text{bpy})_3]^{2+}(\text{PF}_6)_2$ the potential was set at both ($+1.4\text{ V}$ and -1.4 V) and values found were nearly identical ($3.98 \times 10^{-5}\text{ cm}^2/\text{sec}$ at $+1.4\text{ V}$ and $9.6 \times 10^{-5}\text{ cm}^2/\text{sec}$ at -1.4 V) to previous literature determinations ($4.2 \times 10^{-5}\text{ cm}^2/\text{sec}$) for this compound. The current time response of for each of the nitroaromatics was converted to $1/t^{1/2}$ vs. i (i is the current in amperes and t is the time in seconds) plotted in Kaleidagraph. A least squares linear regression was performed with fitting parameters of the slope yielding the diffusion coefficients $D(\text{cm}^2/\text{sec})$ from known concentration C_o^* (mol/cm^3) for each of the nitroaromatics from the Cottrell equation Eq. (2.1) [80].

$$i(t) = i_d(t) = \frac{nFAD_o^{1/2}C_o^*}{\pi^{1/2}t^{1/2}} \quad (2.1)$$

In this equation n is the number of equivalents, F is Faraday's constant ($9.6485 \times 10^4\text{ C/equivalent}$), and A (0.0314 cm^2) is the area of the electrode. The supporting electrolyte for each of these determinations was tetrabutylammonium hexafluorophosphate (TBAH

$\mu = 0.1\text{M}$). Before each measurement of the diffusion coefficient of the nitroaromatic was determined, the measurement of the solution (solvent with supporting electrolyte) contribution to the observed diffusion coefficient was determined and analyzed in the exact same manner as mentioned above. The current time response of the solution was minimal and subtraction produces no noticable change in the diffusion coefficient measurements for the nitroaromatics nor for the $\text{Ru}(\text{bpy})_3^{2+}(\text{PF}_6)_2$. For the diffusionally controlled regime of electron transfer the bimolecular steady-state rate is given by the Debye-Smoluchowski equation Eq. (2.2) [82], where $D = D_d + D_a$ and a' = the effective

$$k_D = 4\pi Da' \quad (2.2)$$

encounter distance. As it has been determined [83] that for bimolecular quenching reactions involving nitroaromatics the quenching occurs through the nitro functionality, the value of a' was assumed to be identical for each of the nitroaromatics used here.

Solution concentration of the $\text{Ru}(\text{bpy})_3^{2+}(\text{PF}_6)_2$ was $3 \times 10^{-5} \text{ M}$ with $\mu = 0.2 \text{ M}$ in tetrabutylammonium perchlorate (TBAP). The concentration of each of the respective quenchers were 0.0015- 0.2 mM as necessary for the reduction of the natural lifetime (τ_o) of the $\text{Ru}(\text{bpy})_3^{2+}(\text{PF}_6)_2$ to $(\tau_o/2)$ as has been previously determined for reliable determination of the linear Stern-Volmer bimolecular quenching rate constants k_q [84,85]. The lifetime data was transformed into quenching rate k_q using the relation of Meyer given in Eq. (2.3).

$$\frac{1}{k_q} = \frac{1}{k_{q'}} + \frac{1}{k_D} \quad (2.3)$$

Where k_q is the measured quenching rate constant and k_q^* is the rate constant of activated quenching and finally k_D is the determined diffusion limited rate constant in the medium used. The data obtained from the fluorescence quenching experiments were plotted as k_q vs. concentration of the quencher and a least squares linear regression analysis was performed using Kaleidagraph and Origin fitting routines based on the linear Stern-Volmer Eq. (2.4).

$$\frac{\tau_o}{\tau} = 1 + k_q[Q]\tau \quad (2.4)$$

Furthermore, the data of the redox potentials measured for the complexes previously determined by Meyer in CH_3CN solvent were converted to ΔG and the quenching rates as $RT\ln k_q$ and fitted to Marcus Theory using two different expressions developed both by Meyer [3] and by Schuster [86].

Bulk electrolysis measurements were performed on solutions of the ruthenium complexes $\sim 3.0 \times 10^{-5}$ M, contained in a previously constructed cell, modified to fit into the optical path of a CARY 17 absorption instrument. This cell has the same general configuration as the standard electrochemical H-cell, with the exception of a reduced volume compartment for the reference electrode. The initial determination of the potential at which the compound was reduced/oxidized was determined from cyclic voltammetry measurements. Bulk electrolysis was carried out 0.2 V past the halfwave potential. Stirring was maintained throughout the experiment by a micro magnetic stir bar.

Optical Spectroscopy

Absorption Spectroscopy

Absorption measurements were performed using a Cary 17 spectrometer retrofitted with the hardware and software design modifications of On-Line Systems Inc. for each of the ruthenium(II) complexes. All absorption measurements were collected using 1cm Suprasil or matched quartz emission cells in aerated or degassed solutions by Ar(g) or freeze/pump/thaw cycles. Absorption spectra were collected throughout the full spectral region encompassing the $d\pi-\pi^*$ (MLCT) and intraligand $\pi-\pi^*$ regions for each of the ruthenium complexes and throughout the Q-band and Soret regions for the porphyrin complexes.

Molar absorptivities for each $[(bpy)_2Ru(Me-bpy)COOH][(PF_6)_2]^{2+}$, $[(bpy)_2Ru^{2+}(Me-bpy)COO^-][(PF_6)]^+$, $[(bpy)_2Ru(Me-bpy)AmH^+][(PF_6)_3]^{3+}$, and the analogous tetramethylated ruthenium complexes were measured on solutions $\sim 2.0 \times 10^{-5}$ M in CH_2Cl_2 (bpy = 2,2'-bipyridine, $Me-bpyCOOH$ = 4-methyl-4'-carboxylic acid-2,2'-bipyridine, $(Me-bpy-AmH^+ = 4\text{-methyl-4'-amidinium-2,2'bipyridine})$. The $[(decb)_2Ru(Me-bpy)COOH][(PF_6^-)_2]^{2+}$ and $[(decb)_2Ru^{2+}(Me-bpy)AmH^+][(PF_6^-)_3]^{3+}$ ($decb$ = 4,4'-diethylcarboxy-2,2'-bipyridine) complexes in which molar absorptivities data were collected in CH_3CN solvent. These molar absorptivities reported for the (bpy) and (decb) complexes in Chapter 5 were determined from Beer-Lambert plots [87] of six points covering an absorption range $4.0\text{-}40 \times 10^{-6}$ M.

Absorption titration for the ruthenium complexes $\sim 2.0 \times 10^{-5}$ M were collected throughout the quencher concentration range $\sim 0.5\text{-}15$ equivalents relative to the Ru(II) polypyridyl concentration. Addition of μl quantities of a stock solution 2.0×10^{-3} M

quencher was used for each of the respective salt-bridge and hydrogen-bonding quenchers. Solution volume was maintained at a constant 5.0 ± 0.15 ml solution volume throughout the titration range.

Absorption data, collected for each of the ruthenium complexes as a function of DBU in CH_2Cl_2 , were performed on samples 2.0×10^{-5} M. Addition of DBU encompassing a range of 0.2 - 10 equivalents of the ruthenium complex concentration was accomplished by the addition of a stock 2.0×10^{-3} M solution of DBU by micropipet. Solution volume was maintained at a constant 5.0 ± 0.15 ml throughout the titration range.

Emission Spectroscopy

Emission measurements were performed using an instrument previously designed and constructed at Michigan State University [88]. This instrument was recently modified to include photon-counting detection, supported by associated hardware and software [89]. Excitation of all samples was accomplished using either of two sources, 150 W Xe or 200 W Xe/Hg lamps. Isotropic emission from the samples was detected using a standard 90° orientation by a dry-ice cooled Hamamatsu R1104 or R943-02 gated photon-counting photomultiplier tube mounted to a single monochromator (2.5 mm / 2.5 mm). All emission measurements were performed at room temperature unless stated otherwise. All samples were contained in 1cm suprasil or matched quartz cells with aerated solutions or that included a high vacuum adaptation design constructed at Michigan State University.

Emission titration measurements for the $[(\text{tmb})_2\text{Ru}(\text{Me-bpy})\text{COOH} (\text{PF}_6)_2]^{2+}$, $[(\text{tmb})_2\text{Ru}(\text{Me-bpy})\text{COO}^- (\text{PF}_6)]^+$ and $[(\text{tmb})_2\text{Ru}(\text{Me-bpy})\text{AmH}^+ (\text{PF}_6)_3]^{3+}$ ($\text{tmb} = 3,3',4,4'$ -tetramethyl-2,2'-bipyridine) complexes were performed using DBU, complimentary salt-bridged benzene and 3,5-dinitrobenzene complexes. For these measurements, concentrations of the respective quencher or base were measured in CH_2Cl_2 solvent. The addition of the 3,5-dinitrobenzamidine quencher covered a range of from 0.5-15 equivalents of the ruthenium complex. For each of the $[(\text{tmb})_2\text{Ru}^{2+}(\text{Me-bpy})\text{COOH} (\text{PF}_6)_2]^{2+}$ and $[(\text{tmb})_2\text{Ru}^{2+}(\text{Me-bpy})\text{AmH}^+ (\text{PF}_6)_3]^{3+}$ complexes, the concentration range of the complementary salt-bridging 3,5 dinitrobenzene was abbreviated relative to that of the $[(\text{tmb})_2\text{Ru}^{2+}(\text{Me-bpy})\text{COO}^-]$ experiment. For the $[(\text{tmb})_2\text{Ru}^{2+}(\text{Me-bpy})\text{COOH}]^{2+}$ the concentration range of the 3,5-dinitrobenzene complex encompassed the range from 0.5-5 equivalents. For the $(\text{tmb})_2\text{Ru}^{2+}(\text{Me-bpy})\text{AmH}^+$ the 3,5-dinitrobenzoate was varied over the concentration range of 0.5 - 10 equivalents relative to the ruthenium complex. Similarly, the concentration range used in the titration with the salt-bridge and hydrogen-bonding functionalized benzene complexes encompassed an identical concentration range to that of the 3,5-dinitrobenzene analogue. However, for the addition of DBU, the concentration range was identical for each of the $[(\text{tmb})_2\text{Ru}^{2+}(\text{Me-bpy})\text{COOH} (\text{PF}_6)_2]^{2+}$ and $[(\text{tmb})_2\text{Ru}^{2+}(\text{Me-bpy})\text{AmH}^+ (\text{PF}_6)_3]^{3+}$ comprising a range of 0.2 to 10 equivalents.

In the emission titration measurements of the reductive electron transfer systems, the concentration of each of the ruthenium complexes was maintained at $\sim 2.0 \times 10^{-5}$ M. The quencher titration range comprised a 0.2 - 2 M equivalent concentration range relative to the concentration of the ruthenium complex. For this series of complexes, the

quencher additions included the addition of DBU, salt-bridge functionalized dimethylaminobenzene complexes, salt-bridge functionalized benzene complexes, and dimethyl-p-toluidine. Each of the emission titration measurements was performed open to air and after freeze/pump/thaw degassing cycles.

Photophysical Measurements

Quantum yield measurements for each of the ruthenium complexes were conducted on the above described emission instrument. The excitation wavelength for these determinations was the 435.8nm Hg line of a 200W Xe/Hg lamp. All measurements were performed at room temperature in either Ar(g) degassed or freeze/pump/thaw degassed solutions. Absolute quantum yields were determined by referencing emitted light to the emission of a standard $\text{Ru}(\text{bpy})_3^{2+}(\text{PF}_6^-)_2$ solution. ($\phi_{\text{em}} = 0.029, 0.062$, for CH_2Cl_2 and CH_3CN [68] respectively). Appropriate corrections for differences between sample and quantum yield standard were applied according to Eq. (2.1). A_s and A_c are the absorbance of the standard (s) and the Ru(II)polypyridyl (c) complex at the excitation

$$\phi_{\text{emc}} = \phi_{\text{ems}} \left(\frac{A_c}{A_s} \right) \left(\frac{I_s}{I_c} \right) \left(\frac{\eta_c}{\eta_s} \right)^2 \quad (2.1)$$

wavelength, I_s and I_c are the integrated emission spectra corrected for photomultiplier characteristics and η_c and η_s are the refractive indices of the solvents of PCET complex and standard, respectively.

Infrared spectroscopy

Infrared measurements were performed with the use of the departmental Nicolet FT-IR instrument. The FT-IR spectra of the CH_2Cl_2 solvent and of the CH_2Cl_2 solvent with the addition of the DBU were collected for baseline corrections. Collection of the FT-IR data for each of the samples required the use of high sample concentrations ($\sim 1 \times 10^{-3}$ M) and the collection of at least 64 (usually 256) scans at 4 cm^{-1} resolution were required for the observation of well resolved spectra for each of the ruthenium complexes.

Association constants were determined for the ruthenium complexes in CH_2Cl_2 following a similar procedure. Stock solutions of ruthenium complex were 9.2×10^{-4} M and 1.1×10^{-3} M and that of the stock solution of complexing salt-bridge functionalized complexes 1.3×10^{-3} M, 9.1×10^{-4} M, 1.15×10^{-3} M and 8.6×10^{-4} M for benzoate, benzamidine, 3,5-dinitrobenzoate, and 3,5-dinitrobenzamidine respectively. The concentrations of the ruthenium complexes were constant throughout the titration procedure. Aliquots of the complexing salt-bridge acceptor complexes were taken volumetrically by micropipet. Each aliquot of the salt-bridge complex was added to a sample vial and the CH_2Cl_2 solvent was removed by evaporation. To this evaporated residue was added the constant volume of ruthenium complex solution. Subsequent to mixing a $100 \mu\text{l}$ aliquot of the resultant solution was added to the $200 \mu\text{m}$ CsI infrared sample cell by syringe.

Nano-Second Lifetime Measurements

Emission decay lifetimes were collected in the LASER Laboratory at Michigan State University. The 504 nm excitation wavelength used for excitation of the $d\pi-\pi^*$ (MLCT) transitions of salt-bridge functionalized *tris*-bipyridyl ruthenium(II) complexes was provided by the third harmonic output (355 nm) of a DCR-2 Nd:YAG laser operating at 10 Hz, pumping a 25-50 psi $H_2(g)$ filled Raman shifting tube. The isolation of the second Stokes-shifted 504 nm light was accomplished with the use of a Pellin-Broca prism placed after the Raman shifting tube to disperse the Stokes and anti-Stokes shifted $H_2(g)$ lines. After dispersion, the 504 nm light was further isolated by passing the beam through an iris diaphragm before being turned by a glass prism. The excitation light was collimated using a telescope and turned once again at a glass prism before reaching the sample. Excitation powers measured at the sample were typically 1-5 mJ/pulse (10 ns FWHM). Reduction of scattered light in the observed emission decay data was accomplished by passing the emission through an appropriate combination of long and short wavelength pass filters placed before the focusing lens to the slit of a SPEX 1702 single pass monochromator. Lifetime decays, monitored at the ruthenium complex emission maxima (unless otherwise stated), were collected with a Hamamatsu R928 PMT operating at 600V. The output of the PMT was signal averaged with a TEK 602A Digitizing Signal Analyzer storage oscilloscope averaging 512 decay traces/lifetime data file. Decay data were stored as two column ASCII files to be manipulated via Kaleidagraph or Origin software packages.

Low Temperature lifetimes

Low temperature (77K) lifetime measurements were made on EPA glass samples contained in 9 mm o.d. NMR tubes immersed in a liquid N₂ Dewar with the windows of the Dewar kept free of condensation by a stream of nitrogen gas. For each ruthenium sample the data set was composed of the average of 512 decay traces per lifetime file.

Temperature Dependent Lifetimes

Temperature dependent lifetimes (-20 – 60°C) were collected with the use of a temperature-controlled cell housing obtained from Hitachi. Cooling or heating of the cell housing was provided by the flow of a solvent mixture of water and ethylene glycol (50:50) in a programmable Neslab chiller. At temperatures below 0°C, condensation on the surface of the cell was prevented with a flow of N₂(g). All samples were freeze/pump/thaw degassed prior to measurement.

Pico-second Lifetime measurements

Lifetimes collected at the picosecond timescale were accomplished with the use of a recently modified TCSPC instrument previously designed and constructed at Michigan State University [90]. The design modifications made were, the inclusion of a Hamamatsu 6 µm R3809U (MCP-PMT) mounted to a CVI 112 0.8 m scanning subtractive double monochromator. The output of the MCP detector was fed to an EG&G 9806 pre-amplifier prior to reaching an EG&G 9307 pico-Timing Discriminator. These modifications were made to reduce transit time spread (TTS) of the monochromator and risetime of the detector and consequently the overall instrument response function for the instrument. Other modifications to the instrument include the introduction of an Ealing

microscope objective, directed through a CVI DPL polarization scrambler after the sample to collimate the luminescence light onto the entrance slit of the monochromator. These modifications give rise to instrument response functions typically 40-50 ps at the selected wavelength ranges used.

Excitation is provided by the output of a synchronously pumped cavity-dumped Coherent 702 dye laser typically operating at a frequency of 3.8 MHz (FWHM 6-8 ps, 13 nJ/pulse) The Coherent Antares 76-s Nd:YAG laser second harmonic (532 nm, 100 ps FWHM, 3W) output provides the pump source for the dye laser. Tunability of the excitation wavelength provided by the 702 dye laser is accomplished with one of the three dye circulators running pyromethene 567, R6G, or LDS 698 laser dyes for access to wavelength ranges through 560-750nm. Doubling, accomplished with an external crystal placed in the beam path, increases the useful range of the 702 dye laser by providing additional excitation wavelengths of 280-375nm. The intermediate wavelength range is adequately covered with the use of the blue-dedicated 702 dye laser providing excitation wavelengths from 420 - 470 nm.

The fast time response necessary for the collection of fluorescence data below the nano-second time-scale requires special electronic design provided by reversed timing single-photon-counting techniques. For reversed timing, the sample luminescence resulting from the excitation pulse provides the start signal at the time to amplitude converter (TAC). Splitting of the excitation beam equally (1" glass cube 50 / 50 beam splitter) prior to sample excitation provides both the excitation and the reference signal which is optically delayed through a 1.0 m external fiber optic cable coupled to a variable length internal fiber optic delay cable. This configuration allows the spacing of the

fluorescence signal and reference laser pulses up to 180 ns. The addition of either of two external 50 m or 100 m fiber optic spools provides the further spacing of the signal and reference laser pulses to a total of 680 ns. Additionally, for the collection of fast events in long fluorescent lifetime samples the excitation frequency may be set continuously from 38 MHz to 1.5 kHz through the 702 dye laser cavity dumper driver. With an external trigger source constructed at Michigan State University the frequency may be further tuned to 1 kHz.

Other modifications of the instrument include the addition of a Tennelec TC 864 replacing the older TC 862, changing the range of the smallest temporal window from 25 to 5 ns. Data collection was accomplished with new 4096 channel Viking Instruments MCA card and data was displayed and stored with the use of Edinburgh FLA-900A software followed by further analyses with Kaleidagraph or Origin software packages

For the $[(tmb)_2Ru(Me-bpy)COO^-][(PF_6)]$ complex titrated with 3,5-dinitrobenzamidine and the $[(decb)_2Ru(Me-bpy)AmH^+][(PF_6)_3]^{3+}$ titrated with N,N'-dimethylaminobenzoate lifetime data collection was accomplished with excitation at 575 nm and emission collected at the emission maximum for each point of the lifetime titration.

Synthesis of Ruthenium Complexes

Synthesis of $[Ru(Me-bpy-COOH)_3]^{2+}$ and $[Ru(Me-bpy-AmH^+)_3]^{5+}$. Complexes were prepared using standard literature procedures A 95% ethanol (10 ml) solution containing 4-methyl-4'carboxylic acid-2,2'-bipyridine (1.0g, 4.1 mmol) or 4-methyl-4'amidinium-bipyridine (4.0g 20 mmol) and $RuCl_3 \cdot (H_2O)_3$ (0.5g 1.9 mmol) were allowed

to reflux for 10 days. The solvent for each complex was evaporated under reduced pressure followed by dissolution in a minimal amount of water and filtered. The deep red PF_6^- salt was obtained by the addition of a saturated aqueous solution of NH_4PF_6 . Further purification of the $[\text{Ru}(\text{Me-bpy-COOH})_3]^{2+}$ complex was accomplished by charging a neutral alumina column with the complex and eluted with CH_2Cl_2 , $(\text{CH}_3)_2\text{CO}$, and MeOH followed evaporation under reduced pressure and washing with anhydrous ethyl ether on a medium frit. For the $[\text{Ru}(\text{Me-bpy-AmH}^+)_3]^{5+}$ complex the purification consisted of charging a silica gel column with the complex and eluting, followed by evaporation under reduced pressure and washing with anhydrous ethyl ether.

Deuteration of samples for lifetime measurements

Deuteration of the dissociable protic substituents of the salt-bridge and hydrogen-bonding interface of $[(\text{bpy})_2\text{Ru}^{2+}(\text{Me-bpyCOOH})][(\text{PF}_6^-)]_2$, $[(\text{bpy})_2\text{Ru}^{2+}(\text{Me-bpy})\text{AmH}^+][(\text{PF}_6^-)]_3$, $[(\text{tmb})_2\text{Ru}^{2+}(\text{Me-bpy})\text{AmH}^+][(\text{PF}_6^-)]_3$ and $[(\text{tmb})_2\text{Ru}^{2+}(\text{Me-bpyCOOH})][(\text{PF}_6^-)]_2$ complexes was accomplished by the addition of each complex and NaOCH_3 to a 50 ml round bottom flask. The contents of the flask were rigorously dried under vacuum and gentle heating. Upon cooling of the flask to ambient a dried degassed solution of MeOD was transferred under vacuum to each of the flasks containing the ruthenium complexes. Subsequent to the addition of ~10 ml of MeOD to each flask the contents were warmed to room temperature and thoroughly mixed for a period of 10 minutes and the excess solvent was removed under vacuum. This procedure was repeated 3-5 times before complete. The confirmation of deuteration was assessed by FAB-MS, IR, and NMR spectroscopy.

CHAPTER 3

PHOTOINDUCED ELECTRON TRANSFER WITHIN AN ELECTRON DONOR-ACCEPTOR ASSEMBLY JUXTAPOSED BY A HYDROGEN-BONDING INTERFACE

Introduction

The ubiquity of electron transfer processes in chemical reactions have led to the investigation of a great variety of model systems designed to address specific questions regarding the factors controlling electron transfer processes [91]. Development of model systems incorporating long range electron transfer reactions has been a central focus in these developments [18].

Pioneered by the observation of long range electron transfer reactions in biological systems, incorporation of structural components found in these systems have been implemented in a variety of different electron transfer models [91]. To better understand the relationship of the biological framework, developments of electron

transfer reactions occurring in proteins, protein complexes and in systems containing synthetic polypeptides, α -helices, β -sheets and β -turns as spacers have been undertaken [12,13,15].

A fundamental design consideration of these photoinduced electron transfer model system investigations is the incorporation of photoexcitable donor molecules capable of either oxidative or reductive electron transfer reactions in the excited state. To this end the photophysical behavior of Ru(II)polypyridine complexes have been the subject of numerous investigations of photoinduced excited state electron transfer reactions. Development of this class of complexes has been extensively investigated in regard to both bimolecular electron transfer reactions and more recently to the study of intramolecular electron transfer reactions[68,92]. Recent examples using these photoexcitable donor molecules may be seen in the chromophore-quencher complexes of Meyer [3,15]. These systems contain both an appended reductive quenching substituent and oxidative substituent covalently tethered by peptide residues to the bipyridyl ligands composing the metal complex. The relative synthetic ease with which bipyridyl ligands may be functionalized make these complexes particularly amenable to the development of electron transfer assemblies. Other recent examples of the mimicry of biological frameworks toward the understanding biological function are found in the work of Ogawa [13]. Similarly, the incorporation of design features representative of reactions occurring in the biological medium have been developed in model systems [93].

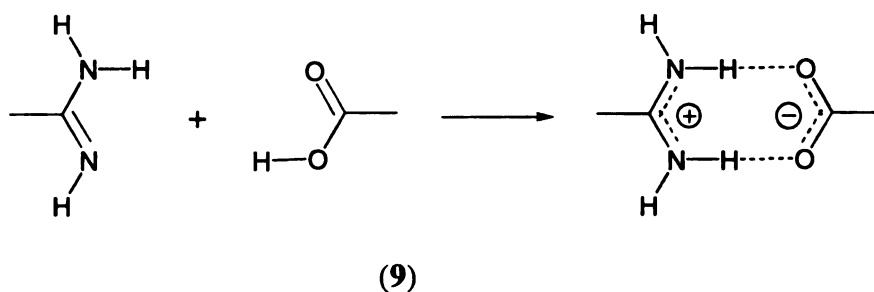
Coupling of proton motion to charge separation is a fundamental mechanism in biological energy conversion systems. The energy storing processes of small molecule activation and the translocation of protons across membranes in the protein and enzymes

of photosynthesis and respiration are predicated upon proton coupled electron transfer (PCET). One approach to investigating the mechanism of PCET is to photoinduce electron transfer within an donor/acceptor pair that is juxtaposed by a proton transfer interface such as those formed from carboxylic acid dimers [62] or guanine-cytosine base-pairs [49]. Electron transfer systems based on the dicarboxylic acid design have previously been described where it was found that electron transfer reactions occur with rates comparable to systems in which the electron transfer donor and acceptor are tethered by a covalent pathway from the standpoint of distance and driving force [62].

The incorporation of a symmetric interface into a system in which the electron donor composed of a carboxylic acid derivatized $\text{Ru}(\text{bpy})_3^{2+}$ complex may be used, requires the modification of one of the bipyridyl ligands with carboxylic acid functionality. These molecules have been previously synthesized in other laboratories [94] and have subsequently been reproduced in the Nocera group [95] in which the carboxylic acid functionality is placed at the 4' position of a bipyridyl ligand. In order to utilize this complex and create an electron transfer reaction, an electron transfer quencher is necessary which can recognize and bind with the complimentary carboxylic acid functionality of the donor complex. One well-known organic oxidant, 3,5-dinitrobenzoic acid, provides this complimentary portion for the creation of a symmetric interface system. The electron transfer donor/acceptor complex generated in solution between these molecules is shown in Figure (9a) below.

The present system based on the photoinduced excited state of a modified *tris*-bipyridyl ruthenium (II) chromophore in CH_2Cl_2 solvent. The results of the findings are compared to systems composed of the introduction of a charged asymmetric amidinium-

carboxylate salt-bridge hydrogen bonding interaction as shown in Figure (3.1), for modified Ru(II) polypyridyl electron transfer donor complexes. Introduction of asymmetry to both the donor and acceptor moieties of the proton transfer interface allows an experimentally reversible configuration such that the direction of the electron transfer reaction may be analyzed in relation to the direction of proton transfer within the salt-bridging interface. The advantages garnered through the incorporation of the charged



asymmetric interface are, foremost, the selective and directional hydrogen-bonding interactions effectively abolishing the competitive self-associations prevalent in the symmetric dicarboxylic acid (COOH_2) system. Furthermore, the charge complementarity of the interface enhances the production of a stable and strong hydrogen-bonding configuration even in solvents having high dielectric constant [95].

The comparison of observed electron transfer rates in these asymmetric systems provides the potential to determine the effects of proton motion within the interface. In this chapter the measurement of the time-resolved quenching of emission intensity by photoexcitation is discussed with specific attention to the kinetic isotope effects observed through selectively introducing deuterated functionalities to the salt-bridge interface components.

Results

Electronic Absorption and Luminescence spectroscopy

Absorption and emission spectra for the three hydrogen-bonding and salt-bridge modified ruthenium(II) electron transfer donors are typical of modified ruthenium(II)polypyridine complexes [68]. The 400 - 500 nm region shows typical, slightly split $d\pi-\pi^*$ (MLCT) absorption bands ($\lambda_{\max} = \sim 450$ for (1), (2) and (3)), and single intraligand $\pi-\pi^*$ absorption bands in the region 260 - 300 nm ($\lambda_{\max} = \sim 285$ nm for (1), (2) and (3)).

The emission spectra for each of the three ruthenium complexes are broad and structureless at room temperature and show vibrational progressions of 1000 - 1500 cm^{-1} upon cooling to $\text{N}_2(\text{l})$ temperatures (77K). Emission maxima of the spectra are found to change position slightly in response to changes in the electronic composition of the ligand set surrounding the metal center. ($\lambda_{\max} = 646$ for (9a), 639 for (9b) and 629 for (9c)). The photophysical characterization data for absorption and emission is summarized in Table 2.

Free energy driving force (ΔG) determinations for each of the electron transfer systems (9a-c) was accomplished by two methods. First, the determination of the free energy of the excited state relative to the ground state by the measurement of the FWHM of the emission band required the estimation made through the use of a relationship previously derived by Meyer [15] with corrections for reorganizational energy of medium frequency vibrational modes of the bipyridyl ligands, using Eq's. (3.1) and (3.2). The operating principle of these Eq's. (3.1 and 3.2) is generalized from a Franck- Condon

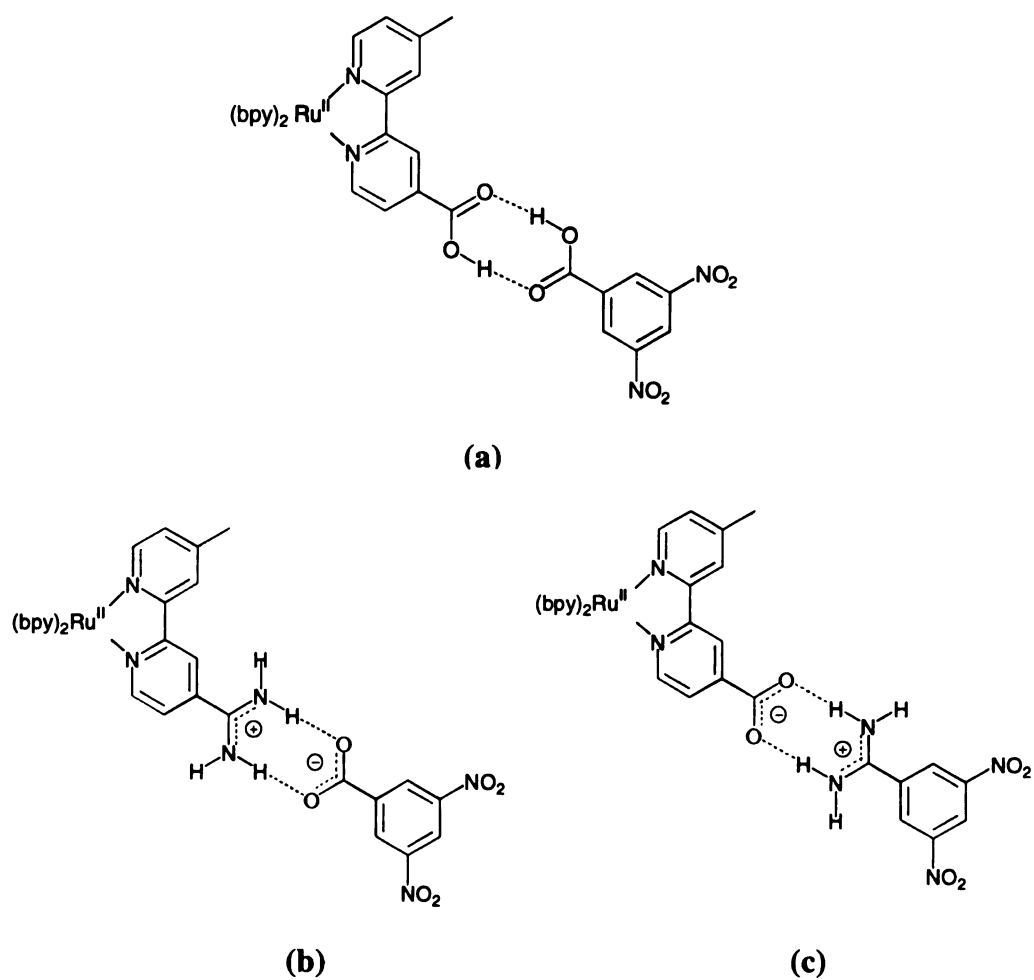


Figure 9 Bipyridyl ligated systems. Symmetric dicarboxylic acid (a) asymmetric amidinium-carboxylate (b) and asymmetric carboxylate-amidinium (c) salt-bridge interfaces for electron transfer studies.

Table 1. Electrochemical data for the three (bpy)₂Ru(II) complexes

Ru (II) compound	$E^{3+/2+}$	ΔE_p (mV)	i_{pa} / i_{pc}
(bpy) ₂ Ru ²⁺ (Mebpy)COOH	1.27	100	1.1
(bpy) ₂ Ru ²⁺ (Me-bpy)AmH+	1.26	65	1.00
(bpy) ₂ Ru ²⁺ (Me-bpy)COO ⁻	1.29	60	1.00

$$E_{0,0} = \Delta G_{es} + \chi \quad (3.1)$$

$$\chi \cong \frac{(\Delta v_{0,1/2})^2}{16 \ln 2 k_B T} \quad (3.2)$$

emission spectral analysis [96] of *tris*-bipyridyl ruthenium(II) complexes derived from the Energy Gap Law considerations of Jortner [97]. The determination of the $E_{0,0}$ is derived from the energy of the emission spectra taken at the maximum. The additional factor χ is a result of the displacement of the excited state potential energy surface relative to the ground state surface. The extent of the displacement and its contribution to the luminescence is accounted for in Eq (3.2) by the incorporation by the measurement of the full width at half maximum (FWHM) of the emission spectrum, as the primary contribution to the spectral bandshape are determined to be due to one vibrations of the bipyridyl ligands (1200 - 1500 cm^{-1}) and to a lesser extent to the metal-nitrogen bond changes (200 - 500 cm^{-1}) resulting from photoexcitation and thermal factors. Entropic considerations are accounted for in the term χ ($\chi = \chi_i + \chi_o$) and are assumed to be small [98].

Measurement of the reduction potentials for the 3,5-dinitrobenzoic acid (DNBA) and the 3,5-dinitrobenzamidinium (DNBA mH^+) results in irreversible electrochemical data by standard cyclic voltammetry techniques. Thus the free energy necessary for the reduction of the oxidative quenchers were determined by the derivation of a linear free energy relationship between the known reduction potential and the bimolecular quenching rate constant of $\text{Ru}(\text{bpy})_3^{2+}$ (CH_3CN $\mu = 0.1$) by a series of nitroaromatic complexes (o, m, and p-dinitrobenzene). The reaction free energy for the bimolecular quenching of these complexes encompasses a range of ($-\Delta G = 0.3\text{V}$). Collection of this

data allows an estimation of the thermodynamic free energy ($-\Delta G$) for the electron transfer reactions of the proton coupled-electron transfer quenchers determined as shown in the following relation Eq. (3.3).

$$\Delta G_{et} = E_{Ru^{2+}} - E_{1/2} Ru^{3+/2+} - Q^{0/-} \quad (3.3)$$

Luminescence and Lifetime Measurements

Each of the three ruthenium complexes $(bpy)_2Ru^{2+}(Me-bpy)COOH$, (**9a**) $(bpy)_2Ru^{2+}(Me-bpy)AmH^+$ (**9b**) and $(bpy)_2Ru^{2+}(Me-bpy)COO^-$ (**9c**) exhibit long lived and monoexponential luminescence in room temperature CH_2Cl_2 solution throughout 4τ of decay data ($\tau = 1100$ ns, 1030 ns and 1300 ns). In these lifetime decays there is no evidence of change in the decay lifetime upon altering the emission detection wavelength. Similarly, the use of excitation wavelength 436, 504 or 532 nm causes no appreciable change in the observed lifetime decay. That these monitored decay lifetimes do not change with alteration of excitation wavelength is consistent with the contention [99] that the emissive state from which the electron transfer occurs in these complexes represents a thermodynamically equilibrated complex on the nano-second time-scale. Additionally, the risetime to the emissive state giving rise to the lifetime decays are not observed to vary.

For each of the synthetically modified Ruthenium complexes the $d\pi-\pi^*$ (MLCT) excited state is well poised for the efficient reduction of the complimentary carboxylic acid, amidinium or carboxylate aliphatic or aromatic electron transfer acceptors. The addition of complimentary hydrogen-bonding or salt-bridge functionalized non-electron transfer active compounds, the emission and the decay lifetimes are altered from the

either the uncomplexed species or the electron transfer complexes. Upon the addition of the hydrogen-bonding or salt-bridge functionalized 3,5-dinitro aromatic quenchers, to the complimentary ruthenium(II) complexes (**9a-c**) there is an observable dramatic attenuation of the luminescence attributable to quenching by an electron transfer mechanism consistent with the observation of the electron transfer quenching of electronically excited *tris*-polypyridyl complexes of ruthenium(II) by nitroaromatics [3]. The lifetime decay data for each of these three systems exhibit biphasic decay with one component dependent upon the concentration of the quencher and one component remaining independent of the concentration of the quencher throughout the quencher concentration range investigated Figures (10) and (11). The concentration dependent component is assigned to bimolecular quenching of the excited state lifetime of unbound ruthenium complex. Bimolecular electron transfer rates for this component of the electron transfer reactions for each of the complexes obeys typical linear Stern-Volmer bimolecular quenching kinetics. Relative quenching determined from the bimolecular component of the lifetime decays for $(\text{bpy})_2\text{Ru}^{2+}(\text{Me-bpy})\text{COOH}$ (**9a**), $(\text{bpy})_2\text{Ru}^{2+}(\text{Me-bpy})\text{AmH}^+$ (**9b**) and $(\text{bpy})_2\text{Ru}^{2+}(\text{Me-bpy})\text{COO}^-$ (**9c**) complexes are 80% , 64% and 49% respectively. Fitting this lifetime decay data versus quencher concentration yields the bimolecular electron transfer rate constants ($k_{\text{et}} = 2.4 \times 10^9 \text{ M}^{-1} \text{ s}^{-1}$ for (**9a**), $1.4 \times 10^9 \text{ M}^{-1} \text{ s}^{-1}$ for (**9b**) and $1.0 \times 10^9 \text{ M}^{-1} \text{ s}^{-1}$ for (**9c**))

The concentration independent component observed in the lifetime quenching experiments for each of the ruthenium complexes exhibit rate constants of $8.0 \times 10^6 \text{ s}^{-1}$, $12.0 \times 10^6 \text{ s}^{-1}$ and $4.3 \times 10^6 \text{ s}^{-1}$ for $(\text{bpy})_2\text{Ru}^{2+}(\text{Me-bpy})\text{COOH}$, $(\text{bpy})_2\text{Ru}^{2+}$

Table 2. Emission Characterization of (bpy)₂Ru(II) complexes

Ru (II) compound	E _o (cm ⁻¹)	Δv _{0,1/2} (cm ⁻¹)	ΔG _{es} (V)
(bpy) ₂ Ru ²⁺ (Mebpy)COOH	15480	2297	2.20
(bpy) ₂ Ru ²⁺ (Mebpy)AmH+	15649	2586	2.26
(bpy) ₂ Ru ²⁺ (Mebpy)COO ⁻	15800	1760	2.18

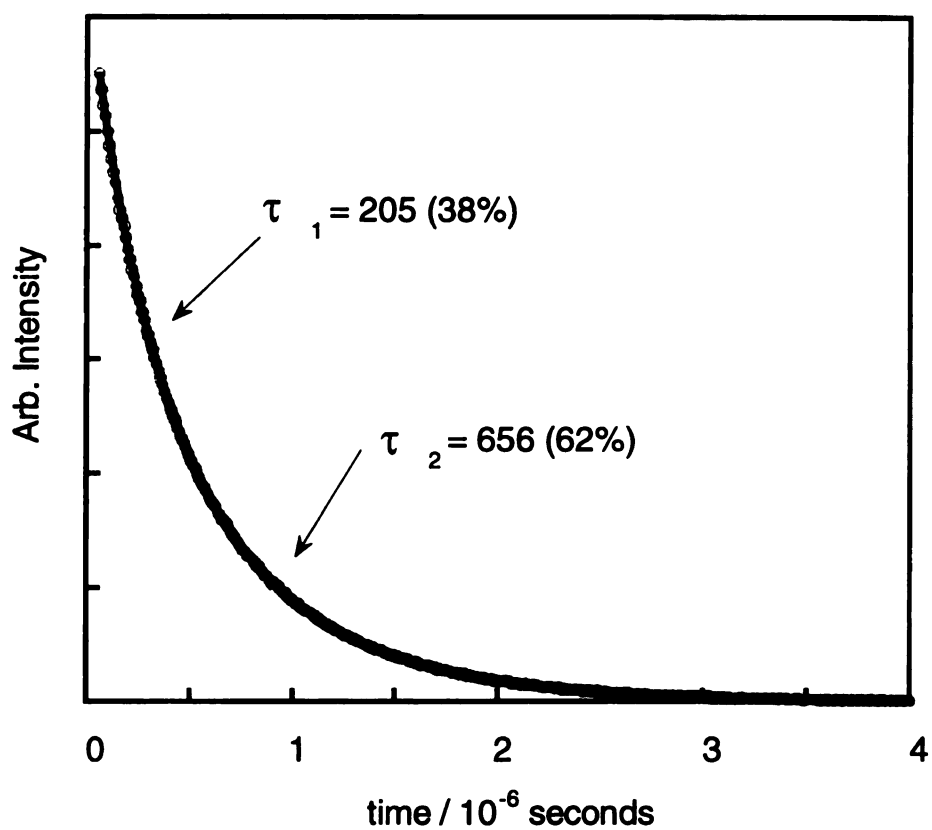


Figure 10. Biexponential fit of lifetime decay indicating concentration-dependent and concentration-independent components of a representative lifetime decay for [(bpy)²Ru²⁺(Me-bpy)AmH⁺] (1.0×10^{-4} M) with complimentary 3,5-dinitrobenzoate [1.5×10^{-4} M].

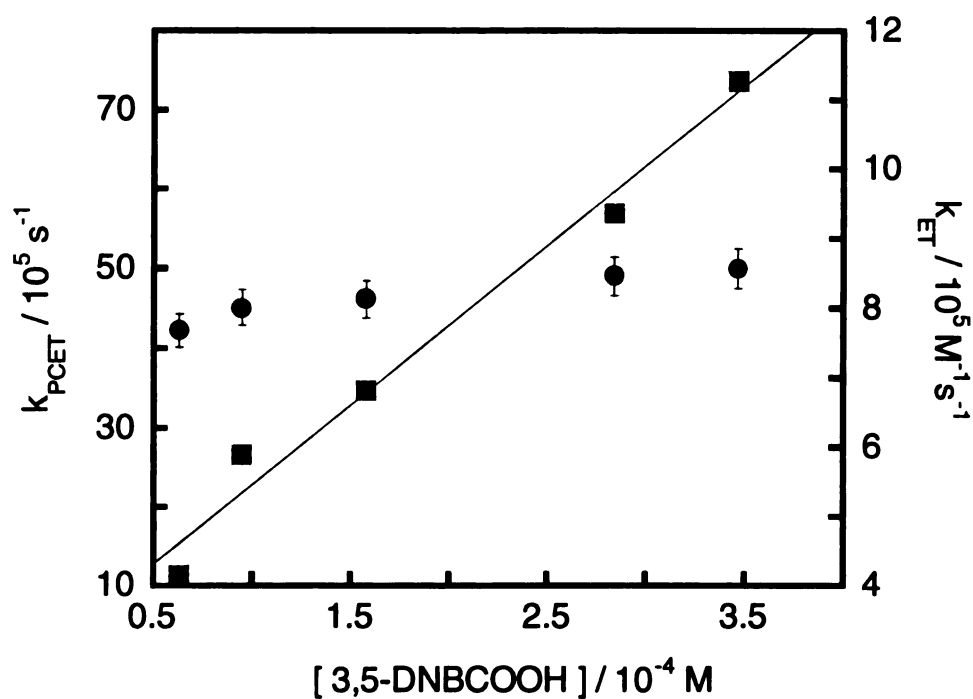
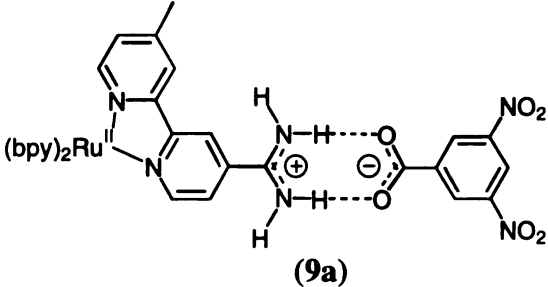
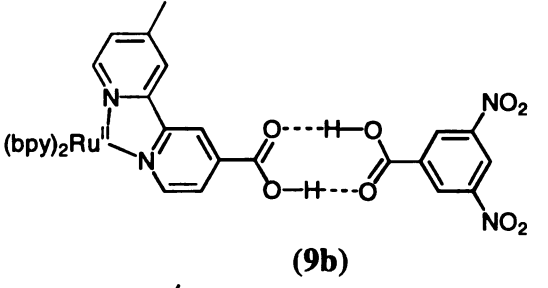
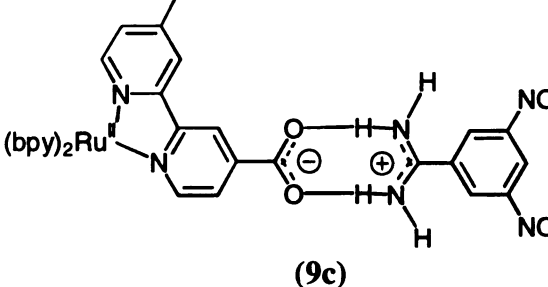
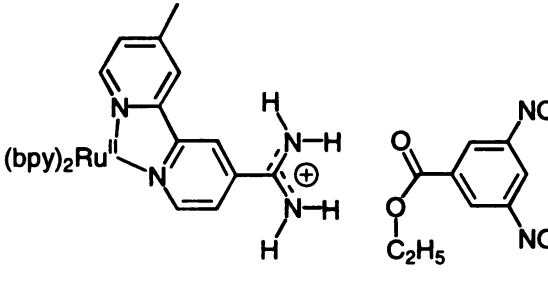


Figure 11. Concentration-independent component (●) and concentration dependent component (■) for the lifetime titration of $(bpy)_2Ru^{2+}(Me-bpy)AmH^+$ [1.0×10^{-4} M] with 3,5-dinitrobenzoate in CH_2Cl_2 at $22^\circ C$.

Table 3. Observed electron transfer rates for concentration-dependent and concentration-independent electron transfer of bipyridine based donor-acceptor complexes in CH₂Cl₂ at 22^oC.

Ru(II) salt bridge complex	ΔG_{ET} / V	$k_{ET}/M^{-1} s^{-1}$	$k_{PCET} s^{-1}$
 <p>(9a)</p>	-0.21	2.4×10^9	4.3×10^6
 <p>(9b)</p>	-0.14	1.4×10^9	8.0×10^6
 <p>(9c)</p>	-0.05	1.0×10^9	12.0×10^6
 <p>(9d)</p>	-0.15	1.9×10^9	—

(Me-bpy)COO⁻ and (bpy)₂Ru²⁺(Me-bpy)AmH⁺ respectively. This component of the lifetime decay data is attributed to proton coupled-electron transfer (PCET) through the symmetric hydrogen bonding or salt-bridge functionalized interfaces. The data for each of the three systems is summarized ($-\Delta G$, k_{et} , and k_{PCET}) in Table 3.

The assessment of these kinetics data is suggestive of electron transfer occurring through the symmetric dicarboxylic acid and the asymmetric salt-bridge hydrogen-bonding interfaces. Validation of the association between electron donor and acceptor reactants in DMSO solution have been shown in NMR titration experiments for (bpy)₂Ru²⁺(Me-bpy)AmH⁺ [95] In DMSO the association constants measured for system (9b) is found to be dependent upon the dielectric constant of the solvent ($K_a = 1197 \pm 93$ M⁻¹ in DMSO and $K_a = 2432$ in CH₃CN). Measurement of the association of complex (9a) reveals an association constant of 702 M⁻¹ in CH₂Cl₂ solvent.

Control experiments for the lifetime measurement using the non-complexing ethyl-3,5-dinitrobenzoate yield monoexponential decays throughout a concentration range comprising that of the 3,5-dinitrobenzene salt-bridge and carboxylic acid quenchers. These experiments reveal no evidence of biphasic decay processes throughout the concentration range of the titration. Supporting the contention that the observed concentration independent component of the lifetime decay data represent an electron transfer reaction occurring as a result of the association of the symmetric hydrogen-bonding or asymmetric salt-bridge complexes.

Discussion

The subtle differences in the concentration independent rate as a function of the change in the direction of the interface suggests that the direction of the interface plays a role in determination the observed electron transfer rate. But by the substitution of the dissociable protons within the interface of electron transfer complexes (**9a**) and (**9b**) the participation of the proton in the electron transfer rates are more clearly shown. The lifetime measurements incorporating the deuterated complex (**9a**) reveals a k_H/k_D rate ratio of 1.5 while the observed kinetic isotope effect observed for the electron transfer complex (**9b**) gives rise to a rate ratio $k_H/k_D = 1.34(3)$

Referring to Table 3 summarizing the electron transfer kinetics for each of the three complexes it may be seen that the relative energetic difference in the driving force between the complexes are small. In fact, the difference between the asymmetric system $(bpy)_2Ru^{2+}(Me-bpy)AmH^+$, 3,5-dinitrobenzoate ($\Delta G = -0.21V$) and the $(bpy)_2Ru^{2+}(Me-bpy)COOH$, 3,5-dinitrobenzoic acid ($\Delta G = -0.14 V$) is merely $-0.07 V$. Yet, despite the smaller driving force for the complex composed of the symmetric $(COOH)_2$ interface the observed intramolecular electron transfer rate is nearly a factor of 2 greater than that observed for the asymmetric (AmH^+,COO^-) interface system. Comparison of the two asymmetric interface systems (AmH^+,COO^-) vs. (COO^-,AmH^+) shows a difference in driving force of $0.15V$ and a difference in observed intramolecular electron transfer rates of only 3.

For each of these systems the energetics of the bipyridyl ligands surrounding the ruthenium play a role in the determination of the electron transfer reaction. Both the

carboxylic acid and amidinium functionalized bipyridyls should have π^* levels lying lower than that of the respective non-functionalized bipyridyl ligand despite the presence of the methyl substituent located at the 4 position. For the carboxylate functionalized bipyridyl ruthenium complex, however, the energy of the bipyridyl π^* level is expected to lie higher than that of the bipyridyl due to the presence of the carboxylate at the 4' position and also due to the additional presence of the methyl at the 4 position. Thus the energetics of the ligands are expected to be $\text{Me-bpy-AmH}^+ < \text{Me-bpy-COOH} < \text{bpy} < \text{Me-bpy-COO}^-$. Respectively. Electrochemical measurements of the reduction potentials $E_{1/2}(\text{Ru}^{2+}/\text{Ru}^{1+})$ and $E_{1/2}(\text{Ru}^{1+}/\text{Ru}^{0})$ of each of the complexes allow an assessment of these energetics and show a qualitative agreement to the expected trend. The relationship of the electrochemical data to the energetic splitting of the MLCT states may be expected since the charge transfer transition results in the placement of the electron in the π^* of the bipyridyl ligand and similarly the electrochemical measurement does likewise. However, the difference being that the charge transfer transition results in the change of the charge of the metal from Ru^{2+} to Ru^{3+} . Yet the irreversibility of the redox couples associated with the COOH and AmH^+ bipyridyl ligands obscure the direct observation and disallow the placement of the relative potentials of the ligands in each complex.

The electrochemical data do, however, allow an assessment of the magnitude of the participation of electron transfer contributions from the ancillary ligands. In a manner similar to that previously noted by Cooley et al. [100] the incorporation of the remote ligands in the observed electron transfer rates may be achieved through the use of Eq's. (3.3) and (3.4) accounting for the effects of the equilibrium established in charge transfer

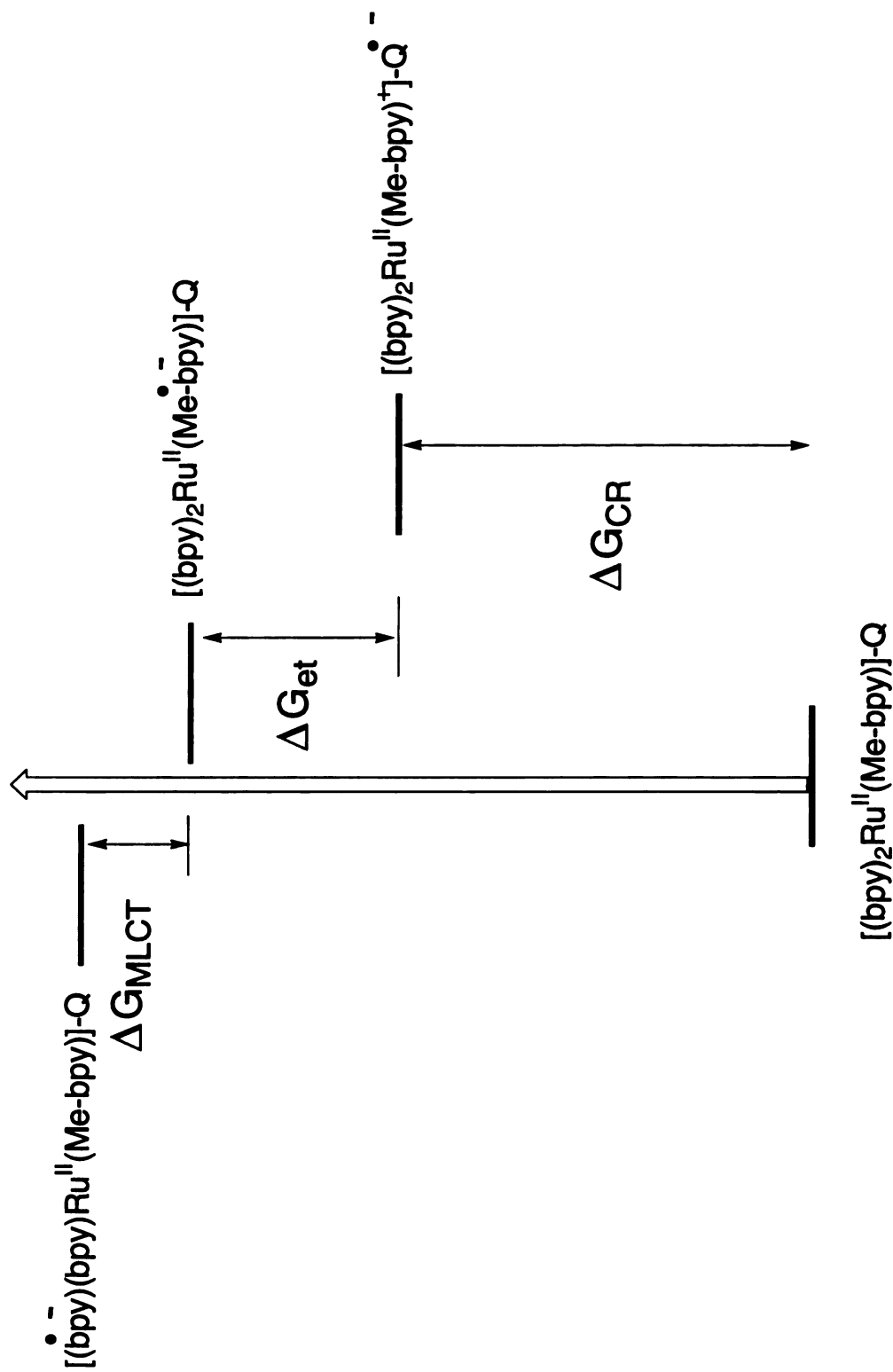


Figure 12. Energetic scheme for the excitation of the Ru(II)polypyridyl complexes $[(bpy)_2Ru^{2+}(Me-bpy)AmH^+]^3+$, $[(bpy)_2Ru^{2+}(Me-bpy)COOH]^2+$ $[(bpy)_2Ru^{2+}(Me-bpy)_2Ru^{2+}(Me-bpy)COO-]^+$ in CH_3CN at $22^\circ C$.

$$\alpha = \frac{K_{eq}}{1 + K_{eq}} \quad (3.3)$$

$$K_{eq} = \left(\frac{\eta_A}{\eta_R} \right) e^{-\left(\frac{E_{AR}}{RT} \right)} \quad (3.4)$$

to ligands η_A and η_R (adjacent and remote bipyridyls) having energetics of similar magnitude yielding the partitioning factor α . The magnitude of α in each of complexes derived from the measurement of the reduction potentials for adjacent bipyridyl ligands (E_A) and remote bipyridyl (E_R) (**9a-c**) is quite small. And more importantly for these complexes (**9a-c**) is the comparison of this energetic difference (E_{AR}) relative to the tris-bipyridyl ruthenium complex in which the value of E_{AR} is found to range from 180 - 200 mV in comparison to that observed for the Me-bpyCOO⁻ (220 mV), and Me-bpyAmH⁺ (210 mV). As a result the energy difference between the reduction potentials of the adjacent and remote bipyridyl ligands for each of the bipyridyls are no more than 50 mV which would yield $\alpha = 0.066$. This value for α is relatively insignificant amounting to 10-15% changes in the observed electron transfer rates. Thus the use of this estimation does not lie far outside of the error expected in collection of the lifetime decay measurements.

Alternatively, the evaluation of the participation of the remote ligands in the observed electron transfer may be determined through the assessment of the free energy of the excited state relative to the ground state for each of the salt-bridge functionalized bipyridyl complexes. Using the relationship given in Eq. (3.1) and (3.2) in combination with the emission spectra for each of the complexes supports these trends for the

changing electronic composition of the bipyridyls, reflected in the relative position of the emission maxima and calculated emission energetics summarized in Table 2. From these estimations it is seen that the energetic difference between the three ligands is quite small and that the excited electron is essentially delocalized over the three bipyridyls of the ruthenium complex.

This distribution of the charge transfer electron density is expected to participate in the observation of the electron transfer rate constant through the hydrogen-bonding interface. The similarity of the charge transfer energetics for transitions to each of the ligands thus obscure a measurement of the direct electron transfer rate constant corresponding to electron transfer through the hydrogen-bonding or salt-bridge interface. As a result these data suggest as has been previously shown for the symmetric $(\text{COOH})_2$ interface that the electron transfer rate exhibits a dependence on the proton interface. However, the data represented by the two asymmetric interface systems $(\text{AmH}^+, \text{COO}^-)$ and $(\text{COO}^-, \text{AmH}^+)$ suggest that the proton motion within the interfaces in an electron transfer reaction may be manifested in ways other than the electronic coupling as the suggested explanation of the observed electron transfer rates in the symmetric dicarboxylic acid interface [66]. In that case the proton displacement from one side of the interface is directly compensated by displacement of the proton at the other side. This symmetric configuration of protons allows a maximization of charge delocalization and the electronic coupling between the donor and acceptor facilitating the electron transfer. Yet, in this interface as a result of the neutral symmetric configuration little dependence upon coupling of the proton to the solvent is expected. However, in the asymmetric interfaces significant charge rearrangement upon proton motion in the interface is

expected [38]. A direct consequence of this charge rearrangement is the coupling of the solvent dipoles to the charge redistribution occurring upon the electron transfer. For each of the asymmetric interfaces the effects of the charge redistribution will be significantly different. In the case of the complex **(9b)** ($\text{AmH}^+, \text{COO}^-$) the electron transfer may influence the resulting proton transfer while for **(9c)** ($\text{COO}^-, \text{AmH}^+$) the proton is located such that the transfer of the proton does not occur. Thus for these two asymmetric systems effects of the proton (charge) within the salt-bridge interface are expected to yield significant coupling to the solvent potentially being manifested as differences in additional Franck-Condon factors for the intramolecular electron transfer event. Furthermore, the charge within the interface establishes a coulombic field over the salt-bridge, which is expected to enhance or attenuate the driving force for the electron transfer reaction. However, for these systems since the relative energetics of the bipyridyl ligands are such that the functionalized and non-functionalized ligands are energetically similar, observation of substantial differences in the electron transfer rate are not evident.

The results of tris-bipyridyl ruthenium(II) systems in which the energetics of the ancillary ligands are synthetically altered such that these issues may be further addressed is the subject of the Chapter 4.

CHAPTER 4

PHOTINDUCED ELECTRON TRANSFER WITHIN A SYNTHETICALLY MODIFIED RUTHENIUM DONOR ACCEPTOR PAIR:THE EFFECT OF SWITCHING THE SALT-BRIDGE INTERFACE

Introduction

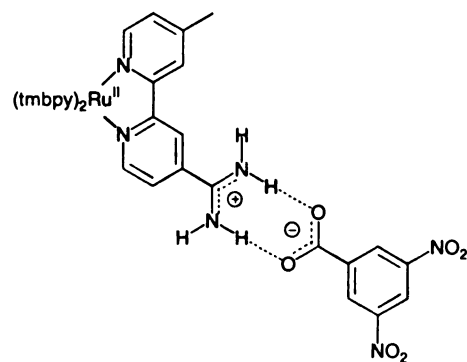
The definition of pathways in electron transfer studies has an established significance in the determination of the factors controlling the overall observed rate constant for an electron transfer event [10]. Specifically, in protein matrices, definition of the pathway for a particular electron transfer system, is principally predetermined by the protein structure. Secondary structure of the protein, composed of β -sheets, β -turns, and α -helices sets the overall tertiary structure of the protein. The shortest distance through this medium by which the electron may reach the acceptor from the donor will be the principle rate determining path. Detailed studies of the relative contributions of each type of protein sequence in relation to the observed electron transfer rates have been assessed

by Gray et al. [14]. More recently, the attachment of electron transfer donor and acceptor moieties to the ends of α -helical oligopeptide monomers [16] have begun to elaborate not only on the pathway through the peptide backbone, but also the direction of electron transfer within the pathway by the attachment of electron transfer donor and acceptor relative to the N-terminus and the carboxy-terminus of the α -helix. By these means effects of the electrostatic field, calculated by vacuum electrostatics to be as large as 10^9 V/m, generated between the ends of the oligopeptide are established. Wasielewski has prepared systems representative of the photosynthetic reaction center implementing the generation of an electrostatic field, by photoinduced electron transfer in a donor-acceptor pair ($d = 8.4$ Å). In these systems the assessment of the effects of an electrostatic field generated as a result of photoinduced electron transfer are monitored by the spectral features of a carotenoid probe molecule. The suggestion that is inferred in this system is the electrostatic field generated as a result of long range charge separation systems may perturb electron transfer in nearby donor acceptor systems, effectively tuning the redox potentials of these species and subsequently modify the electron transfer rate constants.

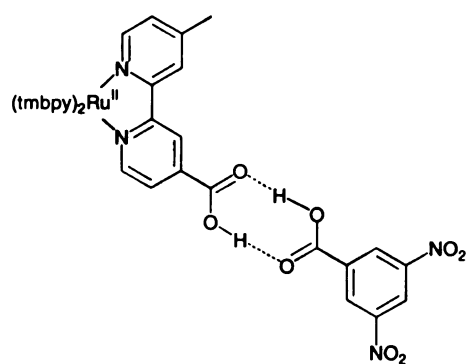
The relative energetics of the $d\pi-\pi^*$ (MLCT) charge transfer transitions in Ru(II) polypyridyl salt-bridge electron transfer complexes are determined by the ligand set. The implementation of ligands of different energetics ultimately may be responsible for influencing the overall pathway traversed by an electron through the intervening medium of an electron transfer donor-acceptor pair. Relative energetic splitting of the MLCT transitions to each of the ligands of a Ru(II) polypyridine complex may be determined through a comparison of electrochemical, absorption and emission data [68]. Although a recent study [71] suggests that an exact correlation does not exist between the

spectroscopic properties and the electrochemical data. Nonetheless, the ground state electrochemical data yields an assessment of the extent of the σ donating and π accepting capacities afforded by each of the ligands complexed to the central metal. Manipulation of the σ donating ability of the ligands via placement of electron donating groups at the ligand destabilizes metal centered $d\pi$ states making a poorer π -accepting ligand. Similarly, the addition of an electron withdrawing functionalities result in the net lowering of the π^* energy of the coordinated ligand resulting in decreases in the energy of the MLCT transition. For *tris*-heteroleptic Ru(II)bipyridyl complexes in which the different ligand substituents vary electronically, the dipole of the $d\pi$ - π^* MLCT charge transfer transition will be predominantly oriented toward the ligand lying at lower energy [71].

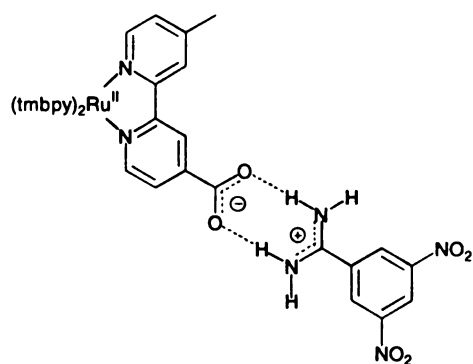
The determination of the localization of the excited electron in Ru(II) polypyridyl complexes has been thoroughly investigated by many different researchers [101]. Consistent with the electrochemical determinations, EPR experiments of chemically reduced $\text{Ru}(\text{bpy})_3^{2+}$ have shown that the signal observed is bipyridine based and is localized. For these complexes photoexcitation leading to the transfer of charge localized at the ligands has been verified by transient absorption and resonance Raman techniques. These investigations suggest that the ligand most easily reduced is the resulting location for the charge transfer. Findings of these studies suggest that the initial population of the electron resides at one ligand at timescales < 10 ns. Recent ultrafast spectroscopic studies have suggested that the localization of the excited state of ruthenium complexes is obtained in the first 500 fs of excitation [76].



(a)



(b)



(c)

Figure 13. Tetramethyl bipyridyl Ru(II) complexes for electron transfer through the salt-bridge interface formed by the association of the complimentary quenchers 3,5-dinitrobenzoate (a), 3,5-dinitrobenzoic acid (b) and 3,5-dinitrobenzamidine (c).

In addition to the splitting of the energetic levels for each of the respective charge transfer transitions, separation of the MLCT energetics with ligand variation has broad consequences in the overall symmetry of the complex. Thus, in addition to the energetic splitting, the different ligand electronic composition may impose a different point group symmetry to the complex, giving rise to electronic transitions having different basic photophysical details [69]. In the simplest sense, a tris-bipyridyl ruthenium complex may be considered as having a D_3 point group in the ground state. However, in the localized model [69,] charge transfer transitions make one of the ligands inequivalent, reducing the symmetry of the complex to a C_2 point group. Substitution of a ligand into a *tris*-bipyridyl ruthenium(II) complex having electronic composition different from the remaining ligands may impose reduced symmetry in the ground state of the complex resulting in an observable changes in the the charge transfer transitions [102]. Thus, the electron transfer donor/acceptor pathway for complexes formed via salt-bridge hydrogen bonding is critical for the determination and observation of an electron transfer rate through the interface.

Three tris-bipyridyl ruthenium(II) complexes used for the formation of the hydrogen-bonding and salt-bridge intramolecular electron transfer complexes $[(tmb)_2Ru^{2+}(Me-bpy)AmH^+]^{3+}$ $[(tmb)_2Ru^{2+}(Me-bpy)COOH]^{2+}$ and $[(tmb)_2Ru^{2+}(Me-bpy)COO^-]^+$ (tmb = 3,3',4,4'-tetramethyl-2,2'-bipyridine, $Me-bpyAmH^+$ = 4-methyl-4'-amidinium-2,2'bipyridine, $Me-bpyCOO^-$ = 4-methyl-4'-carboxylate-2,2'-bipyridine) incorporated these design features. Association of these complexes with the respective complimentary electron transfer quenchers 3,5-dinitrobenzoate ($DNBCOO^-$), 3,5-

dinitrobenzoic acid (DNBCA) and 3,5-dinitrobenzamidine (DNBA mH^+) respectively are shown in Figure (13).

Results

Electrochemistry

Results of the electrochemical measurements indicate that the three hydrogen-bonding salt-bridge functionalized complexes (**13a-c**) are typical for ruthenium(II) polypyridyl complexes in CH_3CN [68,103]. Since the reduction of the two protonated 3,5-dinitrobenzene quenchers 3,5-dinitrobenzamidine $^+$ (DNBA mH^+) and 3,5-dinitrobenzoic acid (DNBA) are irreversible by standard electrochemical techniques the determination of the potentials for these compounds was obtained by measurement of the deprotonated quenchers these potentials for each of the quenchers are shown in Table 4. These measurements suggest that the effective change in the potential upon protonation/deprotonation is 0.1 V.

Electronic Absorption and Luminescence photophysical characterization

For the $[(\text{tmb})_2\text{Ru}^{2+}(\text{Me-bpy})\text{COOH}]^{2+}$, $[(\text{tmb})_2\text{Ru}^{2+}(\text{Me-bpy})\text{AmH}^+]^{3+}$ and $[(\text{tmb})_2\text{Ru}^{2+}(\text{Me-bpy})\text{COO-}]^+$ complexes addition of the (tmb) ligands slightly alter the appearance and position of the absorption bands relative to those observed for complexes composed of 2,2'-bipyridyl ligands as seen in the absorption spectra for the three ruthenium complexes shown Figure (14).

For the $[(\text{tmb})_2\text{Ru}^{2+}(\text{Me-bpy})\text{AmH}^+][(\text{PF}_6)_3]$ complex (**13a**) the $d\pi-\pi^*$ (MLCT) absorption band indicates a distinct splitting with two maxima ($\lambda_{\text{max}} = 427$ and 490 nm).

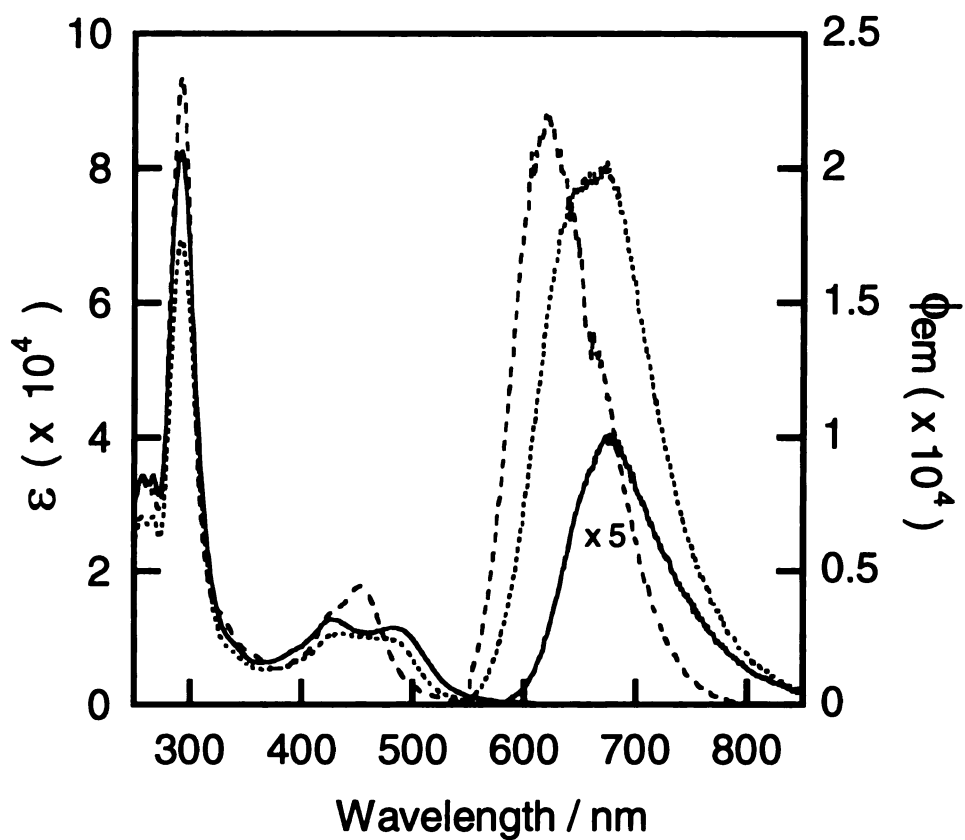


Figure 14 Absorption and Absolute emission of the three Ru(II) electron transfer complexes: $[(tmb)_2Ru^{2+}(Me-bpy)AmH^+]^{3+}$ (line), $[(tmb)_2Ru^{2+}(Me-bpy)COO^-]^+$ (dashed line), and $[(tmb)_2Ru^{2+}(Me-bpy)COOH]^{2+}$ (dotted line).

The intraligand $\pi-\pi^*$ absorption band has a single maxima ($\lambda_{\max} = 292$ nm), while the $[(\text{tmb})_2\text{Ru}^{2+}(\text{Me-bpy})\text{COOH}][(\text{PF}_6)_2]$ (**13b**) absorption spectra resembles that for the amidinium modified complex. However, the splitting of the $d\pi-\pi^*$ (MLCT) region is not nearly as distinct, still the observation of two maxima ($\lambda_{\max} = 433$ and 478 nm) are observed. The intraligand $\pi-\pi^*$ absorption spectra for this complex lies isoenergetically with that of the amidinium $\pi-\pi^*$ absorption band ($\lambda_{\max} = 292$ nm). Finally, the $[(\text{tmb})_2\text{Ru}^{2+}(\text{Me-bpy})\text{COO}^-][(\text{PF}_6)]$ (**13c**) complex exhibits an absorption spectra very similar to that observed for the *tris*- tetramethyl bipyridyl complex $[\text{Ru}(\text{tmb})_3]^{2+}[(\text{PF}_6)_2]$ having $d\pi-\pi^*$ (MLCT) absorption band maxima ($\lambda_{\max} = 456$ nm) and a less pronounced shoulder ($\lambda_{\max} = 426$ nm). The intraligand $\pi-\pi^*$ absorption for this complex is also found to be isoenergetic with the amidinium and carboxylic acid intraligand absorption bands ($\lambda_{\max} = 292$ nm). Absorption spectra for each of the protonated complexes (**13a**) and (**13b**) are typical for Ru(II)polypyridyl complexes having one or more ligands of distinctly different electronic composition [102]. The electronic absorption and emission spectral parameters for these three complexes as well as for three independently synthesized tris-homoleptic complexes formed from the respective ligands composing the electron transfer donor complexes are found in Table 5.

Emission spectra from 500 - 800 nm for each of the three Ru(II)polypyridyl complexes used in the intramolecular electron transfer studies are shown in Figure (14). Each of the emission spectra show broad gaussian shaped emission bands. For the $[(\text{tmb})_2\text{Ru}^{2+}(\text{Me-bpy})\text{AmH}^+][(\text{PF}_6)_3]$ the maxima of the emission is found ($\lambda_{\max} = 678\text{nm}$). For the complexes $[(\text{tmb})_2\text{Ru}^{2+}(\text{Me-bpy})\text{COOH}][(\text{PF}_6)_2]$ and $[(\text{tmb})_2\text{Ru}^{2+}(\text{Me-bpy})\text{COO}^-]$

Table 4. Electrochemical data for (tmb)₂Ru(II) complexes in CH₃CN at 22⁰C. E_{1/2} (V) vs. SCE.

Ru(II)polypyridyl	E _{1/2} (Ru ^{3+/2+})	E _{1/2} (Ru ^{2+/1+})	E _{1/2} (Ru ^{1+/0})	E _{1/2} (Ru ^{0/-})
(tmb) ₂ Ru ²⁺ AmH ⁺	1.02	-1.17*	-1.62	-1.82
(tmb) ₂ Ru(II)COOH	1.04	-1.06*	-1.65	-1.91
(tmb) ₂ Ru(II)COO-	1.02	-1.14*	—	—
(tmb) ₃ Ru(II)	1.01	-1.63	-1.82	-2.07

*irreversible redox couples values are estimated from the midpoint of the cathodic half of the cyclic voltammetric wave

Supporting electrolyte (0.1 M TBAH)

[(PF₆)] the emission maxima are found (λ_{max} = 658 and 618 nm) respectively. Quantum yield measurements for each of these complexes determined relative to a standard [Ru(bpy)₃²⁺] [(PF₆)₂] in CH₂Cl₂ yield values greatly reduced relative to CH₃CN as has been previously found for similar Ru(II)polypyridyl complexes [68]. Summary of the electronic absorption and emission data for each of the three electron transfer donor complexes (**13a-c**) and those for the three *tris*-heteroleptic complexes are given in Table5. Upon cooling to 77K each of the complexes give rise to distinct vibrational progressions ($\Delta\nu_{\text{av}}$ = 1480, 1850 and 1800 cm⁻¹) for [(tmb)₂Ru²⁺(Me-bpy)AmH⁺][(PF₆)₃], [(tmb)₂Ru²⁺(Me-bpy)COOH][(PF₆)₂] and [(tmb)₂Ru²⁺(Me-bpy)COO-][(PF₆)] respectively, typical of tris-bipyridyl ruthenium(II)complexes. Furthermore, lifetimes of low temperature glass samples are (τ = 4.38, 6.0 and 4.9 μ s) respectively, reflective of lifetimes for similar complexes [68].

Association Constants

The Ru(II)polypyridyl complexes appended with the amidinium and carboxylate functionalities readily form the salt-bridge with their complimentary acceptors in solution. Solution association of the respective components for each of the electron transfer complexes have been thoroughly characterized by NMR methods in DMSO-d₆ [79]. Determinations of the stoichiometry and strength of the interaction show 1:1 association from Job's plots and yield binding constants of 386 M⁻¹ and 2297 M⁻¹ for the [(tmb)₂Ru²⁺(Me-bpy)AmH⁺]³⁺ and [(tmb)₂Ru²⁺(Me-bpy)COO-]⁺ with the 3,5

Table 5. Ru(II) polypyridyl emission characterization data in CH₂Cl₂ 22⁰C. Excitation by Xe/Hg lamp at 435.8 nm

Ru(II) polypyridyl	λ_{max}	ϕ ($\times 10^2$)	$(\Delta\nu_{0,1/2})^2$ (cm^{-1})	ΔG_{es} (V)
(tmb) ₂ Ru ²⁺ AmH ⁺ (PF ₆) ₃	678	0.22	2278	2.23
(tmb) ₂ Ru ²⁺ COOH(PF ₆) ₂	658	2.6	2496	2.22
(tmb) ₂ Ru ²⁺ COO ⁻ (PF ₆)	618	2.1	2470	2.31
Ru ²⁺ (COOH) ₃ (PF ₆)	626	–	2105	2.22
Ru ²⁺ (AmH ⁺) ₃ (PF ₆) ₅	673	–	2476	2.17

dinitrobenzoate (DNBCOO⁻) and 3,5-dinitrobenzamidine (DNBA⁺) acceptors respectively.

The electrostatic interaction of the complimentary charges of the electron transfer donor and acceptor components comprising the salt-bridge are expected to yield significant association constants in CH₂Cl₂ solvent in which the solvent dielectric is ($\epsilon = 8.9$). Previously, it has been found for the association of the respective salt-bridge complexes that lowering of the solvent dielectric from DMSO-d₆ ($\epsilon = 48$) to CD₃CN ($\epsilon=36$) results in significant increases in the observed association constant [104]. However, the determination of the association constants in CH₂Cl₂ by NMR methods are not easily measured. For the [(tmb)₂Ru²⁺(Me-bpy)AmH⁺]³⁺-3,5-dinitrobenzoate complex absorption titrations reveal significant changes in the d π - π^* (MLCT) absorption region concomitant with increased concentrations of the complimentary 3,5 dinitrobenzoate in solution. Specifically, the split MLCT coalesces upon salt-bridge formation maintaining an isosbestic point at 487 nm as seen in Figure (15). Fitting of this data by the method of Wilcox [105] for the changes in the absorption spectra at 495 nm reveals association constants of $5.6 \times 10^5 \text{ M}^{-1}$. When the titration is instead performed with the benzoate complex similar changes in the absorption spectra are observed, revealing a slightly enhanced association constant of $8.5 \times 10^5 \text{ M}^{-1}$. Greater association for this complex is expected, as there are no electron withdrawing nitro groups present reducing the negative charge at the salt-bridge interface. For the complex formed by the association of [(tmb)₂Ru²⁺(Me-bpy)COOH]²⁺ with 3,5-dinitrobenzoic acid the changes observed in the

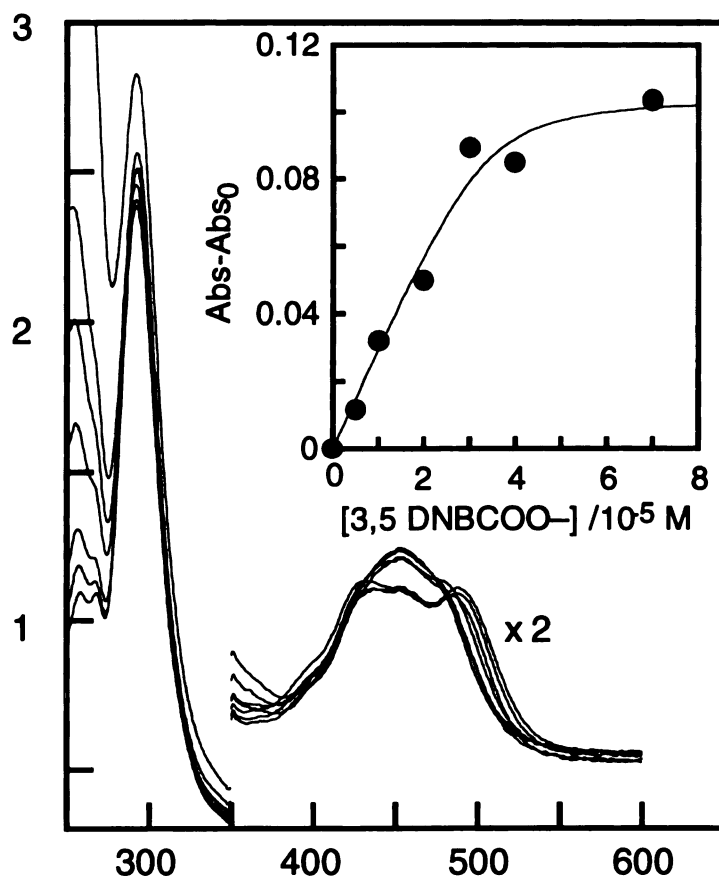


Figure 15 Association constant determination from Absorption titration of $[(\text{tmb})_2\text{Ru}^{2+}(\text{Me-bpy})\text{AmH}^+]^{3+}$ (3.0×10^{-5} M) with 3,5-dinitrobenzoate in CH_2Cl_2 . Inset plot shows the change in absorbance at 495 nm through the titration.

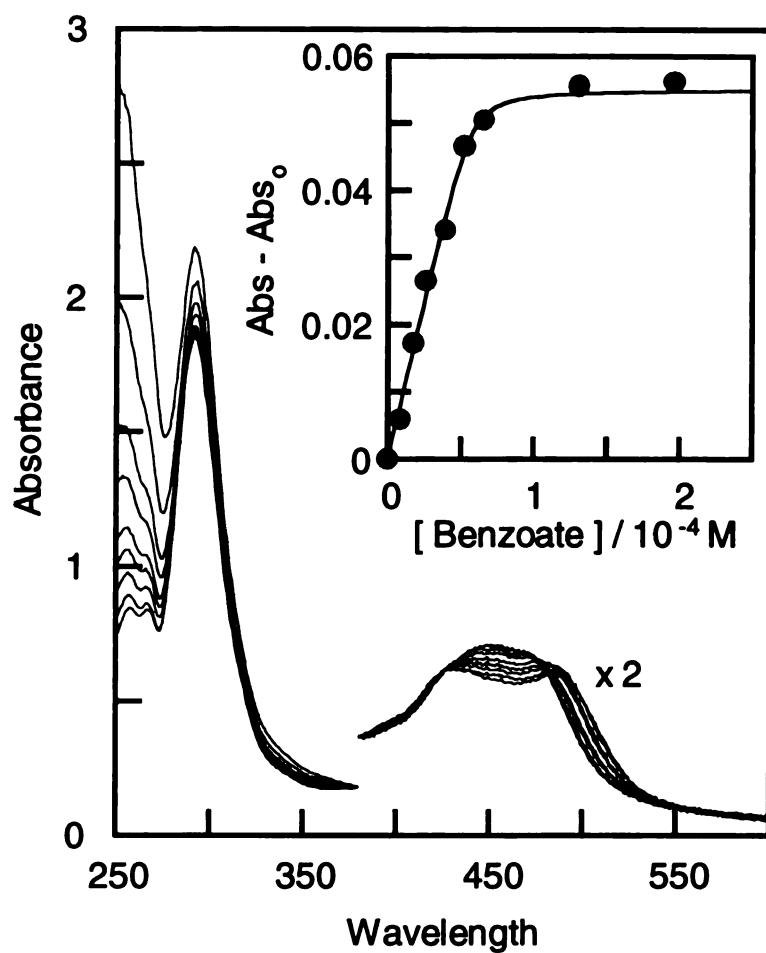


Figure 16. Association constant determination from Absorption titration of $[(tmb)_2Ru^{2+}(Me-bpy)AmH+]^{3+}$ ($3.0 \times 10^{-5} M$) with benzoate in CH_2Cl_2 . Inset plot shows the change in absorbance at 470 nm through the titration.

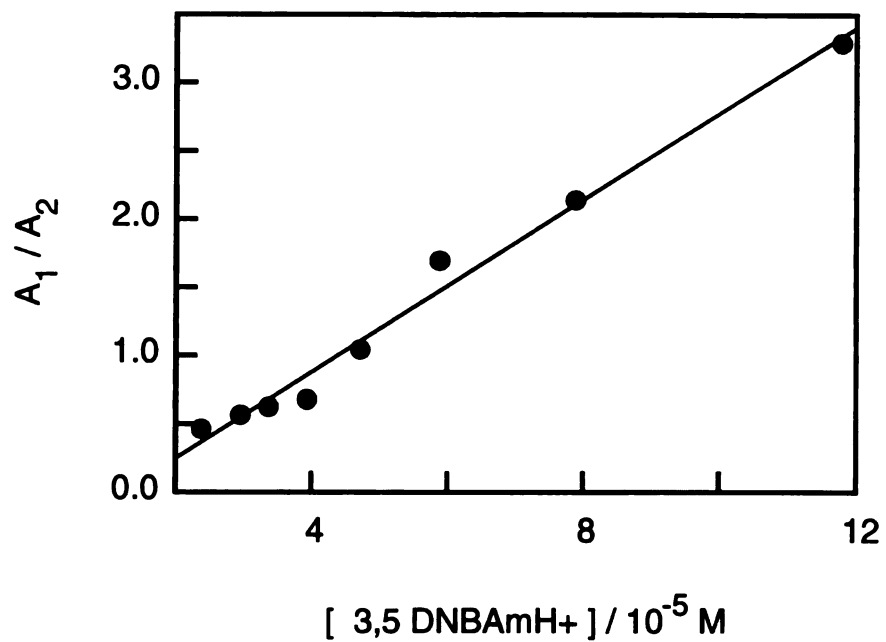


Figure 17. Association constant from the ratio of biexponential fit function prefactors (A_1 and A_2) of the lifetime decay of $[(\text{tmb})_2\text{Ru}^{2+}(\text{Me-bpy})\text{COO}^-]^+$ (0.10 mM) titrated with 3,5-dinitrobenzamidine.

absorption titration are not and this complex gives rise to association constants $K_a = \leq 1000 \text{ M}^{-1}$, similar to previous determinations of the association constant of $[(\text{bpy})_2\text{Ru}^{2+}(\text{Me-bpy})\text{COOH}]-3,5\text{-DNBA}$ complex found to be 702 M^{-1} . Titration of $[(\text{tmb})_2\text{Ru}^{2+}(\text{Me-bpy})\text{COO}^-]^+$ complex with the complimentary 3,5-dinitrobenzamidine does not reveal absorption changes lending accurate assessment of the association constant by absorption methods. However, infrared measurements performed with benzamidine monitoring the change of the C=N stretching region of the benzamidine complex reveal $K_a = 10^5 \text{ M}^{-1}$. Assessment of the association constant for this complex from the pre-exponential factors A_1 and A_2 of biexponential fitting of the lifetime data yield association constants for the complex $> 3.0 \times 10^4 \text{ M}^{-1}$ is shown in Figure (17).

The design of the excited state of the Ru(II)polypyridyl complex is crucial to a proper kinetics study of the electron transfer reactions of these complexes. Thus tetramethylating the ancillary bipyridyl ligands is necessary, as upon photoexcitation into the $d\pi-\pi^*$ (MLCT) state of the complex the oxidative electron transfer reaction may proceed by two potential different pathways.

For a complex in which the lowest energy MLCT excited state is localized on the salt-bridge modified Me-bpy ligand, photoexcitation will place the transferring electron directly into the PCET pathway. Alternatively, a lowest energy MLCT excited state involving the ancillary bipyridyl ligand will remove the excited electron from the PCET pathway. Consistent with this expectation as shown in Table 6 the energetic splitting of

the tetramethylated bipyridyl is removed from the PCET reaction pathway and thus the photoexcitation produces the desired orientation of the charge transfer transition.

Determination of Ru(II)polypyridyl complex energetics

The data in Table 5 allow the evaluation of the free energy of the excited state of each of the complexes. Analysis of the emission profiles of the three homoleptic complexes $[\text{Ru}^{2+}(\text{tmb})_3]^{2+}$, $[\text{Ru}^{2+}(\text{Me-bpyCOOH})_3]^{2+}$ and $[\text{Ru}^{2+}(\text{Me-bpyAmH}^+)_3]^{5+}$ allows the determination of the energy of the excited state for charge transfer to the salt-bridge functionalized ligands for each of the complexes. Accordingly, the evaluation of the excited state energy for the complexes may be determined according to the procedure developed by Meyer [2] and by Schuster [86] as described in Chapter 3. The data determined by this method are given in Table 5.

Luminescence and Lifetime Measurements

In the absence of electron transfer quenchers for each of the complexes exhibit long lived and monoexponential luminescence over 4τ of the decay data having lifetimes $\tau = 860, 770$ and 1030 ns for $[(\text{tmb})_2\text{Ru}^{2+}(\text{Me-bpy})\text{AmH}^+]^{3+}$, $[(\text{tmb})_2\text{Ru}^{2+}(\text{Me-bpy})\text{COOH}]^{2+}$ and $[(\text{tmb})_2\text{Ru}^{2+}(\text{Me-bpy})\text{COO-}]^+$ respectively.

Upon the addition of the complimentary benzoate, benzamidinium or benzoic acid complexes, energetically incapable of electron transfer reaction, the luminescence for each of the complexes is slightly altered. For the $[(\text{tmb})_2\text{Ru}^{2+}(\text{Me-bpy})\text{AmH}^+]^{3+}$ complex the emission is found to shift 10 nm to the blue and undergoes a concomitant 10% relative increase in the emission intensity. For the $[(\text{tmb})_2\text{Ru}^{2+}(\text{Me-bpy})\text{COOH}]^{2+}$ very

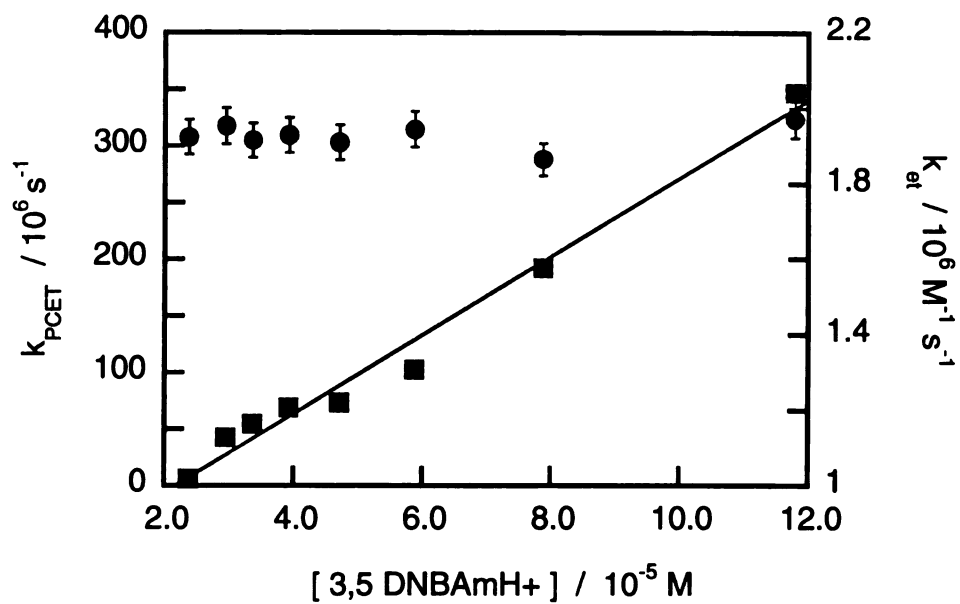


Figure 18 Concentration-dependent (■) and concentration-independent (●) observed rate constants for the quenching of [(tmb)₂Ru²⁺(Me-bpy)COO⁻]⁺ (0.10 mM) by 3,5-dinitrobenzamidinium in CH₂Cl₂

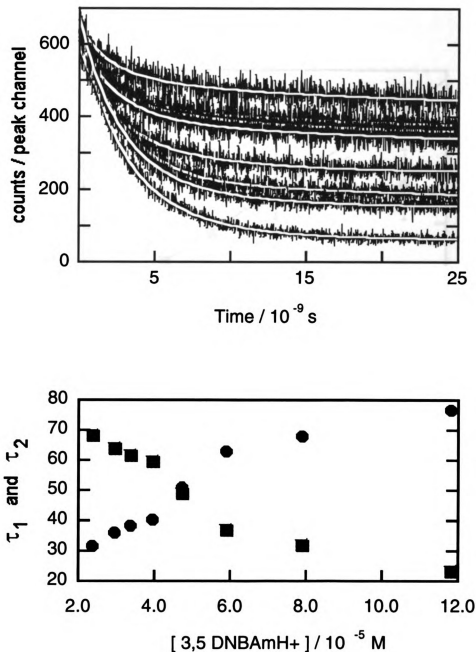


Figure 19. Top panel. Lifetime decay data for the quenching reaction between $[(\text{tmb})_2\text{Ru}^{2+}(\text{Me-bpy})\text{COO-}]^+$ and 3,5-dinitrobenzamidinium. Biexponential fitting of the decay data is indicated with the solid line. Bottom panel. Relative percentages of the biexponential fitting of the decay data from Top panel.

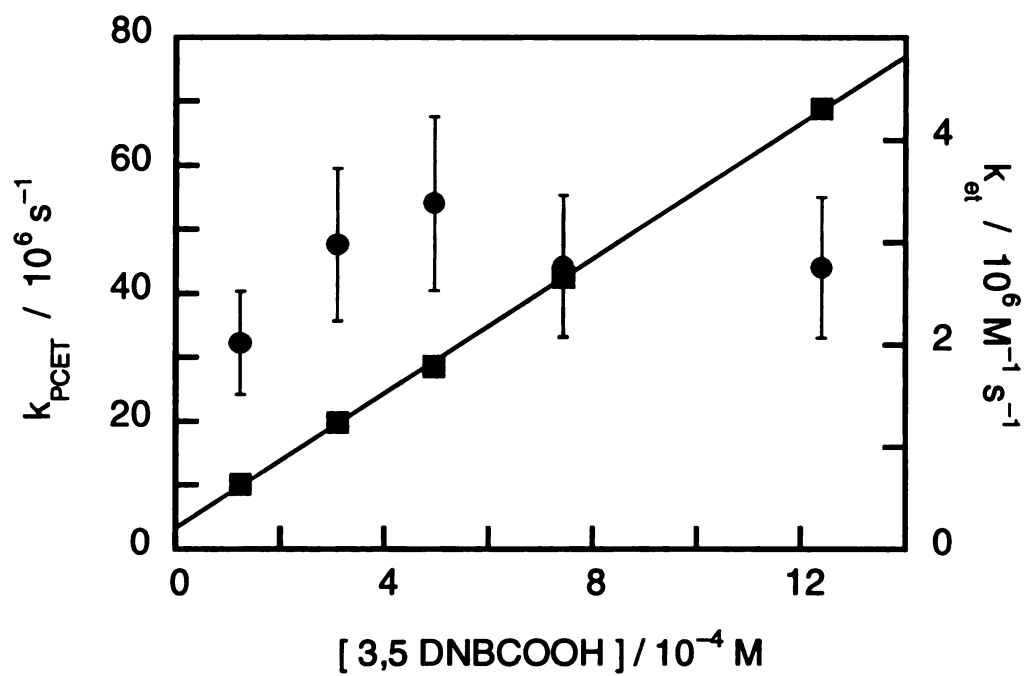


Figure 20. Concentration-dependent (■) and concentration-independent (●) observed rate constants for the quenching of $[(\text{tmb})_2\text{Ru}^{2+}(\text{Me-bpy})\text{COOH}]^{2+}$ (0.06mM) by 3,5-dinitrobenzoic acid in CH_2Cl_2 .

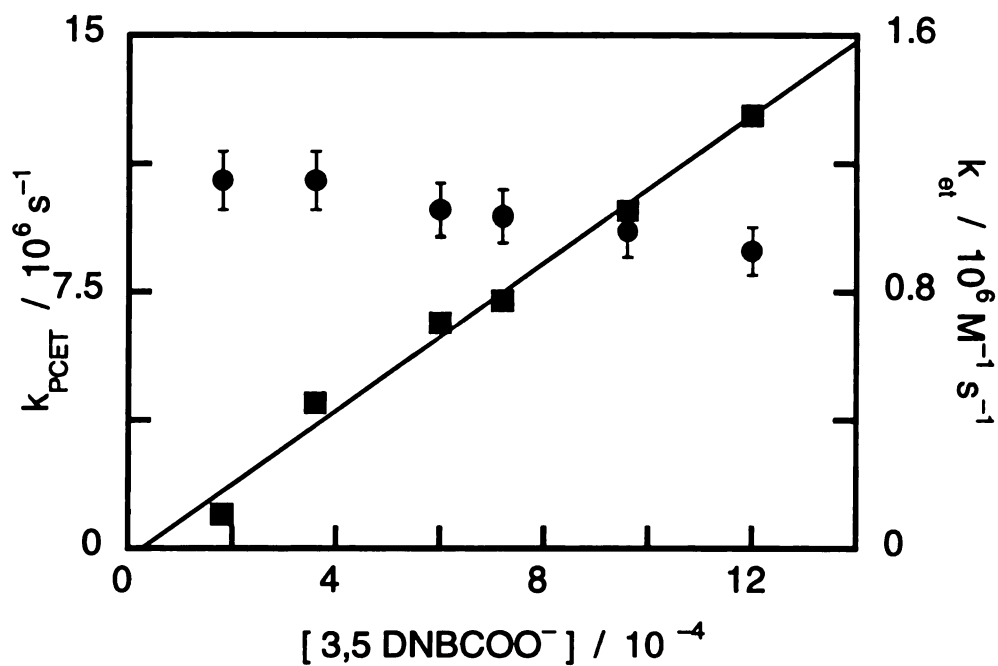
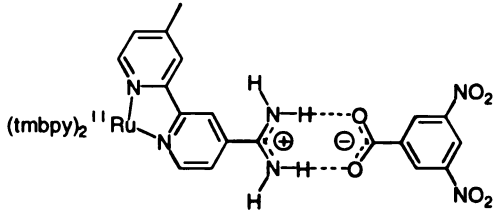
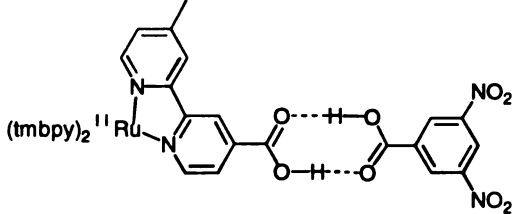
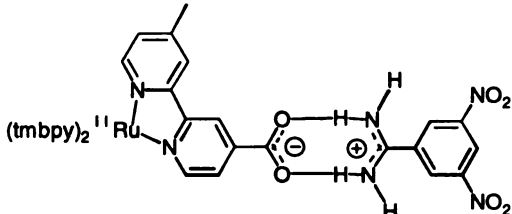


Figure 21. Concentration-dependent (■) and concentration-independent (●) observed rate constants for the quenching of [(tmb)₂Ru²⁺(Me-bpy)AmH⁺] (0.064mM) by 3,5-dinitrobenzoate in CH₂Cl₂.

Table 6. Rates for concentration-dependent and concentration-independent quenching of (tmb)₂Ru(II) electron transfer complexes.

Salt Bridge Complex	$\Delta G^0 / \text{eV}$	k_{ET} ($\times 10^9 \text{ M}^{-1} \text{ s}^{-1}$)	k_{PCET} ($\times 10^6 \text{ s}^{-1}$)
 <p>(13a)</p>	-0.14	1.2	8.4
 <p>(13b)</p>	-0.34	3.3	43
 <p>(13c)</p>	-0.23	3.2	310

little difference is observed in emission spectra upon addition of benzoic acid showing only a slight 5 nm red shift observed concomitant with little 5% relative change in the emission intensity. For the $[(\text{tmb})_2\text{Ru}^{2+}(\text{Me-bpy})\text{COO-}]^+$ the addition of benzamidinium results in observation of a 10 nm red shift of the emission maximum and a 10% increase in the emission intensity. Lifetimes obtained for each of the complexes bound to benzoate, benzamidinium, and benzoic acid are long lived having excited state lifetimes of $\tau = 1200, 470, \text{ and } 895 \text{ ns}$ for $[(\text{tmb})_2\text{Ru}^{2+}(\text{Me-bpy})\text{COO-}]^+$, $[(\text{tmb})_2\text{Ru}^{2+}(\text{Me-bpy})\text{AmH+}]^{3+}$ and $[(\text{tmb})_2\text{Ru}^{2+}(\text{Me-bpy})\text{COOH}]^{2+}$ respectively. Upon the addition of the complimentary 3,5-dinitrobenzene quenchers the luminescence is dramatically quenched.

Excited state lifetimes of each of the tetramethylated Ru(II) complexes in the presence of the quenching 3,5 dinitroaromatic complexes are biphasic. One component of the emission decay is clearly dependent upon the concentration of the quencher whereas the other component remains concentration-independent. Concentration-dependent lifetimes for these complexes are attributed to bimolecular electron transfer quenching of the unbound Ru(II)polypyridyl complexes. For this component, the quenching obeys typical linear Stern-Volmer quenching kinetics yielding electron transfer rates given in Table 6. The observed bimolecular electron transfer rates for each of these three complexes are found in Table 7. Similar observations are found for equi-exergonic reactions of Ru(II)polypyridyl complexes with nitroaromatic quenchers [3] consistent with the determination of bimolecular electron transfer reactions in these complexes. Of greater relevance to the investigation of PCET are the attendant concentration-independent rate constants, which are attributed to the unimolecular electron transfer of each complex associated by the hydrogen bonding salt- bridge interactions. For the two

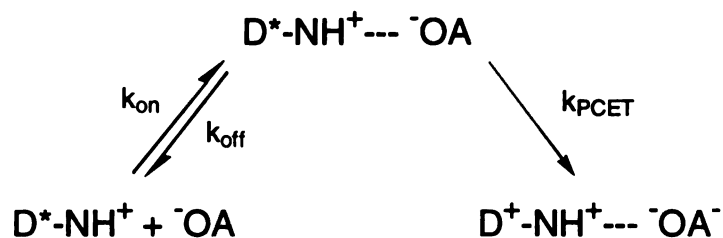
salt-bridging complexes $[(\text{tmb})_2\text{Ru}^{2+}(\text{Me-bpy})\text{COO-}]^+$ and $[(\text{tmb})_2\text{Ru}^{2+}(\text{Me-bpy})\text{AmH+}]^{3+}$ the observed differences in the unimolecular rates are seen to depend significantly on the salt-bridge and its orientation with respect to the electron transfer pathway as is seen in Figures (19-22)

Discussion

The observation of luminescence lifetime quenching in these complexes is indicative of electron transfer occurring through the salt-bridge interface. For each complex the bimolecular component of the lifetime corresponds well with the static quenching results. For the $[(\text{tmb})_2\text{Ru}^{2+}(\text{Me-bpy})\text{COO-}]^+$ associated with 3,5 dinitrobenzamidine 83 % relative quenching in the emission experiments is observed over a range identical to that used in the lifetime quenching experiments. In the determination of the bimolecular contribution to the observed lifetime quenching the relative change in the free complex quenching component is found to be 67 % quenched. Finally, for this complex the measurement of the fast PCET component of the quenching allows the additional assessment to be made for the relative quenching of the free Ru(II) complex by the analysis of the pre-exponential factors of the biexponential curve fitting. In Figure (18) contributions from both concentration-independent PCET component A_1 and the concentration-dependent component A_2 reveal 80% quenching of the free complex lifetime through the concentration range. This is strong support that the quenching occurs by electron transfer and furthermore, that the mechanism of the quenching is the same. In the bimolecular quenching observed in static quenching experiments for the $[(\text{tmb})_2\text{Ru}^{2+}(\text{Me-bpy})\text{AmH+}]^{3+}$ complex formed with the

complimentary 3,5-dinitrobenzoate quencher similar observations are made revealing a relative reduction of the emission intensity by 37% and quenching of the free complex lifetime measurements a relative change in lifetime of 67 % are observed.

Several issues of the electron transfer relevant to the association constant determinations in the two salt-bridge complexes (13a) and (13c) are important for the establishment of the intracomplex electron transfer rate constant. The interaction between the electron transfer donor and acceptor in a non-covalent system is predicated upon the establishment of an equilibrium between bound and unbound quencher during the long excited state lifetime $\sim 1\mu\text{s}$ ($k_r = 1.0 \times 10^6 \text{s}^{-1}$) of the ruthenium complexes. A manifestation of this equilibrium process is the competition of the rate of the electron



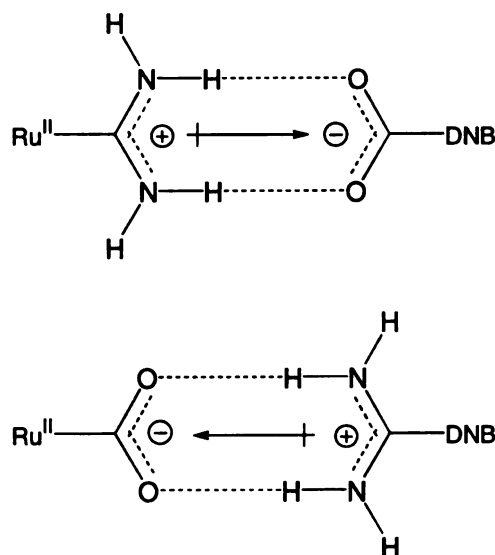
(4.1)

transfer relative to the dissociation rate of the quencher complex. If the rate of the interaction of the two complimentary species in solution may be considered as limited only by diffusion, then the maximal rate at which the two species may encounter one another is approximately k_D for $\text{CH}_2\text{Cl}_2 = 4 \times 10^{10} \text{M}^{-1} \text{s}^{-1}$ in CH_2Cl_2 solvent and not substantially different in CH_3CN , k_D being established for nitro aromatic oxidative electron transfer quenchers as $2 \times 10^{10} \text{M}^{-1} \text{s}^{-1}$ [3]. For the $[(\text{tmb})_2\text{Ru}^{2+}(\text{Me-bpy})\text{COO}^-]^+$ complex the association constant between the two species is found from the A_1/A_2 ratio

of the biexponential fitting of the lifetime decay to be $3.2 \times 10^4 \text{ M}^{-1}$. The maximal off rate for this complex (**13c**) will effectively be $1.25 \times 10^6 \text{ s}^{-1}$. The observed PCET rate for this complex is $310 \times 10^6 \text{ s}^{-1}$, yielding a $k_{\text{PCET}}/k_{\text{off}}$ ratio of 250. For the remaining two systems, the observed PCET rate constant is found to be $43 \times 10^6 \text{ s}^{-1}$ for $[(\text{tmb})_2\text{Ru}^{2+}(\text{Me-bpy})\text{COOH}]^{2+}$ (**13b**) and $8.4 \times 10^6 \text{ s}^{-1}$ for $[(\text{tmb})_2\text{Ru}^{2+}(\text{Me-bpy})\text{AmH}]^{3+}$ (**13a**). In each case the maximal expected off rate constant will be $4 \times 10^7 \text{ s}^{-1}$ ($k_{\text{PCET}}/k_{\text{off}} = \sim 10$) and $7.1 \times 10^4 \text{ s}^{-1}$ ($k_{\text{PCET}}/k_{\text{off}} = 120$), respectively. Thus only in the $(\text{COOH})_2$ system will the effect of the excited state equilibrium be significant, as the observed PCET rate constant is of the same order of magnitude as the predicted off rate. However, the equilibrium established in the electron transfer measurements is with the electronically excited Ru(II) complex and not the ground state complex, as is measured by the absorption titrations. Yet the typical ΔpKa for Ru(II)polypyridyl complexes between ground and excited state is ~ 3 ; for instance, Ru(II) bipyridyls directly appended with carboxylic acids exhibit ΔpKa of 2.5 [106,68]. Hence the observed intramolecular electron transfer decay rates well exceed the equilibration rates, and intramolecular electron transfer occurs for a static complex. This is not the case for the symmetric dicarboxylic acid complex (**13b**) in which it is expected that the PCET rate is complicated by a dynamic equilibrium between the donor and the acceptor.

In addition to the charges at the interface significantly enhancing the association constants for each of the salt-bridge functionalized complexes as is reflected in the association constant determinations. The charge at the interface is expected to be directly affected by the presence of the nitro groups of the quenchers. For the amidinium this is expected to increase the relative positive charge, and conversely for the carboxylate the

electron withdrawing nitro groups are expected to stabilize the negative charge at the interface thus reducing the strength of the salt-bridging interaction. A direct relationship may be expected between the association constant and the electronic coupling as the efficiency of the electronic coupling may be manifested in the differences in the strengths of the salt-bridging interaction [107]. The stronger interaction of the salt-bridge will be expected to enhance the mixing of the donor and acceptor states relative to the symmetric dicarboxylic acid (COOH)₂ interface in which it has been previously assessed that the electronic coupling is $\sim 10\text{cm}^{-1}$ [66]. Infrared data for the two salt-bridge complexes (13a) and (13c) suggest that the shifts of the amidinium C=N stretch change by 20 cm^{-1} in the complex formed from $[(\text{bpy})_2\text{Ru}^{2+}(\text{Me-bpy})\text{AmH}^+]^{3+}$ with 3,5-dinitrobenzoate C=N



(4.2)

stretches changing from while for $[(bpy)_2Ru^{2+}(Me-bpy)COO-J]^+$ with benzamidinium a 25 cm^{-1} shift is found. These shifts are consistent with shifts found for C=N in schiff base complexes [108].

More significantly, is the effect of charge in the salt-bridge on the observed, differences in the intramolecular electron transfer rates. In complex **(13a)** the permanent dipole ($\delta^+\delta^-$) of the (AmH⁺,COO⁻) salt bridge lies in the direction of electron transfer whereas in **(13c)** the electron transfer opposes the (COO⁻,AmH⁺) salt-bridge dipole as schematically represented in Figure (4.2). Additionally, internal electrostatic fields created as a result of the charged salt-bridge interface affecting the rates of electron transfer by altering the driving force of the reaction in the complex relative to that for the isolated constituents [109]. Using typical bond distances for $Ru(bpy)_3^{3+/2+}$, and dinitrobenzene^{0/-} and the amidinium-carboxylate salt-bridge, a determination of the field effect for these interfaces from the Eq. (4.2) yields 0.37 V. The magnitude of the internal

$$E_c = \frac{q_1q_2}{\epsilon r} \quad (4.2)$$

field effect is expected to be will be favorable for complex **(13a)** and thus unfavorable for complex **(13c)** effectively augmenting the relative driving force for intramolecular electron transfer in complex **(13a)**. The thermodynamic attenuation of the electron transfer rate constant for **(13c)** may be further augmented by a greater reorganizational energy associated with the salt-bridge. In **(13a)** accompanying proton transfer (from the Ru(II) amidinium donor to the carboxylate acceptor) can stabilize the charge of the electron as it develops on the acceptor. In this case, since the proton charge is strongly coupled to the solvent dipoles, as with the electron, charge shift within the salt bridge

may be accompanied by significant solvent polarization thereby giving rise to additional Franck-Condon factors for the electron transfer reaction. This is not the case for (13c). Here, the proton is already residing on the acceptor, and hence it is likely to remain upon the arrival of the electron.

The assessment of the electron transfer rates found for each of the asymmetric salt-bridge interfaces may be analyzed in terms of semi-classical electron transfer theory as given in Eq. (4.3). Under the assumption that the electronic coupling (V_{ab}) of the two interfaces is the same and equal to 20cm^{-1} , and furthermore, that the outer-sphere

$$k_{et} = \frac{2\pi}{\hbar} |V_{ab}|^2 (4\lambda k_B T)^{-1/2} \exp\left[-\frac{(\Delta G + \lambda)^2}{4\lambda k_B T}\right] \quad (4.3)$$

contribution (λ_o) to the reorganizational energy (λ) of each system may be found from a two-sphere dielectric continuum model [2,110] ($\lambda = \lambda_o + \lambda_i$) according to Eq. (4.4). Substituting into Eq. (4.4) the diameter of the Ru(II) polypyridine ($d = 14.5 \text{ \AA}$,

$$\lambda_o = \left(\frac{e^2}{4\pi\epsilon_o} \right) \left(\frac{1}{2r_D} + \frac{1}{2r_A} - \frac{1}{R_{DA}} \right) \left(\frac{1}{\epsilon_{op}} - \frac{1}{\epsilon_s} \right) \quad (4.4)$$

$r_D = 7.25 \text{ \AA}$) and for the dinitrobenzene complexes ($d = 7.1 \text{ \AA}$, $r_A = 3.55 \text{ \AA}$) estimated from molecular modeling (Spartan) and that the inner sphere reorganizational energy for each interface is the same and equal to a maximum expected [111] value $\lambda_i = 0.25\text{V}$ yielding $\lambda = 0.75\text{V}$. The ϵ_{op} and ϵ_s for CH_2Cl_2 are the optical dielectric constant (the

square of the refractive index) 2.03 and the static dielectric constant 9.08 respectively e^2 the charge for and electron and $4\pi\epsilon_0$ the vacuum permittivity, yield the expected electron transfer rates based upon the free energy of reaction [AmH⁺,COO⁻ ($\Delta G = -0.14V$)] and [COO⁻,AmH⁺ ($\Delta G = -0.34 V$)] for each interface system [k_{et} (AmH⁺,COO⁻) = $214 \times 10^6 s^{-1}$] and that for the switched analogue [k_{et} (COO⁻,AmH⁺) = $3240 \times 10^6 s^{-1}$]. Thus each of these predicted electron transfer rates are found to be effectively 25 and 10 times greater for each of the (AmH⁺,COO⁻) and (COO⁻,AmH⁺) interfaces respectively. Further modifying the semi-classical electron transfer equation to bring the theoretical rates to the observed values again assuming that the electronic coupling for each interface is the same requires increasing the reorganizational energy λ for each (AmH⁺,COO⁻) and (COO⁻,AmH⁺) interfaces to 1.2 and 1.15V respectively or $\sim 0.5V$ greater than the predicted reorganizational energy found from the simple spherical reactant continuum dielectric models.

Recently, Cukier [67] has shown that a representation for observed electron transfer rates in asymmetric proton coupled-electron transfer systems may be given according to Eq's. (4.5) and (4.6). Here the additional reorganizational energy associated

$$k_{et} = \frac{2\pi}{h} |V|^2 (E_s k_B T)^{-1/2} \sum_{v=0} \left| \langle O_i | v_f \rangle \right|^2 \exp - \left[\frac{(E_s + \Delta G + h\omega v)^2}{4E_s k_B T} \right] \quad (4.5)$$

$$\left| \langle O_i | v_f \rangle \right|^2 = \left(e^{-S} \frac{S^p}{p!} \right) \quad (4.6)$$

with the coupling of the proton to the solvent is given as a summation over available proton vibrational levels, Eq. (4.6), initial (i) and final (f) associated with the localization of the proton during the electron transfer event.

These results show that intervening salt bridges can significantly affect the rates of intramolecular electron transfer reactions and may provide an insight into the coupled proton/electron transfer events found in photosynthetic [112] and respiratory [113] biological systems and the more recent example given by Brzezinski [47] in cytochrome *c* oxidase.

CHAPTER 5

PHOTOINDUCED REDUCTIVE ELECTRON TRANSFER WITHIN AN ELECTRON DONOR-ACCEPTOR PAIR:ASSESSMENT OF THE REVERSAL OF THE ELECTRON TRANSFER DIRECTION

Introduction

The directionality of electron transfer processes is crucial to the effective function of many biological organisms. This necessity for directional electron transfer reactions is of fundamental importance to the storage of solar energy for conversion to necessary metabolites. Necessarily this scheme requires maintainance of a stable charge separated state which can undergo useful chemical reactions in competition with the deleterious back electron transfer reaction. A means by which this may be accomplished is to control the direction of the electron transfer reaction. A premier example of the directional electron transfer reactions coupled to chemical reactions is found in photosynthetic [112] and respiratory [113] biological systems. Prevention of the energy wasting back electron transfer effectively accomplishes the the task. A particular objective recently has been the

mechanistic and theoretical experiments detailing directional electron transfer in the photosynthetic reaction center. Absorption of light in and subsequent energy transfer to the special pair leads to the selective and directional electron transfer through the L subunit rather than the structurally identical M subunit. Recent investigations have applied a variety of different spectroscopic techniques aimed at unraveling the details of this directionality [17]. Many suggestions are centered on the dielectric asymmetry of the RC environment, the Coulombic (electric field) asymmetry has been shown in the work of Honig as a potential explanation, and also the incorporation of hydrogen-bonding interactions of particular residues of the peptide backbone encompassing the reaction center have all been suggested as playing potential roles in the asymmetric electron transfer in this system.

Yet another recent example indicating directional and specific electron transfer has been shown in cytochrome *c* oxidase in which the rate of electron transfer along the heme *a*₃ is found to be 10⁴ times greater than that observed along the nearly identical (structurally and distance) heme *b* pathway. Furthermore in this system the potential control of the observed electron transfer rate has implicated the coupling of proton transfer. Yet the nature and complexity of each of these systems, photosynthetic reaction centers and the cytochrome *c* oxidase do not allow the thorough investigation of each of the speculated controlling interactions.

The design of model systems based upon the electron transfer reactions of Ru(II)polypyridyl systems functionalized with salt-bridging substituents allow the control of the direction of electron transfer reactions. To this end a systematic series of *tris*-bipyridyl ruthenium(II) complexes was designed to explore reductive electron transfer

reactions. This orientation of electron transfer donor and acceptor maintain the previously developed directionality of the asymmetric hydrogen-bonding salt-bridge interface while reversing the direction of the electron transfer. Thus, use of the oxidation capacity of the excited state of the Ru(II)polypyridyl complexes allows an electron transfer to be elicited from an organic donor associated through the salt-bridge interface. Electron transfer reactions for this orientation of donor and acceptor may be regarded as a hole transfer where the excitation of the charge transfer state of the ruthenium complex creates a metal centered Ru^{3+} hole upon formation of which an electron is transferred from the acceptor through the salt-bridge functionalized bipyridine.

Crucial to the unambiguous observation of electron transfer in these Ru(II)polypyridyl systems is the energetic splitting of the MLCT states between the ancillary and salt-bridge functionalized bipyridine ligands. For bipyridine based systems charge transfer to the ligand having the lowest lying reduction potential results in the localization of the excited state electron at the amidinium functionalized bipyridine. For the carboxylate functionalized complex, due to the higher energy MLCT transition of carboxylate, electron localization is maintained at the ancillary bipyridine ligands. To further facilitate the resultant excited state charge transfer localization onto ancillary ligands, electron withdrawing substituents have been incorporated, specifically, two 4,4'-diethylcarboxy-2,2'-bipyridine (decb) ligands. Four Ru(II) systems Figure (23a-d) have been synthesized composed of the electron transfer acceptor complexes $[(\text{bpy})_2\text{Ru}^{2+}(\text{Me-bpy})\text{AmH}^+]^{3+}$, $[(\text{bpy})_2\text{Ru}^{2+}(\text{Me-bpy})\text{COO}^-]^+$, $[(\text{decb})_2\text{Ru}^{2+}(\text{Me-bpy})\text{AmH}^+]^{3+}$ and $[(\text{decb})_2\text{Ru}^{2+}(\text{Me-bpy})\text{COO}^-]^+$ (bpy = 2,2'-bipyridine, decb = 4,4'-diethylcarboxy-2,2'-bipyridine, Me-bpyAmH⁺ = 4-methyl-4'-amidinium-2,2'-bipyridine, and Me-bpy-COO⁻ =

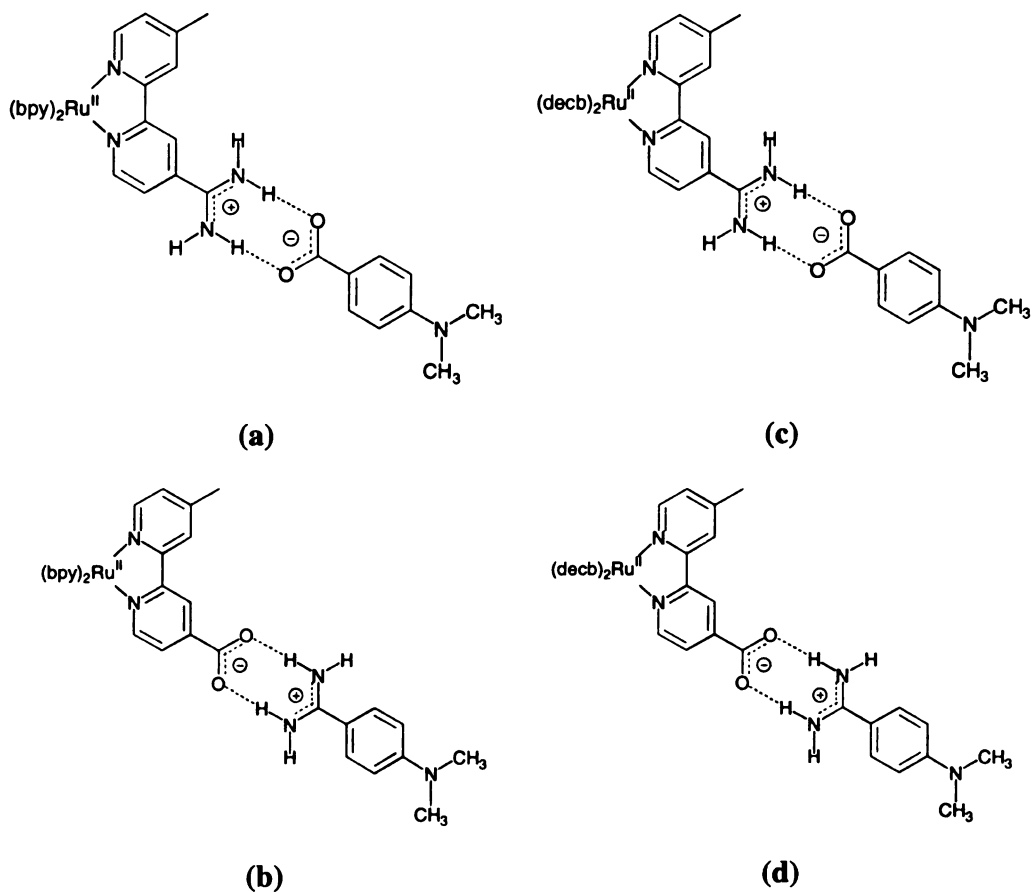


Figure 22. Ru(II)polypyridyl complexes for reductive electron transfer quenching (a) $[(bpy)_2Ru^{2+}(Me-bpy)AmH]^+{}^{3+}$ (b) $[(bpy)_2Ru^{2+}(Me-bpy)COO^-]^+$, (c) $[(decby)_2Ru^{2+}(Me-bpy)AmH]^+{}^{3+}$ and (d) $[(decby)_2Ru^{2+}(Me-bpy)COOH]^{2+}$. Figures shown are the salt-bridged complexes formed from the 1:1 association with N,N'-dimethylaminobenzoate and N,N'-dimethylaminobenzamidinium

4-methyl-4'-carboxylate-2,2'-bipyridine) upon formation of the salt-bridge with the organic donors N,N'-dimethylaminobenzoate and N,N'-dimethylaminobenzamidinium.

Results

Electronic Absorption / Emission Spectroscopy

Absorption profiles for the two bipyridine complexes are typical for Ru(II)bpy complexes [68] having a high energy $\pi-\pi^*$ intraligand absorption band and a low energy $d\pi-\pi^*$ MLCT absorption band. These spectral features are maintained for the amidinium and carboxylate modified complexes. Absorption and emission spectra for each of the ruthenium complexes are shown in Figures (24) and (25). The distinguishing differences evident in the absorption spectra for the two (decb) modified complexes of moderate intensity observed at the low energy tail of the intense intraligand band and high energy tail of the MLCT are typical of complexes with alkyl and ester modified bpy ligands. For instance, Ru(II)*tris*(decb) exhibits transitions at 355 and 407 nm [103a], which are energetically coincident with the additional transitions appearing in the absorption spectra of the amidinium modified ($\lambda_{\text{max}} = 356$ and 405 nm) and carboxylate modified ($\lambda_{\text{max}} = 366$ and 400 nm) (decb) complexes. Similarly, Ru(II) *tris*(dimethylbipyridine) shows absorption features at 328 and 360 nm [114]. These transitions of the alkyl and ester modified bpy ligands are believed to be MLCT in character. Summary of the electronic absorption spectra for each of the Ru(II) complexes are given in Table 7. Figures (26 - 29) display the changes for each of the Ru(II) bpy complexes (23a-d) occurring upon the

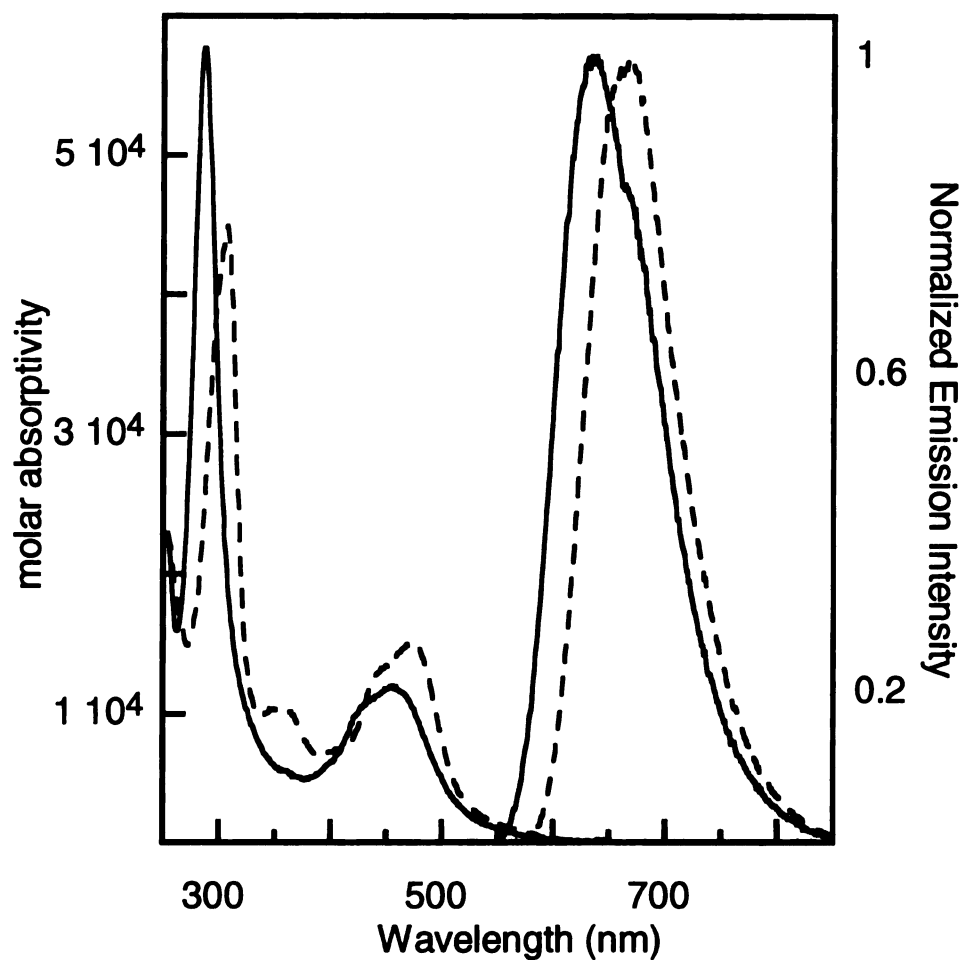


Figure 23. Absorption and emission spectra for amidinium functionalized electron transfer donor complexes $[(bpy)_2Ru^{2+}(Me-bpy)AmH^+]^{3+}$ and $[(decb)_2Ru^{2+}(Me-bpy)AmH^+]^{3+}$ in aerated CH_3CN solution.

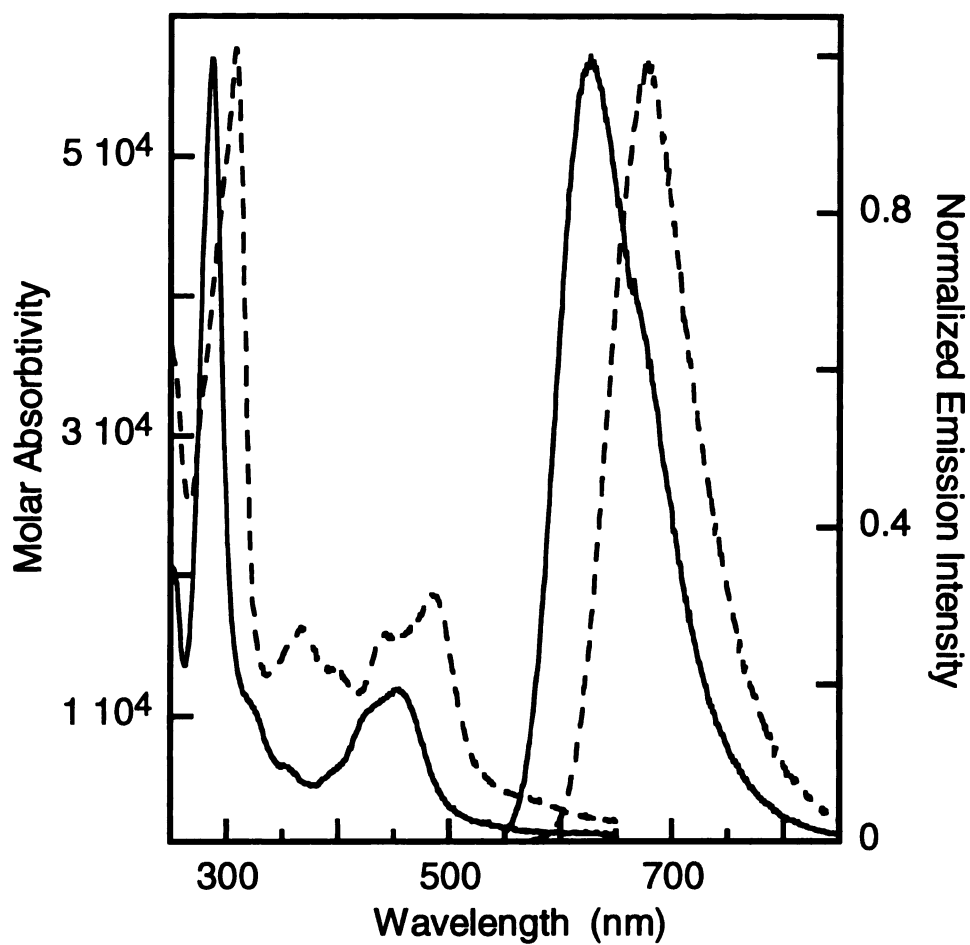


Figure 24. Absorption and emission spectra of carboxylate functionalized electron transfer donor complexes $[(bpy)_2Ru^{2+}(Me-bpy)COO-]^+$ and $[(decb)_2Ru^{2+}(Me-bpy)COOH]^{2+}$ in aerated CH_3CN solvent.

Table 7. Absorption data for (dec_b)₂Ru(II) and (bpy)₂Ru(II) complexes

Ru(II) polypyridyl complex	$\lambda(\text{cm}^{-1})$	$\epsilon (\pi-\pi^*)$	$\lambda(\text{cm}^{-1})$	$\epsilon (\text{d}\pi-\pi^*)$
(dec _b) ₂ Ru ²⁺ (me-bpy)AmH ⁺	32680	44668	21186	14978
(dec _b) ₂ Ru ²⁺ (me-bpy)COOH	32468	62685	20534	18527
(bpy) ₂ Ru ²⁺ (me-bpy)AmH ⁺	34722	58301	21930	11894
(bpy) ₂ Ru ²⁺ (me-bpy)COO ⁻	34965	55996	22026	12017

addition of the complimentary N,N'-dimethylaminobenzoate (DMABCOO-) and N,N'-dimethylaminobenzamidine (DMABAmH⁺) quenchers. Pronounced shifts in the absorption profile for each of the complexes are observed. Whereas the MLCT transitions remain relatively unperturbed, the intensity of the intraligand transition increases, as does the intensity of the weak transition on the low energy tail. These spectral changes are attributable to the formation of the electron transfer complexes Figure (23 a-d). As observed from the insets of Figures (26-29), the inverse of the change in the absorption cross-section scales linearly with the inverse of the quencher concentration. Benesi-Hildebrand treatment [115] of these data yields the association constants given as inserts to Figures (26-29).

Luminescence Spectra

Emission spectra for each of the (decb) and (bpy) amidinium and carboxylate complexes are shown in Figure (24) and (25) respectively. Corresponding energy maxima, quantum yields, and excited state lifetimes are listed in Tables 8 and Table 9. The appreciable red shift in the emission maxima observed for each of the decb complexes is in accordance with the stabilization of the MLCT excited state resulting from the greater electron withdrawing ability of the bpy modified with the 4,4'-dicarboxy substituents. The energy of the MLCT transitions to each of the (bpy) and (decb) complexes may be determined using the procedure of Meyer Eq's. (3.1) and (3.2) in Chapter 3. For the (decb) complexes, as indicated from the red-shifted emission in Figures (24) and (25) the $d\pi \rightarrow \pi^*$ (decb) MLCT excited state is considerably stabilized

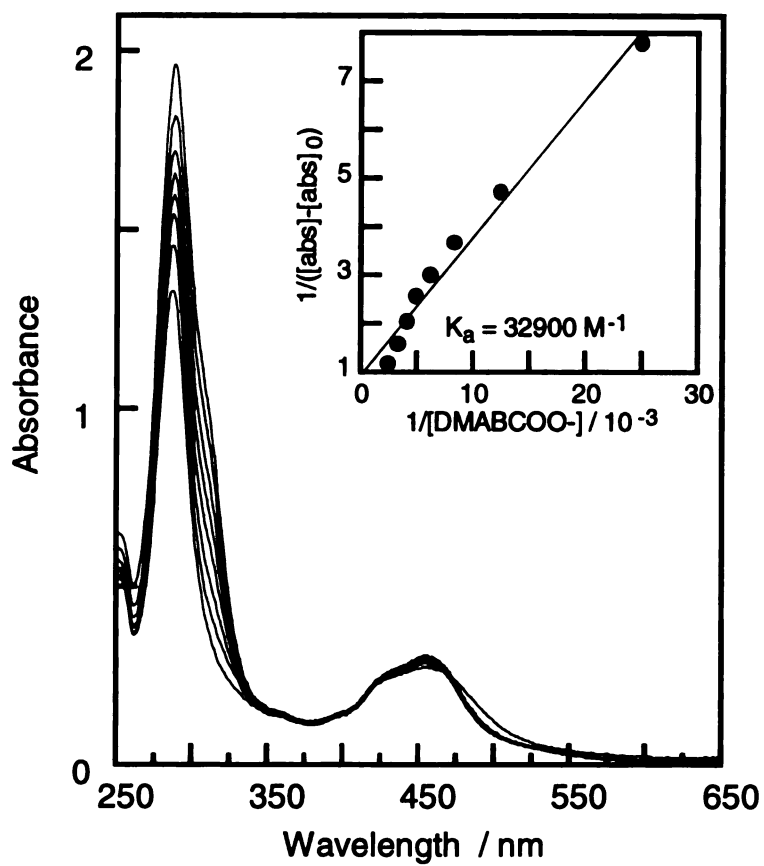


Figure 25. Absorption titration of $[(bpy)_2Ru^{2+}(Me-bpy)AmH^+]$ ($2.0 \times 10^{-5} \text{ M}$) by N,N'-dimethylaminobenzoate in CH_3CN .

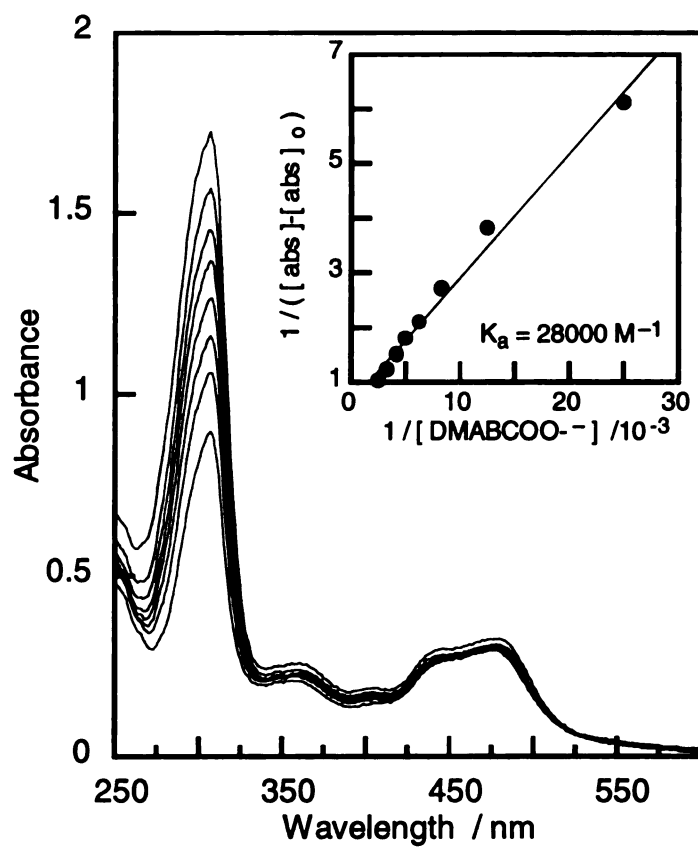


Figure 26. Absorption titration of $[(decb)_2Ru^{2+}(Me-bpy)AmH^+]^{3+}$ ($2.0 \times 10^{-5} \text{ M}$) with N,N'-dimethylaminobenzoate in CH_3CN

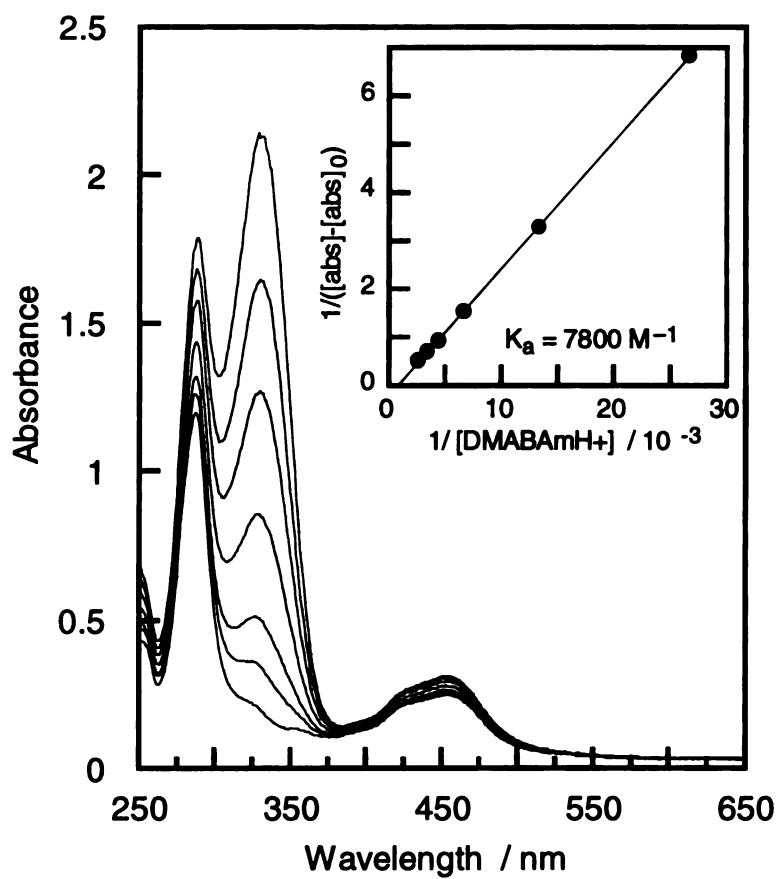


Figure 27. Absorption titration of $[(bpy)_2Ru^{2+}(Me-bpy)AmH^+]^{3+}$ with N,N' -dimethylaminobenzamidinium in CH_3CN .

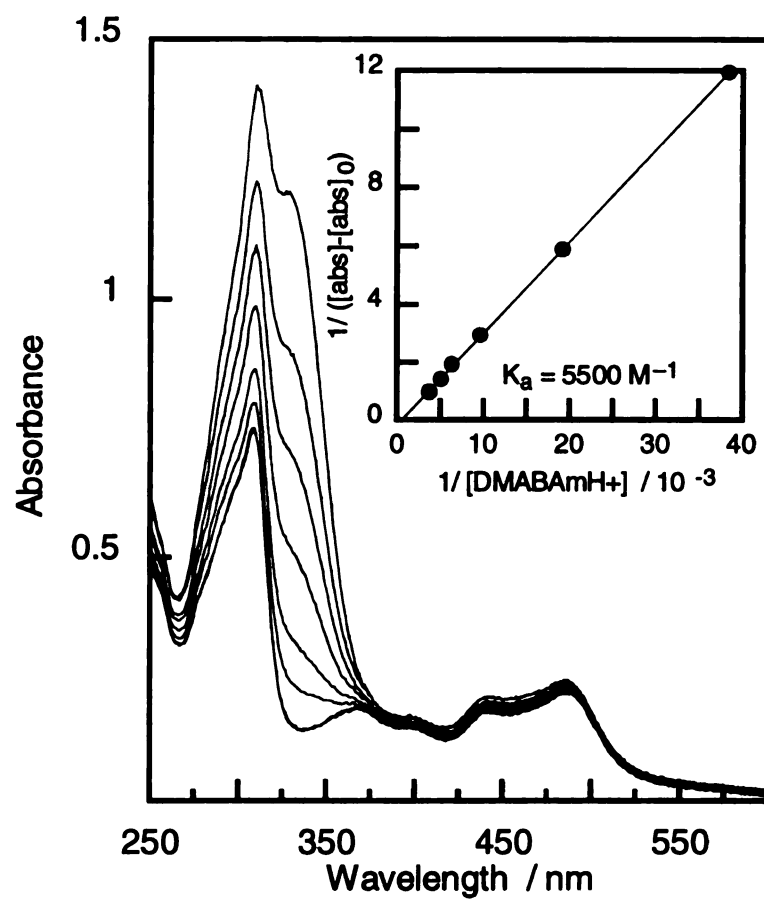


Figure 28. Absorption titration of $[(\text{decb})_2\text{Ru}^{2+}(\text{Me-bpy})\text{COO-}]^+$ with N,N' -dimethylaminobenzamidinium in CH_3CN .

with respect to that of (bpy). Estimates of the $\text{Ru}(\text{decby})_3^{2+}$ MLCT from electrochemical data [103,116] gives $\Delta G_{\text{es}} = 2.05$ eV as compared to $\Delta G_{\text{es}} (\text{Ru}(\text{bpy})_3^{2+*}) = 2.15$ eV [15]. Moreover, the $d\pi \rightarrow \pi^*$ (decby) MLCT is energetically stabilized relative to the MLCT excited states of Mebpy-amH^+ and Mebpy-COO^- . Previous analysis of the emission spectra of the homoleptic Mebpy-amH^+ and Mebpy-COO^- $\text{Ru}(\text{II})$ complexes with Eqs. 3.1 and 3.2 places the MLCT excited states for these ligands at 2.09 and 2.22 eV, respectively. Consistent with the stability for the charge transfer transition of the (decby) complexes are the long excited state lifetimes. Lifetimes for each of the four $\text{Ru}(\text{II})$ polypyridyl complexes (**23a-d**) are summarized in Table 9.

Eqs. (3.1) and (3.2) are also necessary for the estimation of excited state redox potential, which provide the relevant driving forces for the reductive quenching reactions of **23a-d**. In the simplest treatment, the excited state reduction potential of the Ru^{II} metal complex can be ascertained from the simple thermodynamic relation: $E_{1/2}(*\text{Ru}^{\text{III}}) = \Delta G_{\text{es}}^0 - E_{1/2}(\text{Ru}^{\text{III}})$ where $E_{1/2}(\text{Ru}^{\text{III}})$ and $E_{1/2}(*\text{Ru}^{\text{III}})$ are the ground state and excited state Ru^{III} reduction potentials, respectively. The redox potentials for the various $\text{Ru}(\text{II})$ polypyridyl complexes are summarized in Table 10. The $\text{Ru}(\text{II})$ complexes undergo reversible one-electron oxidation as indicated by $i_{\text{p,a}}/i_{\text{p,c}}$ ratios of 1.10 ± 0.10 . Anodic to cathodic peak separations (ΔE_{p}) were greater than 59 mV, but were comparable to that measured for ferrocene, thereby establishing that deviations of ΔE_{p} from the theoretical limit are primarily due to uncompensated cell resistance.

Table 8. Emission Data for (dec_b)₂Ru(II) and (bpy)₂Ru(II) complexes in CH₃CN.

Ruthenium Complex	$\lambda_{\text{em}}(\text{cm}^{-1})$	$\Delta\nu_{0,1/2}(\text{cm}^{-1})$	$\chi(\text{cm}^{-1})$	$\Delta G_{\text{es}}(\text{eV})$
(dec _b) ₂ Ru ²⁺ (me-bpy)AmH ⁺	14950	2070	1885	2.09
(dec _b) ₂ Ru ²⁺ (me-bpy)COOH	14800	1900	1588	2.03
(bpy) ₂ Ru ²⁺ (me-bpy)AmH ⁺	15750	2470	2684	2.28
(bpy) ₂ Ru ²⁺ (me-bpy)COO ⁻	15850	2000	1760	2.18

Table 9. Photophysical Characterization for (dec_b)₂Ru(II) and (bpy)₂Ru(II) complexes in CH₃CN.

Ruthenium Complex	$\phi_{\text{(em)}}$	$\tau/\mu\text{s}$
(dec _b) ₂ Ru ²⁺ (me-bpy)AmH ⁺	0.1053	1.30 (5.20) ^{a)}
(dec _b) ₂ Ru ²⁺ (me-bpy)COOH	0.0960	1.50 (5.50) ^{a)}
(bpy) ₂ Ru ²⁺ (me-bpy)AmH ⁺	0.0835	1.06 (5.45) ^{a)}
(bpy) ₂ Ru ²⁺ (me-bpy)COO ⁻	0.0738	1.18 (5.30) ^{a)}

a) lifetimes for each of the Ru(II)polypyridine complexes measured at 77K in EtOH:MeOH glass (4:1 v/v).

Lifetime Quenching Electron Transfer Measurements

The long-lived luminescence from the Ru(II) polypyridyl complexes is preserved upon formation of the salt-bridge in the absence of an electron donating group. Addition of benzoate to acetonitrile solutions of $[(bpy)_2Ru^{2+}(Mebpy-AmH^+)]^{3+}$ (**23a**) and $[(decb)_2Ru^{2+}(Mebpy-amH^+)]^{3+}$ (**23c**) lead to a modest attenuation in the observed excited state lifetimes ($\tau = 975$ and 1330 ns, respectively), which remain relatively independent of benzoate concentrations. Similarly, long-lived excited state lifetimes of 900 and 1130 ns are observed for $[(bpy)_2Ru^{2+}(Mebpy-COO^-)]^+$ (**23b**) and $[(decb)_2Ru^{2+}(Mebpy-COO^-)]^+$ (**23d**) associated to benzamidinium. The Ru(II) excited state luminescence of (**23a**) and (**23c**) is dramatically quenched when phenyl of benzoate is substituted with the dimethylaniline. This result is consistent with an electron transfer quenching mechanism, which is a well-established reaction between electronically excited Ru(II) *tris*(polypyridyl) complexes and dialkylamine aromatic electron donors [3]. Biexponential decay kinetics are observed for each of the amidinium functionalized complexes where one lifetime component of the emission decay is dependent on the concentration of donor and the other is not over a $DMABCOO^-$ concentration range of 0.062 to 1.24 mM ($[(bpy)_2Ru^{2+}(Mebpy-AmH^+)]^{3+} = 0.051$ mM) Figure (30). The concentration-dependent lifetimes obey typical linear Stern-Volmer quenching kinetics and the bimolecular rate constants of $6.4 \times 10^8 \text{ M}^{-1} \text{ s}^{-1}$ for (**23a**) and of $3.5 \times 10^8 \text{ M}^{-1} \text{ s}^{-1}$

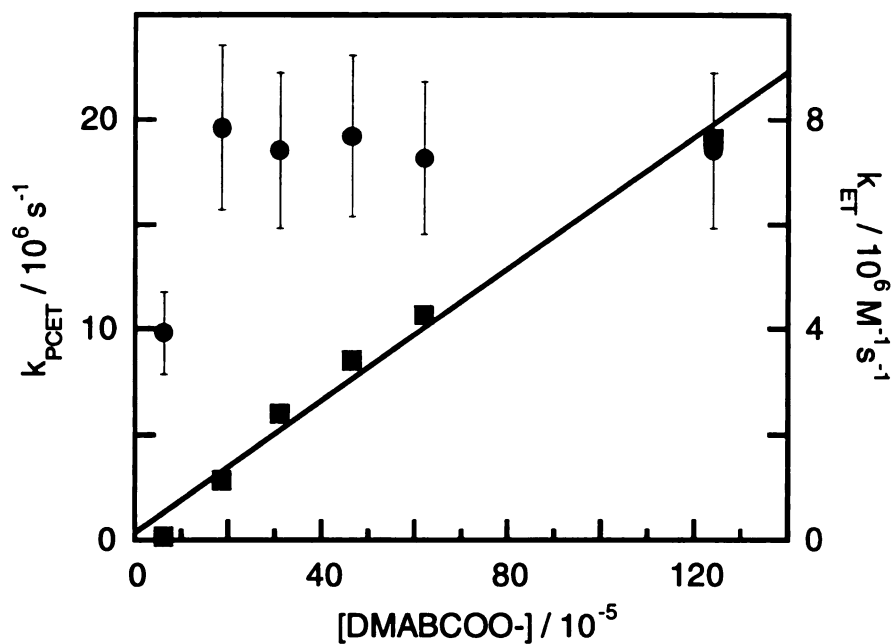


Figure 29. Concentration-independent (●) and concentration-dependent (■) observed rate constants for the quenching of $[(\text{bpy})_2\text{Ru}^{2+}(\text{Me-bpy})\text{AmH}^+]^{3+}$ by N,N'-dimethylaminobenzoate in CH_3CN .

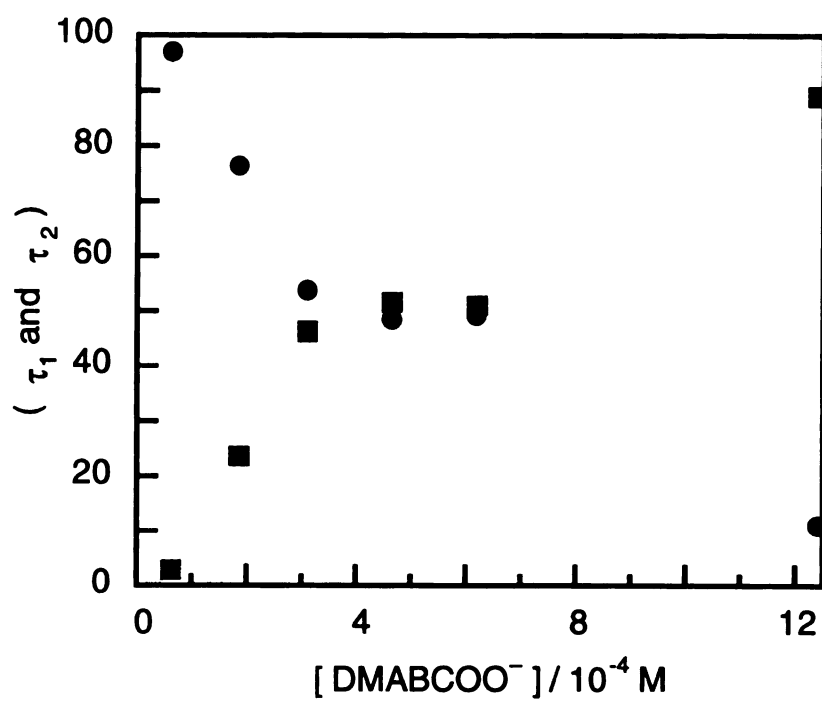


Figure 30. Ratio of pre-exponential factors A_1 (■) and A_2 (●) from biexponential fitting of the quenching data for $[(bpy)_2Ru^{2+}(Me-bpy)AmH^+]^{3+}$ with N,N'-dimethylamino-benzoate.

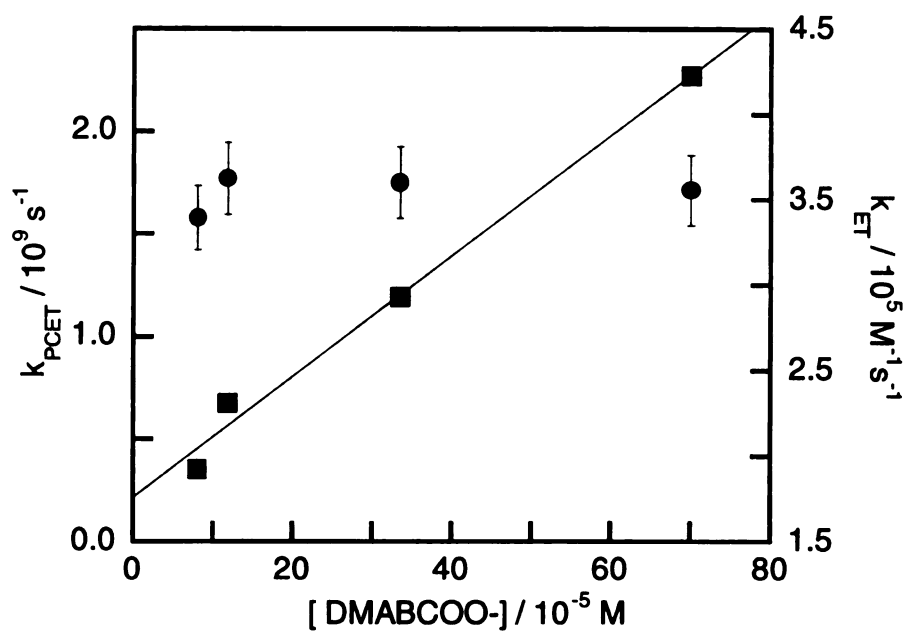


Figure 31. Concentration-independent (●) and concentration-dependent (■) observed rate data for the quenching of $[(\text{decb})_2\text{Ru}^{2+}(\text{Me-bpy})\text{AmH}^+]^{3+}$ by N,N'-dimethylaminobenzoate in CH_3CN .

for **(23c)** accord well with the kinetics of equi-exergonic bimolecular reactions between $\text{Ru}(\text{bpy})_3^{2+}$ and dialkylanilines [3]. Analyses of the concentration- independent lifetime decay curves yield intramolecular rate constants of $1.9 \times 10^7 \text{ s}^{-1}$ and $1.7 \times 10^9 \text{ s}^{-1}$ for **(23a)** Figure (30) and **(23c)** Figure (32), respectively. The independence of the rate constant on quencher concentration is consistent with an electron transfer quenching reaction occurring within the associated pair of **(23a)** and **(23c)**. When the interface is carboxylate and amidinium moieties are interchanged on the Ru(II) acceptor and DMAB donor, no electron transfer quenching of the Ru(II) luminescence is observed. The lifetime of **(23b)** and **(23d)** is invariant with the addition of DMABAmH^+ over a quencher concentration range of $1.0 - 140 \times 10^{-5} \text{ M}$. The significant differences in the electron transfer reactivity between the **(23a,23c)** and **(23b,23d)** systems are reflected in the electron transfer driving forces. Table 10 lists the estimated driving forces for the reaction of the various systems as determined from the following relation: $\Delta G^0 = E_{1/2}(\text{Q}^{+/0}) - E_{1/2}(*\text{Ru}^{\text{II/I}})$ where $E_{1/2}(*\text{Ru}^{\text{II/I}})$ was determined as described above and $E_{1/2}(\text{Q}^{+/0})$ is determined from redox potential measurements. For N,N'-dimethylaminobenzamidinium, a reversible half-wave potential at 1.10 V vs. SCE was observed in the cyclic voltammogram. Conversely, N,N'-dimethylaminobenzoate (TBA^+ salt) was electrochemically irreversible as evidenced by the presence of only an anodic wave in the cyclic voltammetric scan. Accordingly, the potential for this compound was estimated from a Marcus curve by using methods previously described by Schuster and co-workers in their estimation of redox potentials for borate quenchers [86]. A linear free

energy relationship for the electron transfer quenching of $^*\text{Ru}(\text{bpy})_3^{2+}$ by aromatic amines has previously been defined by Meyer [3]. The Marcus curve for the quenching reaction was verified by re-determining the rate constants from emission lifetime decay curves of selected quenchers (dimethyl-*p*-toluidine, diethylaniline, and tetramethyl-*p*-phenylenediamine) under identical experimental conditions. The measured bimolecular rate constants were corrected for diffusional effects and found to be $\pm 10\%$ the values previously measured by Meyer et. al. The corrected observed rate constant for N,N'-dimethylaminobenzoate was $3.1 \times 10^8 \text{ M}^{-1} \text{ s}^{-1}$, falling within the linear range of the Marcus free relationship for aromatic amines ($0.20 < \Delta G_0 < -0.25$). Correlation to the Marcus plot gives a redox potential of 0.70 V vs. SCE. It must be emphasized that the Marcus curve in Meyer's study is constructed for neutral quenchers whereas for the correlation here, the quencher is anionic. Thus the observed rate constant from which the redox potential is determined is compromised to the extent that work term corrections have not been applied. At the high ionic strengths $\mu = 0.1 \text{ M}$ at which the quenching reaction was performed, however, the error associated with work term contributions is expected to be small ($< 0.1 \text{ V}$) according to standard Debye-Hückel formalisms. To ensure that work terms were indeed insignificant in our analysis, we determined the reduction potential of N,N'-dimethylaminobenzamidinium from the same Marcus curve. A corrected, observed rate constant of $1.1 \times 10^5 \text{ M}^{-1} \text{ s}^{-1}$ yielded a $E_{1/2}$ of 1.09 V vs. SCE, which is excellent agreement to the electrochemically measured $Q^{+/0}$ reduction potential of 1.10 V vs. SCE, Table 11.

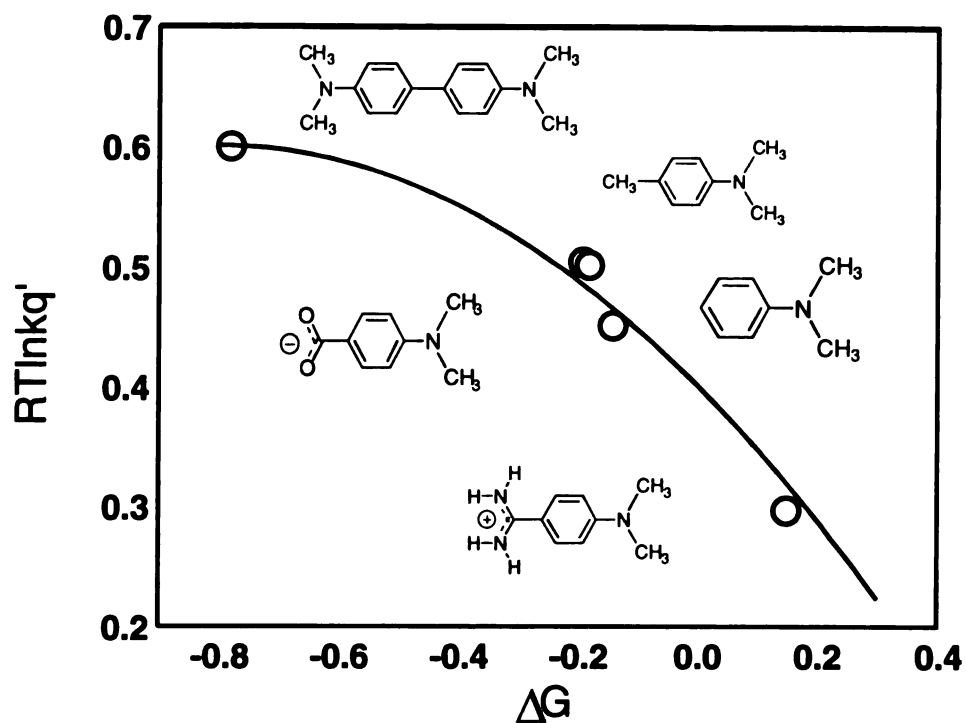
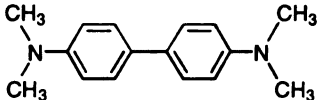
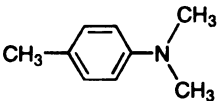
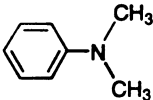
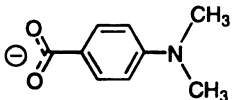
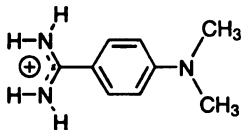


Figure 32. Marcus fit of bimolecular electron transfer rates constants for the kinetic determination of redox potentials of the reductive quenchers N,N'-dimethylaminobenzoate and N,N'-dimethylaminobenzamidinium in CH_3CN $\mu = 0.1$ 22°C

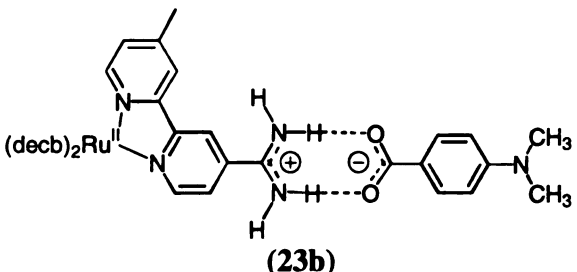
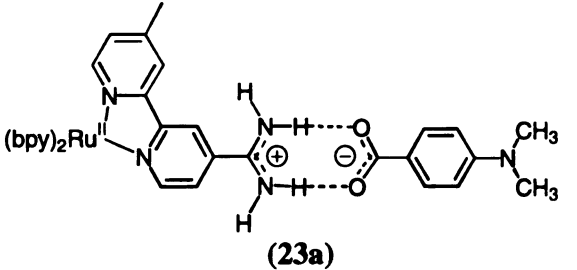
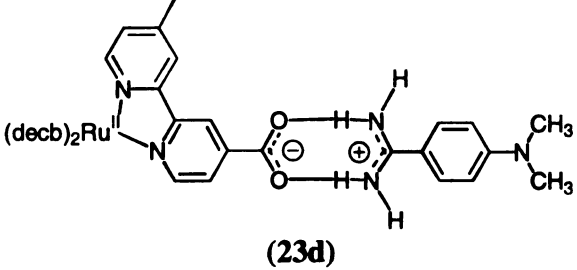
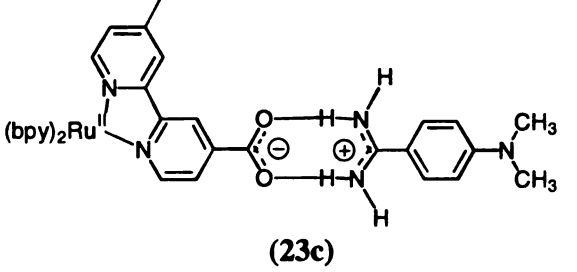
Table 10. Redox potentials and rate constants for the bimolecular quenching reactions between $\text{Ru}(\text{bpy})_3^{2+}$ and the reductive electron transfer quenchers.

Reductive quencher	$k_q \times 10^7$ ($\text{M}^{-1}\text{s}^{-1}$)	$E_{1/2}$ (V)	ΔG_{et} (V)
 (TMPD)	1450	0.12	-0.78
 (DM-p-T)	945	0.71	-0.19
 (DEA)	4.7	0.76	-0.14
 (DMABCOO-)	34	0.70 ^{a)}	-0.08
 (DMABAmH+)	0.105	1.09	0.15

Tetramethyl-p-phenylenediamine (TMPD), dimethyl-p-toluidine (DM-p-T), diethylaniline (DEA), N,N'-dimethylaminobenzoate (DMABCOO⁻) and N,N'-dimethylaminobenzamidinium (DMABAmH⁺).

a) Redox potential determined from Marcus fit of quenching data.

Table 11. Rates for concentration-dependent and concentration-independent quenching of (decb)₂Ru(II) and (bpy)₂Ru(II) salt-bridge electron transfer complexes.

Ru(II) salt bridge complex	ΔG_{ET} / V	k_{ET} / M ⁻¹ s ⁻¹	k_{PCET} s ⁻¹
 <p>(23b)</p>	-0.39	3.5×10^8	1.7×10^9
 <p>(23a)</p>	-0.52	6.4×10^8	1.9×10^7
 <p>(23d)</p>	0.17	8×10^4	—
 <p>(23c)</p>	0.35	—	—

Discussion

Amidinium-carboxylate salt bridge complexes (**23a**) and (**23b**) readily form in CH₃CN solutions. The exceptionally high association of the salt bridge agrees well with Jorgensen's classification for two favorable secondary interactions composing the hydrogen bonded interface [36], bolstered by the stabilization imparted by the molecular recognition of the negatively charged carboxylate by the positively charged amidinium. The significantly higher K_{assoc} of (**23a**) is consistent with an increased basicity of the carboxylate group conferred by the electron donating dimethylamino group, resulting in a stronger hydrogen bonding interaction than that observed for switched interface system (**23c** and **23d**).

Consistent with the equilibrium measurements, the Ru(II) excited state undergoes electron transfer with unbound and bound donor when the reaction is exergonic. The luminescence from $[(\text{bpy})_2\text{Ru}^{2+}(\text{Mebpy-amH}^+)]^{3+}$ and $[(\text{dec b})_2\text{Ru}^{2+}(\text{Mebpy-amH}^+)]^{3+}$ is efficiently quenched by DMABCOO⁻. That the bimolecular rate for the reaction of the bpy complex, (**23a**), is greater than that of the decb complex, (**23c**), is sensible in light of the greater driving force of the bimolecular electron transfer reaction of the former ($\Delta\Delta G = 0.13$ V). Along these lines, the inversion of the relative ordering of the rate constants, and their large difference (**23a** is $\sim 10^2$ less than that of its decb congener **23b**), for the salt-bridge assembled acceptor-donor pair appears peculiar. We believe that the origins of this behavior arise from disparate MLCT energetics and consequently electronic structure of the Ru(II) polypyridyl acceptor complex.

The electron transfer reaction of **(23a)** is established by photogenerating a hole at the Ru(II) center by MLCT excitation. Figure **(34)** shows the relative energy levels of the different ligand systems as established from the spectral fits of the emission profiles of the homoleptic complexes and data from the literature. The energy ordering $\text{decb} \sim \text{Mebpy-amH}^+ \ll \text{bpy}$ follows a simple trend where the energy of the MLCT excited state increases as the electron withdrawing ability of the substituents on the polypyridyl rings decreases. In the case of **(23a)**, simple Boltzmann considerations suggest that MLCT excitation places an electron on the Mebpy-amH^+ and thus the electron transfer pathway contains a photoreduced Mebpy ligand. For **(23c)**, the decb and Mebpy-amH^+ MLCT excited states are nearly equi-energetic and therefore the photoexcited electron is partly removed from the electron transfer pathway. In an electronic sense, the transferring electron traverses a less obstructed pathway from DMAB to the photogenerated hole on the metal. Similar observations for the oxidative quenching reaction of amidinium- and carboxylate-modified Ru(II) polypyridyls by dinitrobenzene were shown in Chapter 4, but the trend is opposite to that observed here. In this case, the photoexcited electron moves away from the metal to an acceptor and the electron transfer pathway is properly established with MLCT of an electron onto the Mebpy ligand to which the salt bridge is attached. This situation is achieved by tetramethylating the ancillary bpy ligand, which raises its MLCT excited state energy well above that of the Mebpy ligand. The photoinduced electron transfer event is cleanly established by MLCT excitation to the Mebpy ligand, from where the electron can smoothly advance to the dinitrobenzoic acid

acceptor. Conversely, the photoexcited electron is removed from the electron transfer pathway when the ancillary bpy is unmodified (owing to the lower energy of the bpy MLCT excited state) and electron transfer proceeds from the remote ancillary ligand. Similar to the magnitude of the effect described here for **(23a)** and **(23c)**, the rate of the properly established electron transfer for the tmbpy complex is 40 times greater than that observed for the more convoluted electron transfer pathway of the bpy complex.

The electronics of **(23b)** and **(23d)** are straightforward with regard to photoinitiating the electron transfer reaction. The energetics for the $d\pi \rightarrow \pi^*$ (polypyridine) MLCT excited state are $\text{decb} < \text{bpy} < \text{Mebpy-COO}^-$. Photoexcitation of **(23a)** and **(23c)** cleanly establishes a hole at the metal ion without any contribution of a photoreduced ligand along the electron transfer pathway. Nevertheless, electron transfer is not observed for either salt-bridge complex **(23b)** or **(23d)**. Moreover, the corresponding bimolecular electron transfer reaction of **(23b)** is absent and that of **(23d)** is negligible. Inspection of the free energies listed in Table x reveal that the electron transfer reactions for these systems are endergonic.

The reactivity difference between the Ru(II) polypyridyl amidinium systems **(23a)** and **(23c)** and carboxylate congeners **(23b)** and **(23d)** is primarily a result in a shift of the DMAB donor potential upon the presence of amidinium at the para position of dimethylaniline. DMAB-AmH⁺ is 0.40 V more difficult to oxidize than DMAB-COO⁻, which is a slightly better reductant than DMA ($E_{1/2} = 0.81$ V vs. SCE). The increased difficulty in oxidizing DMAB-AmH⁺ is sufficiently destabilizing to drive the electron transfer reactions of **(23a)** and **(23c)** energetically uphill. Within the **2/4** series, the further

decrease in driving force of **(23c/23d)** finds its origins in the unfavorable $\text{Ru}^{\text{II/I}}$ redox potential, which is largely ligand-centered in $\text{Ru}(\text{II})$ polypyridyl complexes. As observed from the energy of the MLCT excited states, which typically track the Ru^{III} reduction potential [100], the reduction potentials of (decb) and (Mebpy-AmH^+) are similar and much less than (bpy) and (Mebpy-COO^-). For this reason, as described above, the overall driving forces among these systems reflect for the most part, the difference in the donor potentials. The reduction potential of **(23a)**, however, is expected to be centered on the bpy ligand, which is born out by the similarity of this complexes Ru^{III} half-wave potential to that of $\text{Ru}(\text{bpy})_3^{2+}$ in CH_3CN ($E_{1/2}(*\text{Ru}^{\text{III}}) = 1.32 \text{ V vs. SSCE}$ [103]). Consequently, the large decrease in the electron transfer driving force for **(23c)** and **(23d)** with regard to **(23a)** and **(23b)** reflects the difference in reducing (bpy) as opposed to the more oxidizing (decb) ligand.

The overall electron transfer kinetics of **(23a)** follows the emerging trend that electron transport through salt bridges is fast for the D-(carboxylate-amidinium)-A complexes. In this orientation, electron transfer is in the direction of the permanent dipole of the salt bridge and the internal electric field contributes favorably to the driving force of reaction relative to the isolated constituents (for which the redox potentials in Table 10 are measured) [16,17]. The thermodynamics may be further augmented by favorable kinetics associated with a D-(carboxylate-amidinium)-A orientation. Charge redistribution within the salt-bridge may be strongly coupled to the solvent dipoles [67], thereby giving rise to Franck-Condon factors in excess of that expected for simple electron transfer. In the case of the D-(carboxylate-amidinium)-A complex, the proton already resides on the acceptor and hence it is likely to remain upon the arrival of the

electron. Franck-Condon factors arising from proton motion within the salt bridge are therefore minimized. On the basis of the thermodynamic and kinetics considerations, we can account for the differences in the oxidative and reductive quenching pathways. For the oxidative quenching reaction, electron transfer should be fast out of the electronically excited Ru(II) complex. Conversely, fast electron transfer into the metal center should be observed for a reductive quenching pathway. In both cases, the orientation of the salt bridge with regard to the direction of electron transfer is the same and favorable with regard to electron transfer. Unfortunately, as was provided in Chapter 4 by a comparative kinetics studies of switched interface systems for the oxidative quenching pathway, a more explicit analysis of the effect of the salt bridge on electron transfer pathway is obviated by the large difference in the electron transfer driving forces of **(23c)** and **(23d)**.

LIST OF REFERENCES

1. a) Spears, K. G. *J. Phys. Chem.* **1995**, *99*, 2469. b) Reid, P. J.; Silva, C.; Barbara, P. F.; Karki, L.; Hupp, J. T.; *J. Phys. Chem.* **1995**, *99*, 2609
2. a) Marcus, R. A. *J. Chem. Phys.* **1956**, *24*, 966. b) Marcus, R. A. *J. chem. Phys.* **1965**, *43*, 679
3. a) Bock, C. R.; Connor, J. A.; Gutierrez, A. R.; Meyer, T. J.; Whitten, D. G.; Sullivan, B. P.; Nagle, J. K. *J. Am. Chem. Soc.* **1979**, *101*, 4815. b) Ballardini, R.; Varani, G.; Scandola, F.; Balzani, V. *J. Am. Chem. Soc.* **1978**, *100*, 7219. c) Creutz, C.; Sutin, N. *Proc. Natl. Acad. Sci. U.S.A.*, **1975**, *72*, 2858
4. Rybak, W.; Haim, A.; Netzel, T. N.; Sutin, N. *J. Phys. Chem.* **1981**, *85*, 2856
5. a) Turro, C.; Zaleski, J. M.; Karabatsos, Y. M.; Nocera, D. G. *J. Am. Chem. Soc.* **1996**, *118*, 6060. b) McClesky, T. M.; Winkler, J. R.; Gray, H. B. *J. Am. Chem. Soc.* **1992**, *114*, 6935 c)
6. Winkler, J. R.; Nocera, D. G.; Yocum, K. M.; Bordignon, E.; Gray, H. B. *J. Am. Chem. Soc.* **1982**, *104*, 5798
7. Nocera, D. G.; Winkler, J. R.; Yocum, K. M.; Bordignon, E.; Gray, H. B.; *J. Am. Chem. Soc.* **1984**, *106*, 5145

8. Winkler, J. R.; Gray, H. B.; *Chem. Rev.* **1992**, 92, 369
9. Moser, C. C.; Keske, J. M.; Warnke, K.; Farid, R. S.; Dutton, P. L. *Nature* **1992**, 355, 796
10. a) Beratan, D. N.; Onuchic, J. N.; Betts, J. N.; Bowler, B. E.; Gray, H. B. *J. Am. Chem. Soc.* **1990**, 112, 7915. b) Onuchic, J. N.; Beratan, D. N. *J. Chem. Phys.* **1990**, 92, 722. c) Onuchic, J. N.; Andrade, P. C. P.; Beratan, D. N. *J. Chem. Phys.* **1991**, 95, 1131. d) Beratan, D. N.; Onuchic, J. N.; Winkler, J. R.; Gray, H. B. *Science* **1992**, 258, 1740
11. Lopez-Castillo, J.-M.; Filali-Mouhim, A.; Van Binh-Otten, E. N.; Jay-Gerin, J.-P. *J. Am. Chem. Soc.* **1997**, 119, 1978
12. a) Isied, S. I.; Ogawa, M. Y.; Wishart, J. F. *Chem. Rev.* **1992**, 92, 381. b) Ogawa, M. Y.; Wishart, J. F.; Young, Z.; Miller, J. R.; Isied, S. I. *J. Phys. Chem.* **1993**, 97, 11456. c) Ogawa, M. Y.; Moreira, I.; Wishart, J. F.; Isied, S. I.; *Chem. Phys.* **1993**, 176, 589.
13. a) Gretchikhine, A. B.; Ogawa, M. Y. *J. Am. Chem. Soc.* **1996**, 118, 1543. b) Ogawa, M. Y.; Gretchikhine, A. B.; Soni, S.-D.; Davis, S. M. *Inorg. Chem.* **1995**, 34, 6423
14. Langen, R.; Chang, I.-J.; Germanas, J. P.; Richards, J. H.; Winkler, J. R.; Gray, H. B.; *Science* **1995**, 268, 1733
15. a) Mecklenburg, S. L.; Peek, B. M.; Erickson, B. W.; Meyer, T. J. *J. Am. Chem. Soc.* **1991**, 113, 8540. b) Mecklenburg, S. L.; Peek, B. M.; Shoonover, J. R.; McCafferty, D. G.; Wall, C. G.; Erickson, B. W.; Meyer, T. J. *J. Am. Chem. Soc.* **1993**, 115, 5479. c) Mecklenburg, S. L.; McCafferty, D. G.; Shoonover, J. R.; Peek, B. M.; Erickson, B. W.; Meyer, T. J. *Inorg. Chem.* **1994**, 33, 2974. d) Opperman, K. A.; Erickson, B. W.; Meyer, T. J. *Inorg. Chem.* **1994**, 33, 5295.
16. a) Franzen, S.; Lao, K.; Boxer, S. G.; *Chem. Phys. Lett.* **1992**, 197, 380. c) Galoppini, E.; Fox, M. A. *J. Am. Chem. Soc.* **1996**, 118, 2299. d) Galoppini, E.; Fox, M. A. *J. Am. Chem. Soc.* **1997**, 119, 5277
17. a) Gosztola, D.; Yamada, H.; Wasielewski, M. R. *J. Am. Chem. Soc.* **1995**, 117, 2041. b) Kharkats, Y. I.; Kuznetsov, A. M.; Ulstrup, J. *J. Phys. Chem.* **1995**, 99,

13545. c) Shigenori, T.; Marcus, R. A. *J. Phys. Chem.* **1997**, *101*, 5031. d) Gunner, M. R.; Honig, B. A. *J. Phys. Chem.* **1996**, *100*, 4276
18. Wasielewski, M. R. *Chem. Rev.* **1992**, *92*, 435
19. Osuka, A.; Nakajima, S.; Maruyama, K.; Mataga, N.; Asahi, T. *Chem. Lett.* **1991**, 1003
20. a) Gust, D.; Moore, T. A.; Moore, A. L.; Lee, S. J.; Bittersmann, E.; Luttrull, D. K.; Rhems, A. A.; DeGraziano, J. M.; Ma, X. C.; Gao, F.; Belford, R. E.; Trier, T. T. *Science* **1990**, *248*, 199. b) Gust, D.; Moore, T. A.; *Adv. Photochem.* **1991**, *16*, 1.
21. Gosztola, D.; Yamada, H.; Wasielewski, M. R. *J. Am. Chem. Soc.* **1995**, *117*, 2041
22. a) Heiler, D.; McClendon, G.; Rogalskj, P. *J. Am. Chem. Soc.* **1987**, *109*, 604. b) Helms, A.; Heiler, D.; McClendon, G. *J. Am. Chem. Soc.* **1991**, *113*, 4325. c) Bashkin, J.; McClendon, G.; Mikamel, S.; Marohn, J. *J. Phys. Chem.* **1990**, *94*, 4757. d) Helms, A.; Heiler, D.; McClendon, G. *J. Am. Chem. Soc.* **1992**, *114*, 6238
23. a) Jordan, K.; Paddon-Row, M. N. *Chem. Rev.* **1992**, *92*, 395. b) Clayton, A. H. A.; Scholes, G. D.; Ghiggino, K. P.; Paddon-Row, M. N. *J. Phys. Chem.* **1996**, *100*, 10912
24. a) Miller, J. R.; Calcaterra, L. T.; Closs, G. L. *J. Am. Chem. Soc.* **1984**, *106*, 3047. b) Closs, G. L.; Calcaterra, L. T.; Green, N. J.; Penfield, K. W.; Miller, J. R. *J. Phys. Chem.* **1986**, *90*, 3673. c) Closs, G. L.; Miller, J. R. *Science*, **1988**, *240*, 440. d) Liang, N.; Miller, J. R.; Closs, G. L. *J. Am. Chem. Soc.* **1990**, *112*, 5353
25. Marcus, R. A. *Ann. Rev. Phys. Chem.* **1964**, *15*, 155
26. a) Levich, V. G.; Dogonadze, R. R. *Dokl. Acad. Nauk SSSR* **1959**, *124*, 123. b) Levich, V. G.; *Electrochem. Eng.* **1965**, *4*, 249.
27. a) Rucker, J.; Cha, Y.; Jonsson, T.; Grant, K. L.; Klinman, J. P. *Biochemistry*, **1992**, *31*, 11489. b) Cleland, W. W.; *Biochemistry*, **1992**, *31*, 317. c) Gerlt, J. A.; Gassman, P. G.; *Biochemistry*, **1993**, *32*, 11943. d) Gerlt, J. A.; Gassman, P. G. *J. Am. Chem. Soc.* **1993**, *115*, 11552. e) Schwartz, B.; Drueckhamer, D. G. *J. Am. Chem. Soc.* **1995**, *117*, 11902

28. Warshel, A.; Russell, S. T.; Churg, A. K. *Proc. Natl. Acad. Sci. USA* **1984**, *81*, 4785
29. a) Huang, S.; Huang, J.; Kloek, A. P.; Goldberg, D. E.; Friedman, J. M. *J. Biol. Chem.* **1996**, *271*, 958. b) Phillips, S. E. V.; Schoenborn, B. P.; *Nature*, **1981**, *292*, 81. c) Nagai, K.; Luisi, B.; Shih, D.; Miyazaki, G.; Imai, K.; Poyart, C.; De Young, A.; Kwiatkowski, L.; Noble, R. W.; Lin, S. H.; Yu, N. T.; *Nature*, **1987**, *329*, 858. d) Springer, B. A.; Sligar, S. G.; Olson, J. S.; Phillips, G. N.; *Chem. Rev.* **1994**, *94*, 699
30. a) Heller, B. A.; Holten, D.; Kirmaier, C. *Science*, **1995**, *269*, 940. b) Allen, J. P.; Artz, X. L.; Williams, J. C.; Ivancich, A.; Albouy, D.; Mattioli, T. A.; Fetsch, A.; Kuhn, M.; Lubitz, W. *Biochemistry*, **1996** *35*, 6612.
31. a) Frey, P. A.; Whitt, S. A.; Tobin, J. B. *Science*, **1994**, *264*, 1927. b) Kato, Y.; Toledo, L. M.; Rebek, J. *J. Am. Chem. Soc.* **1996**, *118*, 8575.
32. a) Frey, P. A.; Whitt, S. A.; Tobin, J. B. *Science*, **1994**, *264*, 1927 b) Tobin, J. B.; Whitt, S. A.; Cassidy, C. S.; Frey, P. A. *Biochemistry*, **1995**, *34*, 6919
33. Warshel, A.; Papazyan, A.; Kollman, P. A.; Cleland, W. W.; Krevoy, M. M.; Frey, P. A. *Science*, **1995**, *269*, 102. b) Scheiner, S.; Kar, T. *J. Am. Chem. Soc.* **1995**, *117*, 6970.
34. Honig, B. A.; Nicholls, A. *Science*, **1995**, *26*, 1144
35. Rabold, A.; Bauer, R.; Zundel, G. *J. Phys. Chem.* **1995**, *99*, 1889
36. a) Pranata, J.; Wierschke, S. G.; Jorgensen, W. L. *J. Am. Chem. Soc.* **1991**, *113*, 2810. b) Jorgensen, W. L.; Pranata, J. *J. Am. Chem. Soc.* **1990**, *112*, 2008
37. Shan, S.; Loh, S.; Herschlag, D. *Science* **1996**, *272*, 97
38. Cukier, R. I. *J. Phys. Chem.* **1996**, *100*, 15428
39. Borgis, D.; Hynes, J. T. *J. Phys. Chem.* **1996**, *100*, 1118
40. Douhal, A.; Lahmani, F.; Zewail, A. H. *Chem. Phys.* **1996**, *207*, 477. For other recent reviews of proton transfer see Michael Kasha Fetschrift *J. Phys. Chem.* **1991**, *95*, 10215 - 10518 And a special Issue on Proton Transfer edited by Barbara and Trommsdorff. *Chem. Phys.* **1989**, *136*, 153 - 360

41. a) Burgess, B. K.; Lowe, D. J.; *Chem. Rev.* **1996**, *96*, 2983. b) Pilato, R. S.; Steifel, E. i. In *Bioinorganic Catalysis*; Reedijk, J., Ed.; Dekker: New York, 1993, p 131. c) Stifel, E. I. In *Molybdenum Enzymes, Cofactors, and Model Systems*; ACS Symposium Series 535; Steifel, E. I., Coucouvanis, D., Newton, W. E., Eds.; American Chemical Society: Washington, DC, 1993, p1. d) Steifel E. I. *Proc. Natl. Acad. Sci. USA* **1973**, *70*, 988.
42. Feig, A. L.; Lippard, S. J. *Chem. Rev.* **1994**, *94*, 759
43. Wallar, B. J.; Lipscomb, J. D. *Chem. Rev.* **1996**, *96*, 2625
44. Solomon, E. I.; Sundaram, U. M.; Machonkin. T. E. *Chem. Rev.* **1996**, *96*, 2563.
45. a) Uhlin, U.; Eklund, H. *Nature*, **1994**, *370*, 53. b) Nordlund, P.; Eklund, h. *J. Mol. Biol.* **1993**, *232*, 123. c) Ekberg, M.; Sahlin, M.; Eriksson, M; Sjoberg, B.-M. *J. Biol. Chem.* **1996**, *271*, 20655. d) Crane, B. R.; Siegel. L. M.; Getzoff, E. D.; *Science* **1995**, *270*, 59. e) Averill, B. A. *Chem. Rev.* **1996**, 2951.
46. Ramirez, B. E.; Malmstrom, B. G.; Winkler, J. R.; Gray. H. B. *Proc. Natl. Acad. Sci. USA* **1995**, *92*, 11949
47. Brzezinski, P. *Biochemistry*, **1996**, *35*, 5611.
48. Miyasaka, H.; Tabata, A.; Ojima, S.; Ikeda, N.; mataga, N. *J. Phys. Chem.* **1993**, *97*, 8222
49. a) Harriman, A.; Sessler, J. L. *J. Am. Chem. Soc.* **1993**, *114*, 388 b) Sessler, J. L.; Wang, B.; Harriman, A. *J. Am. Chem. Soc.* **1993**, *115*, 10418
50. Osuka, A.; Shiratori, h.; Yoneshima, R.; Okada, T.; Taniguchi, S.; Mataga, N. *Chem. Lett.* **1995**, 913
51. Aoyama, Y.; Asakawa, Y.; Matsui, Y.; Ogoshi, H. *J. Am. Chem. Soc.* **1991**, *113*, 6233
52. Hayashi, T.; Miyahara, T.; Matsui, Y.; Ogoshi, H.; *J. Am. Chem. Soc.* **1993**, *115*, 2049

53. Lindsey, J. S.; delaney, J. K.; Mauerzall, D. C.; Linschitz, H. *J. Am. Chem. Soc.* **1988**, *110*, 3610
54. Hunter, C.; Sanders, J.; Beddard, G.; Evans, S. *J. Chem. Soc. Chem. Comm.* **1989**, 1765
55. Kuroda, Y.; Ito, M.; Sera, T.; Ogoshi, H. *J. Am. Chem. Soc.* **1993**, *115*, 7003
56. Hage, R.; Krijnen, B.; Warnaar, J. B.; Hartl, F.; Stufkens, D. J.; Snoeck, T. L. *Inorg. Chem.* **1995**, *34*, 4973
57. a) Ram, M. S.; Skeens-Jones, L.M.; Johnson, C. S.; Zhang, X. L.; Stern, C.; Yoon, D. I.; Selmarten, D.; Hupp, J. T. *J. Am. Chem. Soc.* **1995**, *117*, 1411b) Binsted, R. A.; Moyer, B. A.; Samuels, G. J.; Meyer, T. J. *J. Am. Chem. Soc.* **1981**, *103*, 2897. b) Binsted, R. A.; McGuire, M. E.; Dovletoglou, A. Seok, W. K.; Roecker, L. E. ; Meyer, T. J. *J. Am. Chem. Soc.* **1992**, *114*, 173. c) Che, C.-M.; Lau, Keung, L.; Lau, T.-C.; Poon, C.-K. *J. Am. Chem Soc.* **1990**, *112*, 5176.
58. Miyasaka, H.; Tabata, A.; Kamada, K.; Mataga, N. *J. Am. Chem. Soc.* **1993**, *115*, 7335
59. Wenograd, J.; Spurr, R. A. *J. Am. Chem. Soc.* **1957**, *79*, 5844
60. Pitzer J. *Phys. Chem.* **1960**, *64*, 886
61. Rambaud, C.; Oppenländer, A.; Pierre, M.; Trommsdorff, H. P.; Vial, J.-C. *Chem. Phys.* **1989**, *136*, 335
62. Turro, C.; Chang, C. K.; LeRoi, G. E.; Cukier, R. I.; Nocera, D. G. *J. Am. Chem. Soc.* **1992**, *114*, 4013
63. Kirby, J. P.; van Dantzig, N. A.; Chang, C. K.; Noera, D. G.; *Tetrahedron Lett.* **1995**, *36*, 3477
64. Kirby, J. P.; van Dantzig, N. A.; Chang, C. K.; Noera, D. G.; *Tetrahedron Lett.* **1995**, *36*, 3477
65. de Rege, P. J. F.; Williams, S. A.; Therien, M. J. *Science* **1995**, *269*, 1409

66. a)Cukier, R. I. *J. Phys. Chem.* **1994**, 98, 2377. b) Zhao. X. G.; Cukier, R. I. *J. Phys. Chem.* **1995**, 99, 945
67. a)Cukier, R. I. *J. Phys. Chem.* **1995**, 99, 16101. b) Cukier, R. I. *J. Phys. Chem.* **1996**, 100, 15428
68. Kalyanasundaram, K. *Photochemistry of Polypyridine and Porphyrin Complexes*; Academic Press: London, 1992: Ch. 6.
69. Krausz, E.; Ferguson, J. *Prog. Inorg. Chem.* **1989**, 37, 293
70. a) Curtis, J. C.; Sullivan, B. P.; Meyer, T. J. *Inorg. Chem.* **1983**, 22, 224. b) Kober, E. M.; Sullivan, B. P.; Meyer, T. J. *Inorg. Chem.* **1984**, 23, 2098 c) Saleh, A. A.; Crutchley, R. J. *Inorg. Chem.* **1990**, 29, 2132
71. Felix, F.; Ferguson, J.; Gudel, H. U.; Ludi, A. *J. Am. Chem. Soc.* **1980**, 102, 4096
72. Paris, J. P.; Brandt, W. W. *J. Am. Chem. Soc.* **1959**, 81, 5001
73. Porter, G. B.; Schl  ffer, H. L. *Ber. Bunsenges. Physik. Chem.* **1964**, 68, 316
74. Crosby, G. A.; Perkins, W. G.; Klassen, D. M. *J. Chem. Phys.* **1965**, 43, 1498
75. a) Klassen, D. M.; Crosby, G. A. *J. Chem. Phys.* **1965**, 43, 1498. b) Demas, J. N.; Crosby, G. A. *J. Mol. Spectrosc.* **1968**, 26, 72. c) Lytle, F. E.; Hercules, D. M. *J. Am. Chem. Soc.* **1969**, 91, 253
76. Damrauer, N. H.; Cerullo, G.; Yeh, A.; Boussie, T. R.; Shank, C. V.; McCusker, J. K. Science, submitted
77. Kober, E. M.; Caspar, J. V.; Lumpkin, R. S.; Meyer, T. J. *J. Phys. Chem.* **1986**, 90, 3722
78. a) Durham, B.; Caspar, J. V.; Nagle, J. K.; Meyer, T. J. *J. Am. Chem. Soc.* **1982**, 104, 4803. b) Wang, R.; Vos, J. G.; Schmehl, R. H.; Hage, R. *J. Am. Chem. Soc.* **1992**, 114, 1964.
79. Kirby, J. P. Ph.D. Dissertation M.S.U. 1997

80. Bard, A. J.; Faulkner, L.R. *Electrochemical methods Fundamentals and Applications*; John Wiley: New York, 1980.
81. Cabianiss, G. E.; Diamantis, A. A.; Murphy, W. R.; Linton, R. W.; Meyer, T. J. *J. Am. Chem. Soc.* **1985**, *107*, 1845.
82. a) Smoluchowski, M. *Z. Phys.* **1916**, *17*, 557. b) Smoluchowski, M. *Z. Phys.* **1916**, *17*, 585. c) Smoluchowski, M. *Z. Phys. Chem.* **1917**, *92*, 129. d) Debye, P. *Trans. Electrochem. Soc.* **1942**, *82*, 265
83. a) Neta, P.; Meisel, D. *J. Phys. Chem.* **1976**, *80*, 519. b) Neta, P.; Simic, M. G.; Hoffman, M. Z. *J. Phys. Chem.* **1976**, *80*, 2018. c) Bakale, G.; Gregg, E. C.; McCreary, R. D. *J. Chem. Phys.* **1977**, *67*, 5788. d) Guthrie, R. D.; Cho, N. S. *J. Am. Chem. Soc.* **1979**, *101*, 4698
84. Stern, O.; Volmer, M. *Z. Phys.* **1919**, *20*, 183
85. Hoffman, M. Z.; Bolletta, F.; Moggi, L.; Hug, G. L. *J. Phys. Chem. Ref. Data.* **1989**, *18*, 219
86. a) Chatterjee, S.; Davis, P. D.; Gottschalk, P.; Kurz, M. E.; Sauerwein, B.; Yang, X.; Schuster, G. B. *J. Am. Chem. Soc.* **1990**, *112*, 6329. b) Murphy, S. T.; Zou, C.; Miers, J. B.; Ballew, R. M.; Dlott, D. D.; Schuster, G. B. *J. Phys. Chem.* **1993**, *97*, 13152. c) Murphy, S.; Schuster, G. B. *J. Phys. Chem.* **1995**, *99*, 511.
87. Struve, W.S. In: *Fundamentals of Molecular Spectroscopy*; John Wiley: New York, 1989.
88. Newsham, R. Ph.D. Dissertation. M. S. U. 1988.
89. Saari, E. A. Ph.D Dissertation Michigan State University 1997
90. L. E. Bowman, K. A. Berglund and D. G. Nocera, *Rev. Sci. Instr.*, **64** (1993) 338
91. Barbara, P. F.; Meyer, T. J.; Ratner, M. A. *J. Phys. Chem.* **1996**, *100*, 13148
92. a) Wilson, G. J.; Launikonis, A.; Sasse, W. H. F.; Mau, A. W.-H. *J. Phys. Chem.* **1997**, *101*, 4860. b) Yonemoto, E. H.; Riley, R. L.; Kim, I. K.; Atherton, S. J.; Schmehl, R. H.; Mallouk, T. E. *J. Am. Chem. Soc.* **1992**, *114*, 8081. c) Yonemoto, E. H.; Saupe, G. B.; Schmehl, R. H.; Hubig, S. M.; Riley, R. L.; Iverson, B. L.; Mallouk, T. E. *J. Am. Chem. Soc.* **1994**, *116*, 4786. d) Larson, S. L.; Elliott, C.

- M.; Kelley, D. F. *Inorg. Chem.* **1996**, *35*, 2070 e) Balzani, V.; Scandola, F. *Supramolecular Photochemistry*: Ellis Horwood: New York, 1991, f) Scandola, F.; Bignozzi, C. A.; Indelli, M. T.; Chiorboli, C.; Bignozzi, C. A. *Top. Curr. Chem.* **1990**, *158*, 73. g) Meyer, T. J. *Acc. Chem. Res.* **1989**, *22*, 163.
93. Kropf, M.; Joselevich, E.; Dürr, H.; Willner, I. *J. Am. Chem. Soc.* **1996**, *118*, 655
 94. Peek, B. M.; Ross, G. T.; Edwards, S. W.; Meyer, G. J.; Meyer, T. J.; Erickson, B. W. *Int. J. Peptide Protein Res.* **1991**, *38*, 114
 95. Roberts, J. A.; Kirby, J. P.; Nocera, D. G. *J. Am. Chem. Soc.* **1995**, *117*, 8051
 96. Kober, E. M.; Caspar, J. V.; Lumpkin, R. S.; Meyer, T. J. *J. Phys. Chem.* **1986**, *90*, 3722. b) Caspar, J. V.; Westmooreland, T. D.; Allen, G. H.; Bradley, P. G.; Meyer, T. J.; Woodruff, W. H. *J. Am. Chem. Soc.* **1984**, *106*, 3492. c) Caspar, J. V.; Kober, E. M.; Sullivan, B. P.; Meyer, T. J. *J. Am. Chem. Soc.* **1982**, *104*, 630. d) Bradley, P. G.; Kress, N.; Hornberger, B. A.; Dallinger, R. F.; Woodruff, W. H. *J. Am. Chem. Soc.* **1981**, *103*, 7441
 97. Engleman, R.; Jortner, J. *Mol. Phys.* **1970**, *18*, 145. b) Freed, K.F.; Jortner, J. *J. Chem. Phys.* **1970**, *52*, 6272
 98. Hupp, J. T.; Neyhart, G. A.; Meyer, T. J.; Kober, E. M. *J. Phys. Chem.* **1992**, *96*, 10820
 99. Demas, J. N.; Adamson, A. W. *J. Am. Chem. Soc.* **1973**, *95*, 5159
 100. a) L. F. Cooley, C. E. L. Headford, C. M. Elliott and D. F. Kelley, *J. Am. Chem. Soc.*, *110* (1988) 6673. b) Cooley, L. F.; Berquist, P.; Kelley, D. F. *J. Am. Chem. Soc.* **1990**, *112*, 2612
 101. (a)Dallinger, R. F., Woodruff, W. H.; *J. Am. Chem. Soc.*, **1979**, *101*, 4391
 (b)McClanahan, S. F., Dallinger, R. F., Holler, F. J., Kincaid, J. R.; *J. Am. Chem. Soc.*, **1985**, *107*, 4853. (c) Chung, Y. C., Leventis, N., Wagner, P. J., Leroi, G. E.; *J. Am. Chem. Soc.*, **1985**, *107*, 1414.(d) Chung, Y. C., Leventis, N., Wagner, P. J., Leroi, G. E.; *Inorg. Chem.*, **1985**, *24*, 1966.(e)Carroll, P. J., Brus, L. E.; *J. Am. Chem. Soc.* **1987**, *109*, 7613.(f) Kumar, C. V., Barton, J. K., Turro, N. J., Gould, I. R.; *Inorg. Chem.*, **1987**, *26*, 1455.(g) Kumar, C. V., Barton, J. K., Gould, I. R., Turro, N. J., Van Houten J.; *Inorg. Chem.*, **1988**, *27*, 648.(h)Yabe, T., Orman, L. K., Anderson, D. R., Yu, S.-C. Xiobing, X., Hopkins, J. B.; *J. Phys. Chem.*, **1990**, *94*, 7128.(i)Yabe, T., Orman, L. K., Anderson, D. R., Yu, S.-C. Xiobing, X., Hopkins, J. B.; *J. Phys. Chem.*, **1990**, *94*, 729.(j) Danzer, G. D., Golus, J. A.,

- Kincaid, J. R.; *J. Am. Chem. Soc.*, **1993**, *115*, 8643. (k) Danzer, G. D., Kincaid, J. R.; *J. Phys. Chem.*, **1990**, *94*, 3976. (l) Schoonover, J. R., Strouse, G. F., Chen, P., Bates, W. D., Meyer, T. J.; *Inorg. Chem.*, **1993**, *32*, 2618. (m) Schoonover, J. R., Chen, P., Bates, W. D., Dyer, R., Meyer, T. J.; *Inorg. Chem.*, **1994**, *33*, 793 (n) Cooley, L. F., Berquist, P., Kelley, D. F.; *J. Am. Chem. Soc.*, **1990**, *112*, 2612. (o) Kober, E. M., Sullivan, B. P., Meyer, T. J.; *Inorg. Chem.*, **1984**, *23*, 2098. (p) Bradley, P. G., Kress, N., Hornberger, B. A., Dallinger, R. F., Woodruff, W. H.; *J. Am. Chem. Soc.*, **1981**, *103*, 7441. (q) Vining, W. J., Caspar, J. V., Meyer, T. J.; *J. Phys. Chem.* **1985**, *89*, 1095
102. Treadway, J. A.; Loeb, B.; Lopez, R.; Anderson, P. A.; Kene, F. R.; Meyer, T. J.; *Inorg. Chem.* **1996**, *35*, 2242 b) Jones, W. E.; Bignozzi, C. A.; Chen, P. Meyer, T. J. *Inorg. Chem.* **1993**, *32*, 1167. c) Strouse, G. F.; Schoonover, J. R.; Duesing, R.; Boyde, S.; Jones, W. E.; meyer, T. J. *Inorg. Chem.* **1995**, *34*, 473 e) Anderson, P. A.; Strouse, G. F.; Treadway, J. A.; Keene, F. R.; Meyer, T. J. *Inorg. Chem.* **1994**, *33*, 3863.
103. a) Wacholtz, W. F.; Auerbach, R. A.; Schmehl, R. H. *Inorg. Chem.* **1986**, *25*, 227. b) Elliott, C. M.; Hershenhart, E. J. *J. Am. Chem. Soc.* **1982**, *104*, 7519. c) Mabrouk, P. A.; Wrighton, M. S. *Inorg. Chem.* **1986**, *25*, 526. d) Hupp, J. T.; Weaver, M. J. *Inorg. Chem* **1984**, *23*, 3639.
104. Kirby, J. P.; Roberts, J. A.; Nocera, D. G.; *J. Am. Chem. Soc.* In press
105. Wilcox, C. S.; In *Frontiers in Supramolecular Organic Chemistry and Photochemistry*; Schneider, H.-J., Durr, H., eds.; VCH: Weinheim, 1991; p 123.
106. a) Giordano, P. J.; Bock, C. R.; Wrighton, M. S.; Interrante, L. V.; Williams, R. F. X. *J. Am. Chem. Soc.* **1977**, *99*, 3187. b) Ferguson, J.; Mau, A. W.-H.; Sasse, W. H. F. *Chem. Phys Lett.* **1979**, *68*, 21. c) Lay, P. A.; Sasse, W. H. F. *Inorg. Chem.* **1984**, *23*, 4125. d) Shimidzu, T.; Iyoda, T.; Izaki, K. *J. Phys. Chem.* **1985**, *89*, 642. e) Nazeeruddin, Md. K.; Kalyanasundaram, K. *Inorg. Chem.* **1989**, *28*, 4251.
107. Gray, H. B.; Winkler, J. R. *Annu. Rev. Biochem.* **1996**, *65*, 537.
108. a) Andersson, L. A.; Loehr, T. M.; Chang, C. K.; Mauk, A. G. *J. Am. Chem. Soc.* **1985**, *107*, 182. b) Ward, B.; Chang, C. K.; Young, R. *J. Am. Chem. Soc.* **1984**, *106*, 3943. c) Hanson, L. K.; chang, C. K.; Ward, B.; Callahan, P. M.; Babcock, G. T.; Head, J. D. *J. Am. Chem. Soc.* **1984**, *106*, 3950
109. Scherer, T.; van Stokkum, I. M. H.; Brouwer, A. M.; Verhoeven, J. W. *J. Phys. Chem.* **1994**, *98*, 10539

110. a) Born, M. *Z. Phys.* **1920**, *1*, 45. b) Kirkwood, J. G. *J. Chem. Phys.* **1939**, *7*, 911. c) Onsager, L. *J. Am. Chem. Soc.* **1936**, *58*, 1486. d) Hush, N. S. *Trans. Faraday Soc.* **1961**, *57*, 557 e) Powers, M. J.; Meyer, T. J. *J. Am. Chem. Soc.* **1978**, *100*, 4393. f) Powers, M. J.; Meyer, T. J. *J. Am. Chem. Soc.* **1980**, *102*, 1289. g) Brunshweig, B. S.; Ehrenson, S.; Sutin, N. *J. Phys. Chem.* **1986**, *90*, 3657. h) Brunshweig, B. S.; Ehrensn, S.; Sutin, N. *J. Phys. Chem.* **1987**, *91*, 4714.
111. a) Dodsworth, E. S.; Lever, A. B. P.; *Chem. Phys. Lett*, **1984**, *112*, 567. b) Dodsworth, E. S.; Lever, A. B. P.; *Chem. Phys*, **1985**, *119*, 61. c) Dodsworth, E. S.; Lever, A. B. P.; *Chem. Phys.* **1986**, *125*, 152. d) Dodsworth, E. S.; Lever, A. B. P. *Inorg. Chem.* **1990**, *29*, 499
112. a) Graige, M. S.; Paddock, M. L.; Bruce, J. M.; Feher, G.; Okamura, M. Y. *J. Am. Chem. Soc.* **1996**, *118*, 9005. b) Okamura, M. Y.; Feher, G. *Annu. Rev. Biochim.* **1992**, *61*, 861. c) Takahashi, E.; Maroti, P.; Wraight, C. In *Electron and Proton Transfer In Chemistry and Biology*; Müller, A., Ratajczaks, H., Junge, W., Dieman, E., Eds.; Elsevier: Amsterdam, 1992; pp 219-236. d) Babcock, G. T.; Barry, B. A.; Debus, R. J.; Hoganson, C. W.; Atamian, M.; McIntosh, L.; Sithole, I.; Yocum, C. F. *Biochemistry* **1989**, *28*, 9557. e) *The Photosynthetic Bacterial Reaction Center-Structure and Dynamics*; Breton, J., Vermeglio, A., Plenum: New York, 1988.
113. a) Wikström, M. *Nature* **1989**, *338*, 776. b) Babcock, G. T.; Varotsis, C. *Proc. SPIE-Int. Soc. Opt. Eng.* **1993**, *1890*, 104. c) Babcock, G. T.; Wikström, M. *Nature*, **1992**, *356*, 301. d) Malmström, B. G. *Acc. Chem. Res.* **1993**, *26*, 332. e) Malmström, B. G. *Chem. Rev.* **1990**, *90*, 1247.
114. G. F. Strouse, J. R. Schoonover, R. Duesing, S. Boyde, W. E. Jones, Jr. and T. J. Meyer, *Inorg. Chem.*, *34* (1995) 473
115. Connors, K. A. *Binding Constants The Measurement of Molecular Complex Stability*; ; John Wiley: New York, 1987.
116. C. M. Elliott and E. J. Hershenhart, *J. Am. Chem. Soc.*, *104* (1982) 7519

APPENDIX A

APPENDIX A

DETERMINATION OF THE ACID-BASE PROPERTIES OF A SERIES OF ELECTRON TRANSFER DONOR-ACCEPTOR PAIRS: ASSESSMENT OF THE pK_a^* AND ΔpK_a IN AQUEOUS SOLUTION

Introduction

Excited state proton transfer reactions of terminal oxo complexes of Re(I), Mn(IV), and Ru(II) have been investigated extensively [57,117]. Still, other proton transfer reactions utilizing the excited states of functionally substituted bipyridyls of *tris*-bipyridyl ruthenium complexes are used in the development of effective solar energy conversion systems [118] and proton transfer reactions have been implicated as playing a role in investigations into the development of photovoltaics [119].

The study of inorganic complexes for solar energy storage applications have provided many examples based upon the *tris*-bipyridyl ruthenium class of complexes [120]. The coordination of bipyridyl ligand to metal atoms make the complexes particularly suitable for pK_a studies. The addition of protonatable substituents at the

periphery of the ligands is synthetically straight-forward and the compounds are easily synthesized. The excited state properties of these complexes have many desirable characteristics, the lifetimes are long compared to the time constant of the proton transfer reaction under study, the luminescence of the excited state is strong and in most cases very dependant upon the degree of protonation.

Protonation/deprotonation investigations utilizing bipyridyl ruthenium complexes have been investigated for more than 25 years [121]. The first example of excited state protonation/deprotonation processes in which both protonated and deprotonated forms of $[(\text{bpy})_2\text{Ru}^{2+}(\text{bpy}-(\text{COOH})_2)[(\text{PF}_6)]$ in a buffered aqueous solvent was studied by Wrighton and coworkers [122]. These studies provided a preliminary insight into the photophysical properties exhibited under changing pH conditions. Since that time the development of Ru(II) complexes utilizing a wide range of protonatable bipyridyl [57,123] and imidazolyl and benzimidazolyl [124] ligands have been reported. Excited state properties of $\text{Ru}(\text{bpy})_3^{2+}$ complexes and synthetic variations, allow convenient control of the energy gap (ΔE between the emissive $^3\text{MLCT}$ state and the deactivating MC state) [67] allowing the design of complex having desirable photophysical characteristics. The depth of the studies of $\text{Ru}(\text{bpy})_3^{2+}$ complexes has allowed their incorporation into both electrochemical and photophysical sensors for the determination of pH in solution [125]. Design of an $\text{O}_2(\text{g})$ sensor based on the protonation/deprotonation properties of Ru(II)polypyridyl complexes has also been reported [126]. Furthermore, these complexes have been implemented as luminescent tags [127] for the study of protein folding/denaturing in aqueous solution as a function of solution pH. More fundamental approaches, have been concerned with implementation of

protonation/deprotonation processes in the activation of substrates and energy conversion schemes [120,128]. Work oriented toward the investigation of protonation/deprotonation processes in the tuning of redox potentials in electron transfer schemes have also appeared [129].

The work presented in this Appendix is comprised of the examination of acid-base properties of these two sets of Ru(II)polypyridyl complexes designed for the study of excited state photoinduced electron transfer reactions; the data is supplemented with that collected by the very capable summer undergraduate research student, Sam Wall. In Chapters 3 and 4 the salt-bridge complexes, Figure 33, presented in non-aqueous aprotic organic solvents, CH₃CN and CH₂Cl₂ have been used in protonation/deprotonation investigations in buffered aqueous solvent. The tendency of a proton to change position within the salt-bridge interface in response to a change in the electronic composition of reactants initiated by the absorption of a photon in electron transfer reactions is an issue of the acidity/basicity of each component of the salt-bridge complex. To this end synthesis of the ruthenium compounds of Figure 33, having different energetics for the ancillary ligands bpy (2,2'-bipyridine) and tmb (4,4' 5,5' tetramethyl-2,2'-bipyridine) were synthesized as a necessary components of the electron transfer investigations (see Chapter 4). The remaining bipyridine ligand, Me-bpyCOOH or Me-bpyAmH⁺ (Me-bpyCOOH = 4'-methyl-4'-carboxy-2,2'-bipyridine and Me-bpyAmH⁺ = 4-methyl-4'-amidinium-2,2'-bipyridine) serve as one half of the salt-bridge electron transfer complex. The investigation of these complexes to gain insight into the propensity of the proton of the salt-bridge interface to change position in response to a change in the electronic

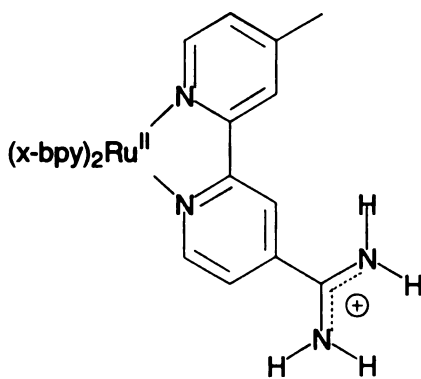
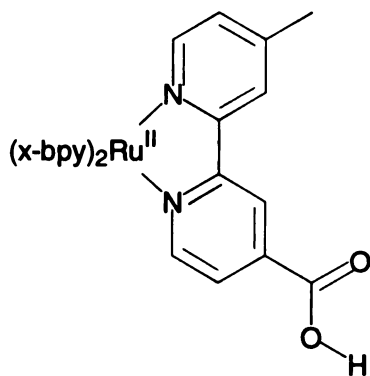


Figure 33. Ru(II)polypyridyl complexes used in the aqueous acid-base property determinations. (a),(b) $[(x\text{-bpy})_2\text{Ru}^{2+}(\text{Me-bpy})\text{COOH}]^{2+}$ {(a) $x = \text{H}$ and (b) $x = (\text{CH}_3)_4$, and (c),(d) $[(x\text{-bpy})_2\text{Ru}^{2+}(\text{Me-bpy})\text{AmH}^+]^{3+}$ {(c) $x = \text{H}$ and (d) $x = (\text{CH}_3)_4$ }.

composition of reactants resulting from the absorption of a photon by the donor, or as a result of the electron transfer reaction in the formation of the charge separated state within the bound complex, and assess this information with regard to the electron transfer reactions of the non-aqueous aprotic solvent systems is the primary aim of this Appendix.

Results

Absorption / Emission Ground and Excited State Acid-Base Reactions of the Ruthenium Complexes

In Figure 34. is shown the absorption titration for each of the carboxylic acid derivatized ruthenium complexes (**33a**) and (**33b**). The insets show the change in the absorption at wavelengths in the respective MLCT region ($\lambda_{\text{max}} = 457$ and 440 nm) and ($\lambda_{\text{max}} = 287$ and 290 nm) for the intraligand $\pi-\pi^*$ region. Observation of Figure 34 shows that for complex (**33a**) there is evidence for two isosbestic points throughout the pH titration at the red and blue edges of the MLCT region located at 400 and 467 nm, while in the bipyridyl $\pi-\pi^*$ region there is evidence for two additional distinct isosbestic points at 274 and 297 nm. The inset titration associated with each plot shows one inflection point located at a pH of approximately 2.0 . For the tetramethylated complex (**33b**) the more clear evidence of two clean isosbestic points located at each side of the MLCT band located at 418 and 477 nm between the pH range 1.85 and 12 are observed. However, at pH below 1.85 the isosbestic point shifts approximately 2 nm to the red and drops slightly in intensity. While it is unlikely that this change in the isosbestic point below pH of 1.85

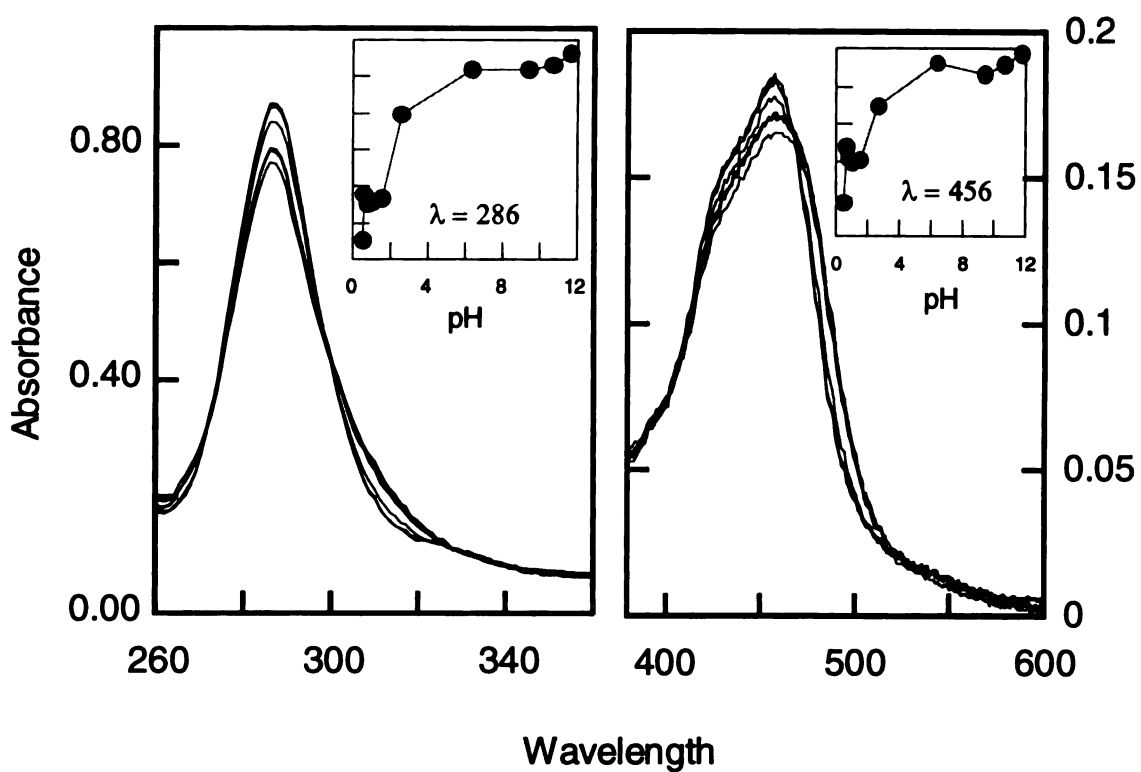


Figure 34. Absorption pH titration of $[(bpy)_2Ru^{2+}(Me-bpy)COOH][(PF_6)_2]$. The spectrum for the intraligand $\pi-\pi^*$ region is shown at the left and the spectrum in the $d\pi-\pi^*$ MLCT region at the right. The inset of each of the plots shows the change of the absorption ($\lambda = 286$ and 456 nm) over the pH range of the experiment.

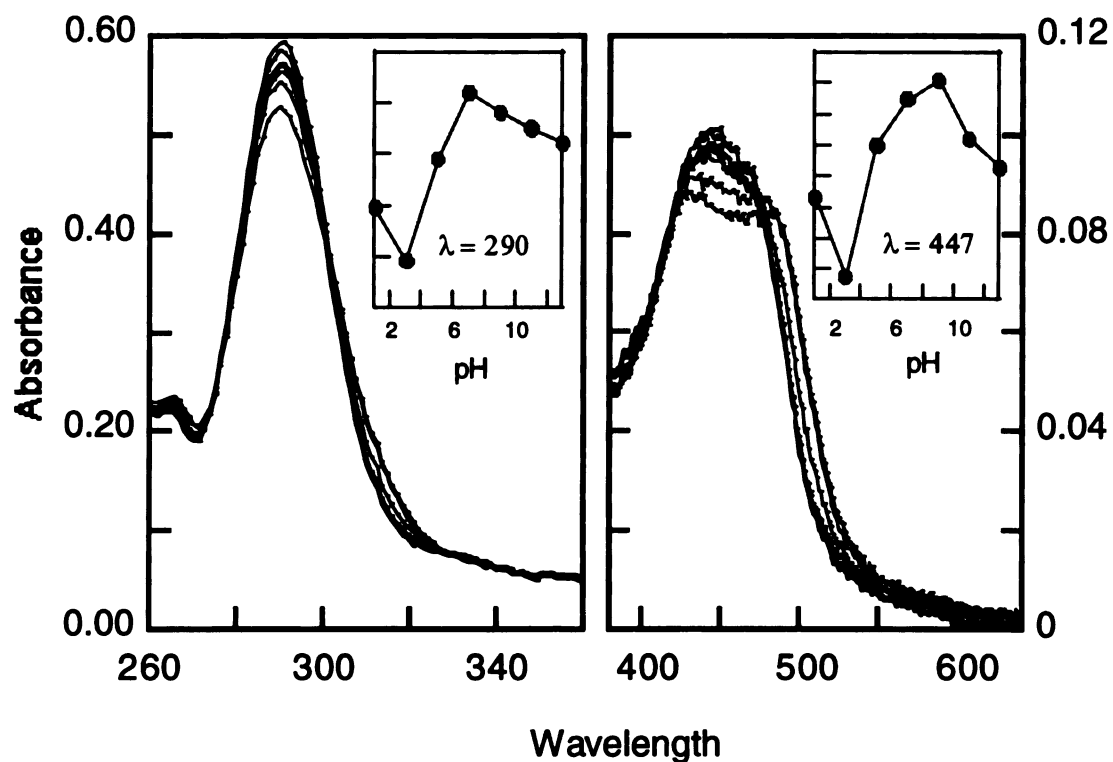


Figure 35. Absorption pH titration of $[(tmb)_2Ru^{2+}(Me-bpy)COOH][(PF_6)_2]$. The spectrum for the intraligand $\pi-\pi^*$ region is shown at the left and the spectrum of the $d\pi-\pi^*$ region is shown at the right. The inset of each of the plots shows the absorption ($\lambda = 290$ and 447 nm) over the pH range investigated.

indicates a second protonation step as has been found in ruthenium complexes having two independent titratable carboxylic acid residues [106] the reversibility leads to the interpretation of the data as due to solution/environmental effects. With reference to Figures 34 and 35 it is seen that for the titration range examined for each of the ruthenium complexes (**33a**) and (**33b**) there is a decreased intensity and broadening of the MLCT band with decreasing pH from 12 to 2.0. In complex (**33a**) the broadening is less substantial than is observed for the tetramethylated complex (**33b**) and little or no evidence of the splitting of the MLCT band as can be readily observed for complex (**33b**) showing evidence of two discernable peak maxima located at 431 and 482 nm.

In Figures 36 and 37 is shown the absorption titration for each of the amidinium derivatized ruthenium complexes (**33c**) and (**33d**). The inset for each region of the spectra both bipyridyl and MLCT show the change in the absorption at wavelengths 457 nm and 440 nm of the MLCT transition for each of these ruthenium complexes. For complex (**33c**) one clean isosbestic point located at 470 nm between the pH range 5 and 12 while at pH below 5 to the lowest pH in the range studied 1.8 a new isosbestic point is observed shifted approximately 3 nm to the red. For complex (**33d**) the same behavior is observed, as found for complex (**33c**) except that for this complex the isosbestic point is located at 479 nm and occurs for the pH range 9.8 to 13.5. At pH below 9.8 through to pH 1.03 the new isosbestic point shifted ~ 2 nm to the red is observed. For each of these complexes the inset absorption change plots mirror the changes in absorption observed throughout the pH range examined. Once again, the shifting isosbestic points are indicative of the establishment of a new equilibria yet for these complexes there are no additional

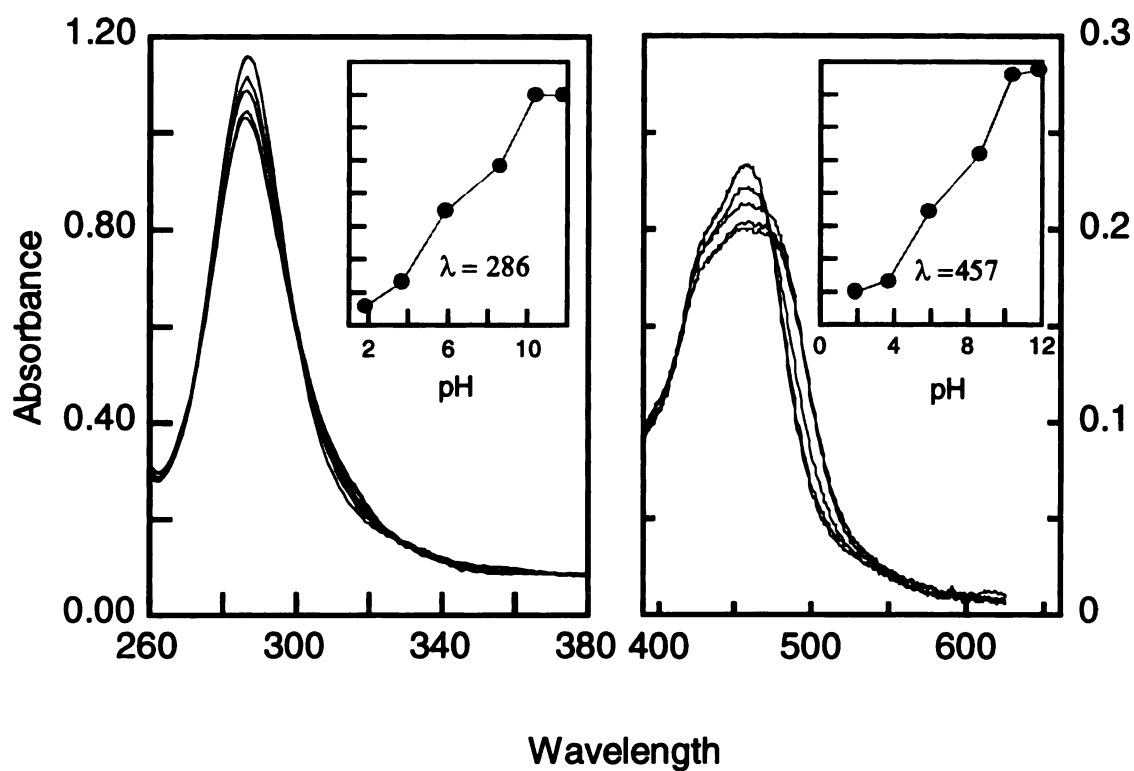


Figure 36. Absorption pH titration of $[(bpy)_2Ru^{2+}(Me-bpy)AmH^+](PF_6)_2$. The spectrum for the intraligand $\pi-\pi^*$ region is shown at the left and the spectrum of the $d\pi-\pi^*$ region is shown at the right. The inset of each of the plots shows the absorbance ($\lambda = 286$ and 457 nm) over the pH range investigated.

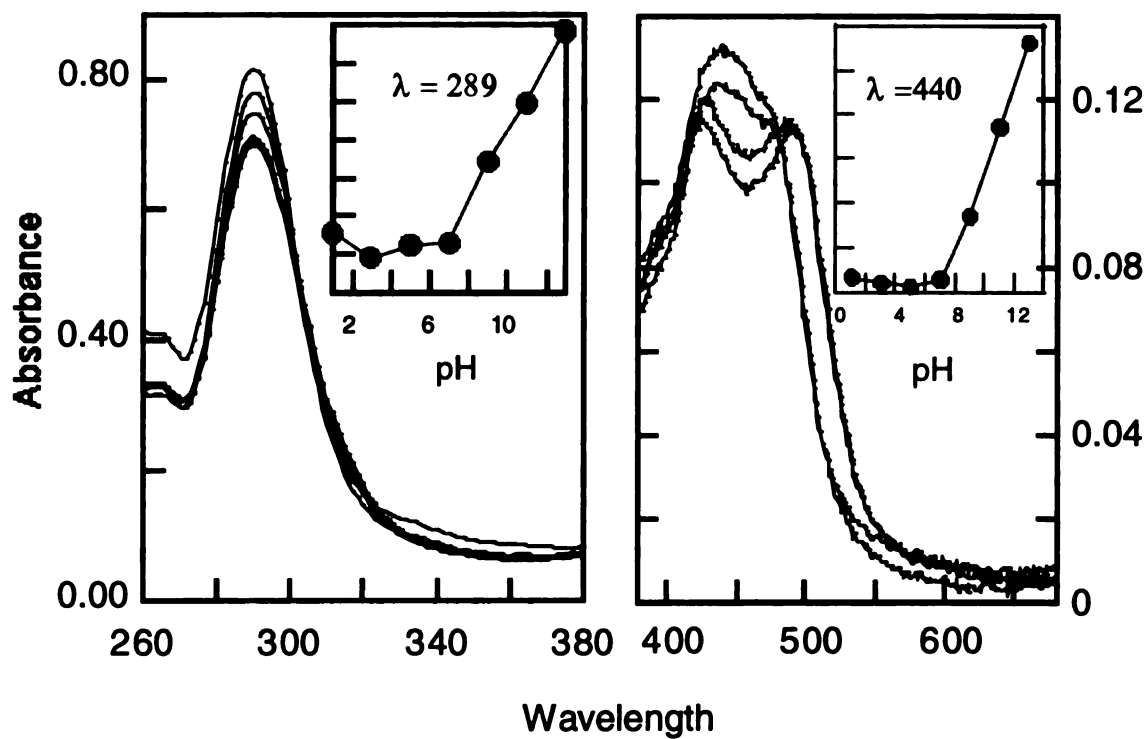


Figure 37. Absorption pH titration of $[(tmb)_2Ru^{2+}(Me-bpy)AmH^+](PF_6)_3$. The spectrum for the intraligand $\pi-\pi^*$ region is shown at the left and the spectrum of the $d\pi-\pi^*$ region is shown at the right. The inset of each of the plots shows the absorption ($\lambda = 289$ and 440 nm) over the pH range investigated.

dissociable substituents. Alternatively, the changes in the isosbestic points may indicate decomposition, although the changes are reversible.

Further observation of the data presented in Figure 36 and 37 reveals a pronounced broadening, and most particularly for the tetramethylated Ru(II) complex, a distinct splitting of the absorption in the MLCT region at low pH. The splitting gives rise to two distinct maxima located at 427 and 491 nm of the MLCT band. Upon increasing the pH the MLCT region shows a coalescence of the absorption band and a shifting of the red edge absorption maxima to higher energy with little or no variation at the higher energy blue edge of the absorption.

In Figures 38 and 39 are shown the emission data and titration profiles of the acid base reactions for the complexes (33a) and (33b). Observation of the emission data presented in Figures 38 and 39, the emission spectra are seen to be broad structureless gaussian shaped profiles typical of $\text{Ru}(\text{bpy})_3^{2+}$ compounds. Insets for each of the figures show the titration profiles as a function of pH over the range of pH 2-10 for (33a) and pH 2-12 for (33b). For these two complexes the position of the emission maxima throughout the titration are found to have opposite trends in regard to the direction of the shift relative to the addition of base. For complex (33a) the protonated emission maximum is found to be located at ~ 650 nm whereas, the deprotonated emission maximum is located at ~ 630 nm. For complex (33b) the protonated emission maximum position is similar to the protonated form of (33a) at 650 nm, yet the deprotonated emission maximum is located approximately 10 nm to the red at 660nm. For each of the complexes the same trend is observed for the change in the emission intensity. For complex (33b) the relative

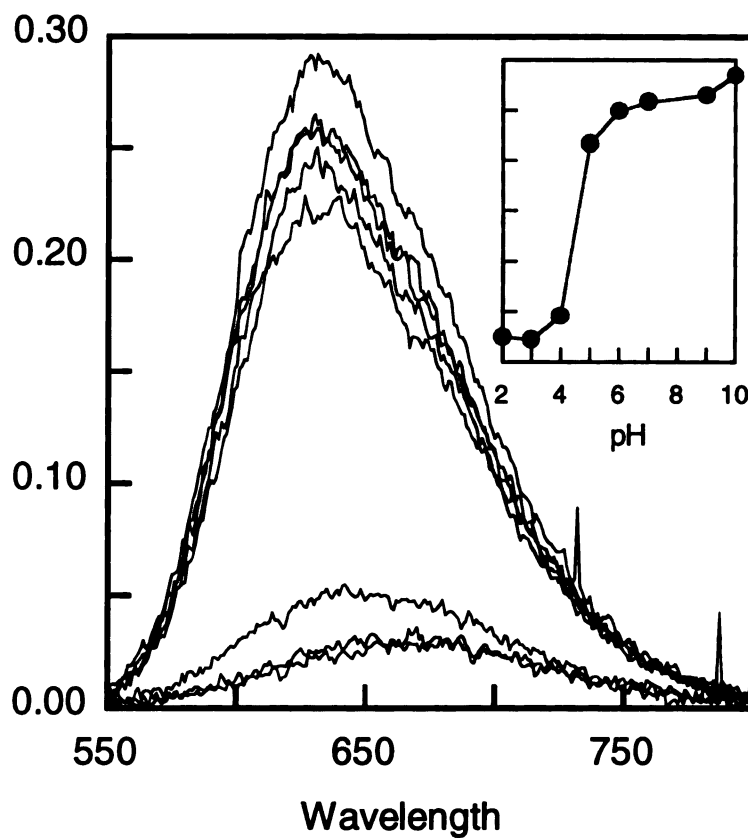


Figure 38. Emission pH titration for $[(bpy)_2Ru^{2+}(Me-bpy)COOH][PF_6]_2$. The inset of the plot indicates the changes of the emission intensity at 630 nm over the pH range investigated.

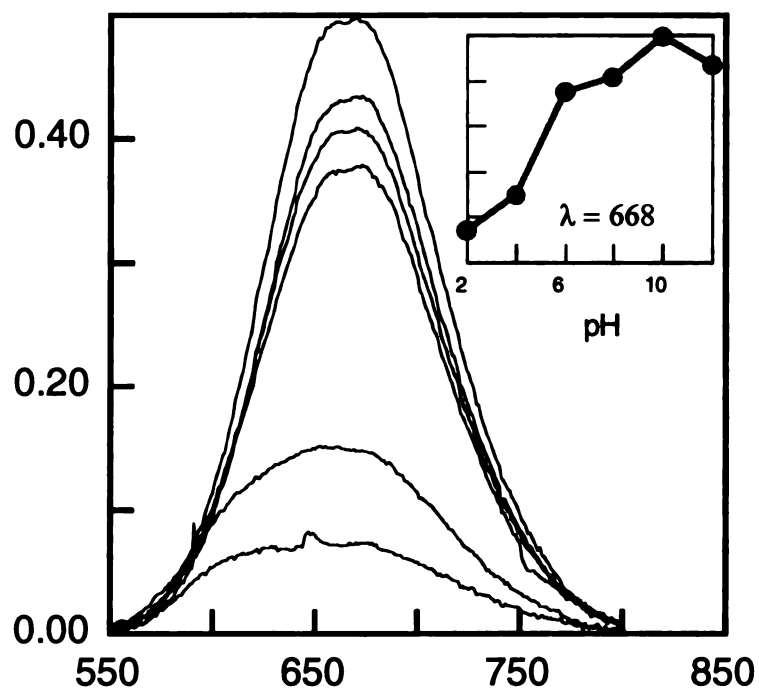


Figure 39. Emission pH titration for $[(\text{tmb})_2\text{Ru}^{2+}(\text{Me-bpy})\text{COOH}][\text{PF}_6]_2$. The inset of the plot indicates the changes of the emission intensity at 630 nm over the pH range investigated.

change in the emission intensity is 10 times more intense at pH of 12 than at pH 2. The 10 nm change of the emission maximum represents a change of approximately 0.028 V or 226 cm^{-1} in the energy of the emissive excited state. That the change is so small is somewhat surprising considering the change in both the extent of delocalization/electronic coupling of the ligand orbitals with the metal centered orbitals throughout the protonation/deprotonation process [130]. Furthermore, the direction of the shift is somewhat contrary to what is expected considering that the deprotonated complex carboxylic acid ligand on becoming a carboxylate is electronically similar to a methyl group, rendering the ligand energetically near to that for a tetramethyl. The inset titration profile for complex (33b) shows data plotted for the emission maxima of both the fully deprotonated complex $\sim 670\text{ nm}$. In this plot of the data indicates a single inflection at pH 4.0-4.5. For complex (33a) there is a more distinct change in the position of the emission maxima. The fully protonated complex at pH 2 has maxima located at 670 nm while for the fully deprotonated complex pH 12 the maxima is located at 630 nm . Throughout this pH range the concomitant change in the intensity of the emission is relatively 10 times more intense at pH 10 than at pH 2. With the change in the emission maxima of 40 nm the change in the energy of the emissive excited state is 0.118 V (948 cm^{-1}). This change in the energy/wavelength of the emission maxima of the excited state concomitant with the protonation/deprotonation process energetically, is consistent with expectation. The loss of a proton at the carboxylic acid of the salt-bridge derivatized ligand results in a dramatic change in the energetics of the complex. Initially the energy of the carboxylic acid functionalized bipyridine ligand lies slightly below that of the 2,2'-bipyridine

ancillary ligands. Yet upon deprotonation the ligand becomes significantly decreased in π accepting ability relative to the ancillary ligands resulting in a reversal of the direction of the charge transfer transition, and the observed emission represents emission predominantly from a charge transfer state localized at the ancillary bipyridyl ligands. The resulting complex resembles energetically the *tris*-bipyridine complex and not surprisingly the emission maximum is nearly the same as for $\text{Ru}(\text{bpy})_3^{2+}$ complex in H_2O solution. The inset of Figure 38 for complex (33a) shows the titration profile through the pH range 2-10. The presentation of the data in the titration profile for the emission maximum of the fully protonated and fully deprotonated complex (data not shown) show similar behavior throughout the titration with inflection point located at pH 4.5 for both plots.

For complex (33c) the data (data not shown) show that at pH below 5 the emission maximum is located at 690 nm while for pH above 7 the emission maximum is located at 670 nm. The relative change in the emission intensity through the titration is 4 times greater at pH 12 than at pH below 5. The change in the emission maximum represents a change of 0.054V (432 cm^{-1}). Furthermore the data for complex (33d) indicate that there is a substantial change in the emission intensity between pH 9 and pH 12 and a plot of the data shows that the inflection point for the titration also lies in this region at pH of ~ 11 . The data for complex (33d) indicates that for the titration through pH 2 to pH 12 similar behavior to that for complex (33c) is observed. The emission maximum shifts to the red throughout the titration beginning at 615 for pH 2 and eventually ending at 665 for pH 12. Throughout the titration it can also be seen that the emission intensity changes by a factor of 5; being greater for the fully deprotonated

complex than for the fully protonated complex. The change of the emission maximum represents a change of 0.152 V (1223 cm^{-1}) difference in the energy of the excited state emission. For this complex there is a dramatic change in the emission intensity between pH 8 and pH 12 and a plot of the titration profile shows the inflection point for the titration occurs in this region at pH 10.0.

Ground State Acid Base Properties of the Free Ligands

For the Ruthenium complexes (33a), (33b), (33c) and (33d) there are four different free ligands of each complex 2,2'-bipyridine, (4,4' 5,5' tetramethyl) 2,2' bipyridine, (4-methyl-4'carboxylic acid) 2,2' bipyridine, and (4-methyl-4'amidinium) 2,2' bipyridine. The acid-base properties of the free ligands provide a direct measure of the interplay of the electronic σ donor strength and π bonding properties affecting the relative energy of the $d\pi-\pi^*$ MLCT transitions. The pKa values for a large variety of coordinating bipyridine ligands have been determined [123j]. Additionally the pKa of the (4-methyl-4'carboxylic acid)-2,2' bipyridine has also been previously determined to be 2.2 for the carboxylic acid substituent, with very little change of the two coordinating nitrogen atom pKa values from the 2,2' bipyridine ligand having values of 0.52 and 4.45 [131]. Assessment of the pKa of the free ligand 4-methyl,4'amidinium-2,2'-bipyridine has not been determined with sufficient accuracy to merit a clear estimate of the pKa, however absorption titration experiments place the pKa between 6-8.5.

Excited State Acid-Base Properties of the Ruthenium Complexes; Lifetime Measurements

The detectable emission of the four ruthenium complexes (33a), (33b), (33c) and (33d) is a benefit that is not universal for ruthenium bipyridyl complexes. This additional piece of information is enormously useful for the determination of the excited state pKa (pKa*) for each of the complexes. Typically the excited state (pKa*) for many molecules may be approximated from emission as a function of pH data using the thermodynamic Förster cycle [132], a knowledge of the energy of E_{0,0} and the changes of the absorption

$$\text{pKa}^* = \text{pKa} + \frac{(0.625)}{T(\nu_B - \nu_{\text{HB}})} \quad (\text{A1})$$

and emission maxima resultant from the protonation/deprotonation process. This relation has been particularly useful for the determination of the pKa* values of many organic compounds. But the spin forbidden charge transfer emission $^3\text{MLCT} \rightarrow ^1\text{A}_1$ G.S. for ruthenium bipyridyl complexes makes the use of this approximation tenuous as the rigorous use of the Förster cycle relationship requires changes shown by the Stokes shift of the emission relative to the absorption having the same spin multiplicity. Herein lies the problem, the absorption spectra of Ru(II)polypyridyl complexes with bipyridine ligands is dominated by the singlet transitions of the MLCT while the emission is predominantly triplet in character, making the approximation of the E_{0,0} for the triplet excited state very uncertain. Thus additional means are necessary for the determination of the pKa*. One such method incorporating corrections for the lifetime of both the

protonated and deprotonated complexes may be derived from these relationships based on the ground state absorption and the excited state emission. To determine pK_a^* more rigorously the changes in the ground and excited state equilibria of the acid-base reactions need to be entered into the equation. The form of the

$$pK_a^* = pK_{a_i} - \log \frac{\tau_{HB}}{\tau_B} \quad (A2)$$

expression is closely related to the Henderson-Hasselbach equation for volumetric acid-base titrations. In this expression τ_{HB} is the lifetime of the protonated complex, τ_B is that for the deprotonated complex and pK_i is the inflection point of the luminescence titration profile. The primary drawback for the application of this equation stems from the necessity of observable luminescence having a lifetime in non-aqueous aprotic solvent longer than the diffusional rate for proton transfer, as typical diffusional rates in solvents such as CH_3CN are approximately $2 \times 10^{10} M^{-1}s^{-1}$ and substantially less in many other solvents. In H_2O solvent this drawback is far less severe as it has been determined that the diffusional rate of the proton is of the order of $>10^{11} M^{-1} s^{-1}$ and has been suggested as being as great as $10^{13} M^{-1}s^{-1}$ in the Grotthuis mechanism [133]. For the Ruthenium complexes (33a,33b) and (33c,33d) there is a significant reduction of the emission intensity and quantum yield concomitant with the reduction of the pH (see above), however, even in the lowest pH solution 0.54 for $[(tmb)_2Ru^{2+}(Me-bpy)COOH]^{2+}$ observable luminescence and measureable lifetimes are found $\tau_{H^+} > 20$ ns ($k_{H^+} > 5 \times 10^7 s^{-1}$). The data of all four complexes is summarized and plotted in Figures 40 and 41. Inspection of the lifetime profiles of complexes (33a) and (33b) in Figure 40 show the

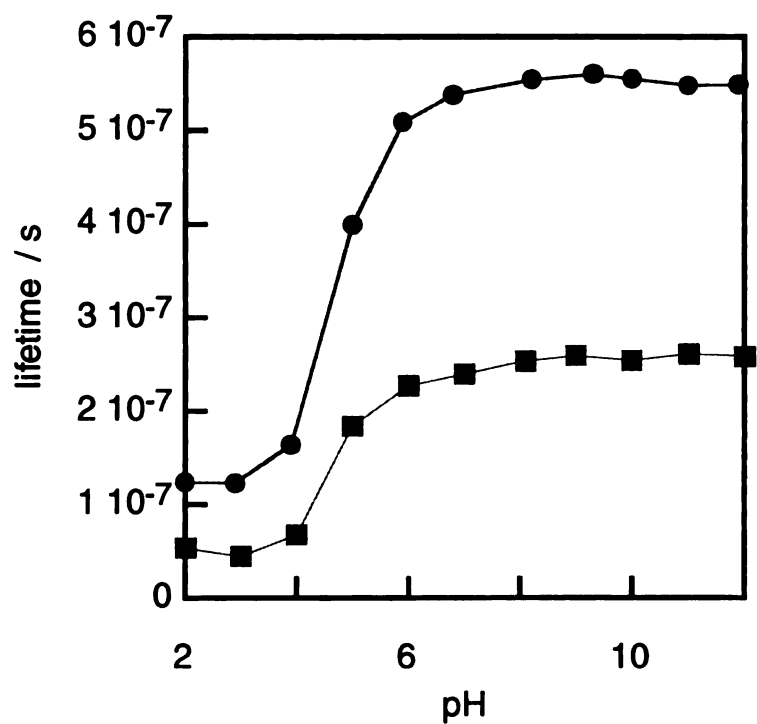


Figure 40. pH dependence of lifetime measurements. Top trace (●) is for the complex $[(bpy)_2Ru^{2+}(Me-bpy)COOH][PF_6]_2$, bottom trace (■) is for the complex $[(tmb)_2Ru^{2+}(Me-bpy)COOH][PF_6]_2$.

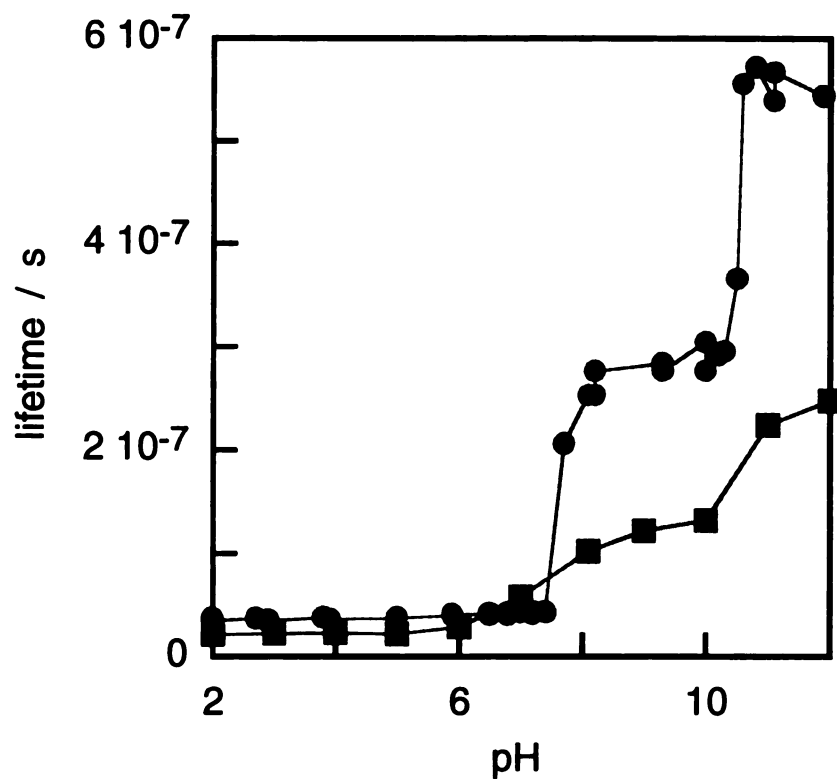


Figure 41. pH dependence of lifetime measurements. Top trace (●) is for the complex $[(bpy)_2Ru^{2+}(Me-bpy)AmH^+][PF_6]_3$, bottom trace (■) is for the complex $[(tmb)_2Ru^{2+}(Me-bpy)AmH^+][PF_6]_3$.

pH vs. lifetime titration data collected for each of the complexes at the emission maxima. For complex **(33a)** it is seen that the protonated complex lifetime is 125 ns ($k_{H^+} = 8.0 \times 10^6 \text{ s}^{-1}$) and that for the deprotonated complex 560 ns ($k_{-H^+} = 1.79 \times 10^6 \text{ s}^{-1}$) yielding a K_a of 4.47 with an apparent inflection point at pH = 5.2. Application of equation **A2** to the emission titration data and the lifetime data yields an assessment of the excited state pKa of 4.4. For complex **(33b)** the lifetime titration profile shows the protonated lifetime to be 50 ns ($k_{H^+} = 2.0 \times 10^7 \text{ s}^{-1}$) and that for the deprotonated complex to be approximately 250 ns ($k_{H^+} = 4 \times 10^6 \text{ s}^{-1}$) yielding a K_a of 5.0 with an apparent inflection point at pH = 4.8. Application of equation **A2** to these emission and lifetime data yield the assessment of the excited state pKa = 4.6.

For the complexes **(33c)** and **(33d)** the lifetime data is less well behaved in that for each of the complexes there are two apparent steps in the protonation sequence as the lifetime profiles show two distinct breaks. For complex **(33c)** the protonated lifetime is found to be approximately 45 ns ($k_{H^+} = 2.22 \times 10^7 \text{ s}^{-1}$) the lifetime at the intermediate step is found to be 275 ns ($k = 3.64 \times 10^6 \text{ s}^{-1}$) and the lifetime of the complex at pH between 10.5 and 12 is 575 ns ($k = 1.74 \times 10^6 \text{ s}^{-1}$). The K_a for the first and second processes is 6.1 with an apparent inflection point a pH 7.8 and that for the second and third processes is 2.1 with an inflection point at pH 10.5. The K_a for the sum of the two processes is thus 8.2. For complex **(33d)** the protonated lifetime is found to be 25ns ($k_{H^+} = 4.0 \times 10^7 \text{ s}^{-1}$) that for the intermediate step is 120 ns ($k = 8.33 \times 10^6 \text{ s}^{-1}$). For the final step a limiting value is not reached , however, using the average of the last two points of the titration a value for the lifetime is found to be 225 ns ($k = 4.44 \times 10^6 \text{ s}^{-1}$). These data then yield

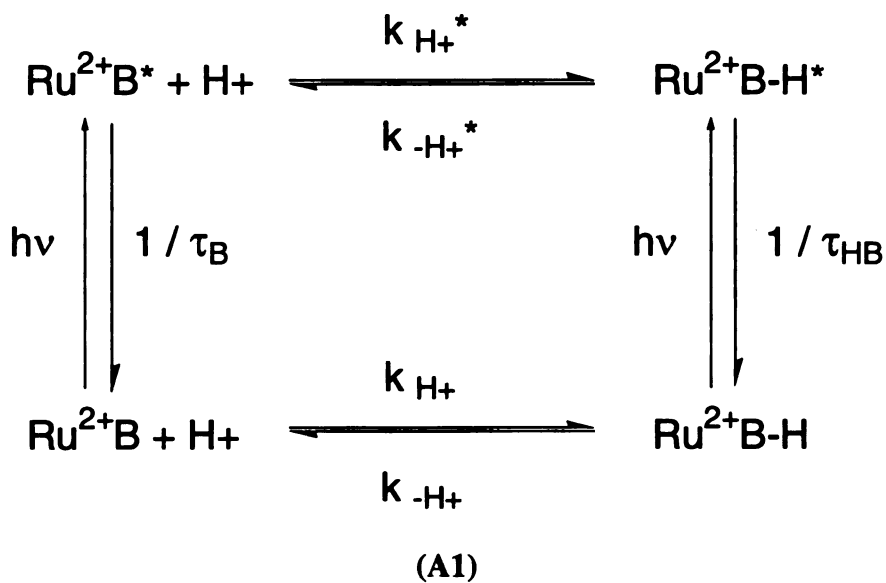
values of 4.8 for the first K_a and 1.9 for the K_a of the last step giving K_a for the overall process of 6.7. The inflection points for these two processes are located at pH 7.2 and 11.0.

Ground State Acid-Base Properties of Salt-Bridge Functionalized 3,5-dinitrobenzene Electron Transfer Quenchers

The acid-base properties of each of the electron transfer quenchers determined by standard volumetric titration procedures [134] were found to be 2.9 ± 0.2 and 8.5 ± 0.3 . The value for the acid functionalized complex is consistent with the pK_a for similar compounds: p-nitrobenzoic acid $pK_a = 3.4$ and benzoic acid $pK_a = 4.2$. However, the pK_a value found for the amidinium functionalized compound is substantially less than expectation. The pK_a reported for benzamidinium as the chloride salt is 11.6 [135]. Addition of the nitro groups would be expected to shift the pK_a to lower values but assessment of the pK_a utilizing linear free energy relationships for both inductive and resonance effects [136] which provide assessment of pK_a values for a great variety of organic complexes in very good agreement with measured values, yield a value of ~ 10 ; substantially higher than this experimental value. It is possible that the influence of the tetraphenyl borate counter ion lends some charge transfer character to the complex possibly lowering the observed pK_a but no assessment can be made to further rationalize this result.

Discussion

The utility of the pKa data derived from the measurement of the photophysical properties of these complexes allows an assessment of the relative tendency of the proton to transfer in response to altered acidity-basicity of the electron transfer donors and acceptors due to photoexcitation of the ruthenium chromophore, but is limited as a means to a simple determination of the intrinsic barrier to proton transfer in non-aqueous solvent. The limitations of the measurements of proton transfer rate constants for each of these ruthenium donors (33a,33b) and (33c,33d) stems from the equilibrium established in the excited state. Since both protonated and deprotonated forms of the complexes are emissive, and furthermore that the lifetime of the protonated form does not satisfy the condition $1/\tau_{HB} \gg k_{-H+}^*$ the deactivation of the excited state protonated complex to ground state protonated complex is in competition with back reaction to give the



deprotonated complex according to the scheme shown in Figure A1. The magnitudes of the K_A^* for each of the ruthenium complexes of ~ 5 is found for three of the four complexes throughout the pH titration range 2-12 the only exception being that observed for complex (33c) showing an apparent value of 6.1. In the limit that the excited state equilibrium is fast with respect to the excited state deactivation the above expression for the determination of the excited state pK_a^* should be modified to account

$$\frac{[HB^+]}{[B]} = \frac{\tau_{HB}(\tau_B - \tau_{obsd})}{\tau_B(\tau_{obsd} - \tau_{HB})} \quad (A3)$$

$$pK_a^* = pK_{a_i} - \log \frac{\tau_{HB}(\tau_B - \tau_{obsd})}{\tau_B(\tau_{obsd} - \tau_{HB})} \quad (A4)$$

for the excited state concentration distribution according to equations A3 and A4. That the lifetimes measured in these experiments show only monoexponential decay over the modest range of wavelengths surrounding the emission maxima observed, is an indication that the above assessment is correct and that the fast equilibrium interconverting the protonated and deprotonated forms gives rise to emission contributions from each species. The addition of large excess of acid or base through the pH titration influences the observed emission and lifetime, driving the equilibrium further toward one side or the other and the lifetime and / or emission of the authentic fully protonated or deprotonated complex is not obtained.

REFERENCES

117. a) Norton, J. *Prog. Inorg. Chem.* **1994**, *42*, 1. b) Thorp, H. H.; Sarneski, J. E.; Brudvig, G. W.; Crabtree, R. H. *J. Am. Chem. Soc.* **1989**, *111*, 9249. c) Liu, W.; Welch, T. W.; Thorp, H. H. *Inorg. Chem.* **1992**, *31*, 4044. d) Manchanda, R.; Thorp, H. H.; Brudvig, G. W.; Crabtree, R. H. *Inorg. Chem.* **1992**, *31*, 4040. e) Goll, J. G.; Liu, W.; Thorp, H. H. *J. Am. Chem. Soc.* **1993**, *115*, 11048. f) Liu, W.; Thorp, H. H. *Inorg. Chem.* **1994**, *33*, 1026. g) Liu, W.; Thorp, H. H. *J. Am. Chem. Soc.* **1995**, *117*, 9822. h) Smith, K.-T.; Romming, C.; Tilset, M. *J. Am. Chem. Soc.* **1993**, *115*, 8681. i) Jones-Skeens, L. M.; Zhang, X. L.; Hupp, J. T. *Inorg. Chem.* **1993**, *31*, 3879
118. Barigelletti, F., Flamigni, L., Guardigli, M., Sauvage, J.-P., Collin, J.-P., Sour, A.; *J. Chem. Soc., Chem. Comm.* **1996**, 1329. b) Grigg, R., Norbert, W. D. J. A.; *J. Chem. Soc., Chem. Comm.* **1992**, 1300
119. a) Lemon, B. I.; Hupp, J. T.; *J. Phys. Chem.* **1996**, *100*, 14578. b) Yan, S. G.; Hupp, J. T. *J. Phys. Chem.* **1996**, *100*, 6867
120. Meyer, T. J. *Acc. Chem. Res.* **1989**, *22*, 163
121. a) Fleischer, E. B., Lavalley, D. K.; *J. Am. Chem. Soc.*, **1972**, *94*, 2599. b) Magnuson, R. H., Taube, H.; *J. Am. Chem. Soc.*, **1975**, *97*, 5129. c) Smith, K. K., Kaufmann, K. J., Huppert, D., Gutman, M.; *Chem. Phys. Lett.*, **1979**
122. Giordano, P. J., Bock, C. R., Wrighton, M. S., Interrante, L. V., Williams, R. F. X.; *J. Am. Chem. Soc.* **1977**, *99*, 3187
123. a) Peterson, S. H., Demas, J. N.; *J. Am. Chem. Soc.*, **1976**, *98*, 7880. b) Peterson, S. H., Demas, J. N.; *J. Am. Chem. Soc.*, **1979**, *101*, 6571. c) Sutton, J. E., Taube, H.; *Inorg. Chem.* **1981**, *20*, 3125. d) Rillema, D. P., Allen, G., Meyer, T. J., Conrad, D.; *Inorg. Chem.*, **1983**, *22*, 1617. e) Crutchley, R. J., Lever, A. B. P.; *J. Am. Chem. Soc.*, **1983**, *105*, 1170. f) Shimidzu, T., Iyoda, T., Izaki, K.; *J. Phys. Chem.*, **1985**, *89*, 642. g) Kirsch-De Mesmaeker, A., Jaquet, L., Nasielski, J.;

- Inorg. Chem.*, **1988**, 27, 4451. h) Shinozaki, K., Kaizu, H., Kobayashi, H.; *Inorg. Chem.*, **1989**, 28, 3675. i) Davila, J., Bignozzi, C. A., Scandola, F.; *J. Phys. Chem.*, **1989**, 93, 1373. j) Hosek, W., Tysoe, S. A., Gafney, H. D., Baker, A. D., Strekas, T. C.; *Inorg. Chem.*, **1989**, 28, 1228. k) Vos, Johannes G.; *Polyhedron* **1992**, 18, 2299. l) Haga, M.-A., Ano, T.-A., Ishizaki, T., Kano, K., Nozaki, K., Ohno, T.; *J. Chem. Soc., Dalton Trans.* **1994**, 263.
124. a) Buchanan, B. E., Vos, J. G., van der Putten, W. J. M., Kelly, J. M., Hage, R., de Graff, Rudolf A. G., Prins, R., Haasnoot, J. G., Reedijk, J.; *J. Chem. Soc. Dalton Trans.*, **1990**, 2425. b) Ryan, E. M.; Wang, R.; Vos, J. G.; Hage, R.; Haasnoot, J. G. *Inorganica. Chimica. Acta.* **1993**, 208, 49
125. a) Grigg, R., Holmes, J. M., Jones, S. K., Norbert, W. D. J. A.; *J. Chem. Soc., Chem. Comm.* **1994**, 185. b) Grigg, R.; Norbert, W. D. J. A. *J. Chem. Soc., Chem. Commun.* 1992, 1300
126. Orellana, G.; Moreno-Bondi, M. C.; Segovia, E.; Marazuela, M. D. *Anal. Chem.* **1992**, 64, 2210
127. Ryan, E. M., Wang, R., Vos, J. G., Hage, R., Haasnoot, J. G.; *Inorg. Chim. Acta.* **1993**, 208, 49
128. a) Gilbert, J. A.; Eggleston, D. S.; Murphy, W. R., Jr.; Geselowitz, D. A.; Gersten, S. W.; Hodgson, D. J.; Meyer, T. J. *J. Am. Chem. Soc.* **1985**, 107, 3855. b) Vining, W. J.; Meyer, T. J. *Inorg. Chem.* **1986**, 25, 2023. c) Rotzinger, F. P.; Munavalli, S.; Conte, P.; Hurst, J. K.; Gratzel, M.; Peru, F.-J.; Frank, A. J. *J. Am. Chem. Soc.* **1987**, 109, 6619. d) Eisenber, R.; Fisher, B. *J. Am. Chem. Soc.* **1980**, 102, 7363. e) Hupp, J. T.; Otruba, J. P.; Parus, S. J.; Meyer, T. J. *J. Electroanal. Chem.* **1985**, 190, 287.
129. a) Haga, M.-A.; Ano, T.-A.; Kano, K.; Yamabe, S. *Inorg. Chem.* **1991**, 30, 3843. b) Marvaud, V.; Launay, J.-P. *Inorg. Chem.* **1993**, 32, 1376
130. Mines, G. A.; Roberts, J. A.; Hupp, J. T.; *Inorg. Chem.* **1992**, 31, 125
131. a) Westheimer, F. H.; Benfey, O. T. *J. Am. Chem. Soc.* **1956**, 78, 5309. b) Nakamoto, K. *J. Phys. Chem.* **1960**, 64, 1420.
132. a) Forster, T. Z. *Naturewiss.* **1949**, 36, 186. b) Forster, T. Z. *Electrochem.* **1950**, 54, 531. c) Weller, A. *Prog. React. Kinet.* **1961**, 1, 189. d) van der Donckt, E. *Prog. React. Kinet.* **1970**, 12, 273. e) Ireland, J. F.; Wyatt, P. A. H. *Adv. Phys. Org. Chem.* **1976**, 12, 131.

133. Smith, K. K., Kaufmann, K. J., Huppert, D., Gutman, M.; *Chem. Phys. Lett.*, **1979**, *64*, 522
134. Skoog, D. A.; West, D. M.; Holler, F. J *Fundamentals of Analytical Chemistry*, 5th ed. Saunders College Publishing.; New York, New York. 1988.
135. a) Albert, A.; Goldcare, R.; Phillips, J.; *J. Chem. Soc.* **1948**, 2240. b) Jaffe, M.; *Chem. Rev.* **1953**, *53*, 191. c) Charton, M. *J. Org. Chem.* **1965**, *30*, 969
136. Perrin, D. D.; Dempsey, B. J.; Sergeant, E. P. *pKa Prediction for Organic Acids and Bases*. Chapman and Hall New York, New York. 1981